

Functionalized double-walled carbon nanotubes for integrated gas sensors

Lin Yang

▶ **To cite this version:**

Lin Yang. Functionalized double-walled carbon nanotubes for integrated gas sensors. Micro and nanotechnologies/Microelectronics. Université Paul Sabatier - Toulouse III, 2017. English. NNT : 2017TOU30254 . tel-01675535v2

HAL Id: tel-01675535
https://laas.hal.science/tel-01675535v2

Submitted on 16 Nov 2018

HAL is a multi-disciplinary open access archive for the deposit and dissemination of scientific research documents, whether they are published or not. The documents may come from teaching and research institutions in France or abroad, or from public or private research centers.

L'archive ouverte pluridisciplinaire **HAL**, est destinée au dépôt et à la diffusion de documents scientifiques de niveau recherche, publiés ou non, émanant des établissements d'enseignement et de recherche français ou étrangers, des laboratoires publics ou privés.

Université Fédérale
Toulouse Midi-Pyrénées

THÈSE

En vue de l'obtention du

DOCTORAT DE L'UNIVERSITÉ DE TOULOUSE

Délivré par :

Université Toulouse 3 Paul Sabatier (UT3 Paul Sabatier)

Présentée et soutenue par :
Lin YANG

le mardi 28 novembre 2017

Titre :

Functionalized double-walled carbon nanotubes for integrated gas sensors

---

École doctorale et discipline ou spécialité :
ED SDM : Nano-physique, nano-composants, nano-mesures - COP 00

Unité de recherche :
LAAS - CIRIMAT

Directeur/trice(s) de Thèse :

Pr. Christophe VIEU
Dr. Emmanuel FLAHAUT

Jury :
Dr. Katia ARAUJO-GUERIN, Université Clermont Auvergne (Président)
Pr. Corinne DEJOUS, Université Bordeaux INP (Rapporteur)
Dr. Madjid ARAB, Université Toulon (Rapporteur)
Pr. Guillaume VIAU, INSA Toulouse, INP (Membre du Jury)
Dr. Emmanuel FLAHAUT, Université Paul Sabatier (Co-advisor)
Pr. Christophe VIEU, INSA Toulouse (Advisor)

Acknowledgement

Time, like water in *Canal du Midi*, flow quietly but so f ast. And now my life as a doctoral student has come to an end. First and foremost I am sincerely and gratefully appreciate my supervisors, Professors **Christophe Vieu** and **Emmanuel Flahaut**. You are excellent mentor for me. It is a pleasure and honor to be your Ph.D. student. I would like to thank you for guiding me, helping me and encouraging me in the scientific world. You are rigorous researcher but also very friendly friends. Working with you was a time under pressure but cheerful. It is precious experience and memory for my career and life. I would also like to thank my team colleagues, Emmanuelle Trevisiol, Christophe Thibault, Frank Carcenac, Alin Cerf, Laurrent Malaquin, Etienne Dague, Aude Delegard, Julie Foncy, Hélène Cayon, Maxime Sahun, Alejandro Kayum Jimenez Zenteno, Aurore Esteve, Emma Desvignes, and Angelo Accardo, and colleagues from other teams, Adrian Laborde, Matthieu Joly, Benjamin Reig, and my colleagues from CIRIMAT lab, Jean-François Guillet, Thomas Lorne, Pierre Lonchambon and Chunyang Nie. Thank you all for giving help to my work and my life in France. I also want to thank my friends who are not involved in my lab-life, Jinhui Wang, Yayu Huang, Longqi Lang, Xu Yang. Thank you for having banquets and treval and sports time with me. It helped me release pressure of work. I also want to thank my friend, Yue Zhao, who is far away in China but keeps in touch with me and support me like a brother.

A special thanks to my father and my mother. I have come to France for three years without one time back to home. They never complain about me but only support me and wait my news every week. Words cannot express my gratitude and remorse. I will cherish your love and work harder to not fail your expectation.

Contents

Acknowledgement i

General Introduction of the Thesis 1

Partie I : Introduction 5

1 Introduction to Carbon Nanotubes 7
1.1 Physics of Carbon Nanotubes 7
1.1.1 Carbon Nanotubes Structure 7
1.1.2 Electronic Properties of CNTs 8
1.1.3 Double Wall Carbon Nanotubes 9
1.2 Synthesis of CNTs 10
1.2.1 Catalytic Chemical Vapor Deposition 10
1.2.2 CNTs Growth Mechanism 11
1.3 CNTs Functionalization 13

2 Carbon Nanotubes Based Gas Sensors 21
2.1 Why is Gas Sensing Important? 21
2.2 Materials for Gas Sensing 22
2.2.1 Conventional Materials 22
2.2.2 Nano Carbon Materials for Gas Sensing 22
2.3 CNTs Gas Sensors 23
2.3.1 Mechanisms of CNTs Gas Sensing 23
2.3.2 State of the Art for Integrating CNTs 25
2.4 Objectives of this Research 28

Partie II : Experiments 37

1 Synthesis and Functionalization of Double wall Carbon Nanotubes and Fabrication of DWCNTs Gas Sensor 39
1.1 Double-walled Carbon Nanotubes Synthesis 39
1.1.1 DWCNTs synthesis *via* CCVD 39

1.1.2 DWCNTs Extraction and Purification . . . 41
1.2 Double-walled Carbon Nanotubes Functionalization . . . 41
1.2.1 Non-covalent Functionalization: Carboxymethyl Cellulose Surfactant Assisted-DWCNTs Suspension . . . 41
1.2.2 Covalent Functionalization . . . 41
1.3 Sensor Fabrication . . . 44
1.3.1 Electrodes Array Fabrication on SiO_2/Si Wafers . . . 46
1.3.2 PDMS Stencils Fabrication . . . 46
1.3.3 Integration of DWCNTs . . . 47
1.4 Characterization . . . 47
1.4.1 Optimization of the Integration Process . . . 47
1.4.2 I/V Characterization . . . 54
1.4.3 Mechanism of Electron Transport in DWCNTs Disordered Films . 58
1.4.4 Consequence for Gas Sensing Mechanisms . . . 61
1.5 Conclusion . . . 62

2 Gas Detection and Results Analysis 65
2.1 Setup for Gas Exposure Experiments . . . 66
2.2 Detection of Pure Compounds . . . 66
2.3 Detection of Compounds inside Water Vapor . . . 67
2.4 Gas Detection Results . . . 68
2.4.1 Detection of pure Compounds . . . 68
2.4.2 Complex Detection . . . 73
2.4.3 Gas Detection Mechanism Discussion . . . 76
2.4.4 Multiple exposure . . . 82
2.4.5 Discrimination . . . 87
2.4.6 Limit of Detection and Calibration . . . 95
2.4.7 Chlorine Detection . . . 100
2.5 Conclusion . . . 100

Partie III : Application Gas Detection in Real Condition 107

1 DWCNTs Sensor Usage in Practice 109
1.1 Alcohol Test . . . 109
1.2 Detecting Trace of Ammonia . . . 111
1.3 Conclusion . . . 112

Partie IV : General Conclusion 113

General Conclusion 113

Appendices i

General Introduction of the Thesis

Since the CNTs have been demonstrated as a gas sensing material[1], the carbon nanotubes (CNTs) based gas sensors have been developed for almost twenty years. According to the type of CNTs that are used, the CNTs based gas sensor can be simply classified as single-walled carbon nanotubes (SWCNTs) based gas sensor and multi-walled carbon nanotubes (MWCNTs) based gas sensor. The ideal CNTs based gas sensor is the one utilizing a single SWCNT layer as sensing material, thus allowing it largest proportion of surface area for absorbing gas molecules, moreover a single SWCNT has distinctive selectivity according to the study of chirality dependence of SWCNT based gas sensor[2]. However, the advantages of SWCNTs in gas sensing research have impeded the development of popularizing SWCNTs based gas sensor. This is due to the fabrication techniques. The fabrication techniques of an individual SWCNT based gas sensors have been developed in two approaches. One method is directly growing SWCNTs on the substrate. The excess SWCNTs are burned in the later process. This method highly requires energy and expensive equipment input. The burn of excess SWCNTs is also a very sophisticated process. Another method is simply depositing an drop of SWCNTs suspension in which there might be a single SWCNT. Thus this method demands lots of repetitive work to successfully fabricate one sensor device as there is high possibility to find none or more than one SWCNT in the drop. Besides, as it has been pointed out the selectivity of SWCNTs based gas sensors depend on the chirality of SWCNTs. Thereby, the individual SWCNT based gas sensors' performance is different one from another if there was no control of chirality of SWCNTs that are used. The low efficiency and high cost, and the essential challenge in the aspect of fabricating gas sensors that are based on individual SWCNT of single chirality make it difficult for massive production. In addition, researchers have also developed a different approach to use CNTs as gas sensing materials by integrating CNTs network. For SWCNTs, because of the fundamental concern[2], furthermore, the SWCNTs of different chiral index can be either semiconducting or metallic, it is better to separate SWCNTs based on their chirality. But there is no such concern for MWCNTs. The MWCNTs are highly conductive. Because the large diameter in MWCNTs reduces the band gap between valence and conduction band, which makes it into a zero-gap semiconductor. Thus, the MWCNTs are normally treated as metallic conductor. But with the increase of number of layers, the aspect ratio is de-

creasing, and there is less surface area in MWCNTs for absorbing gas molecules. Thus the best choice is using DWCNTs which are the simplest MWCNTs and exhibit largest aspect ratio among MWCNTs.

In this Thesis work, we have focused on the optimization of integration of DWCNTs networks and studied the raw and functionalized DWCNTs sensors for detecting simple chemical vapor in different conditions. The DWCNTs gas sensors are easy to fabricate with the method we use and require very low cost to the respect of material consumption, technologies involved. The fabrication does not specifically rely on the substrate. Thus the DWCNTs can be integrated on hard or flexible substrates. It is also suitable for mass production. The functionalized DWCNTs sensors are sensitive to various gas species. The oxidized DWCNTs sensors are able to detect ammonia of sub *ppm* concentration in the presence of high concentration (ca. 5700 *ppm*) water vapor. The sensitivity of oxidized DWCNTs sensors is also very stable upon prolonged ammonia vapor exposure in the presence of high concentration water vapor. Finally we test the oxidized DWCNTs sensors in real-life use, such as alcohol drinking detection, residual of ammonia detection. Compared to commercial breathalyzer, our sensor costs ten times less and is able to detect alcohol drinking where it is out of the detection limit of commercial breathalyzer. The oxidized DWCNTs sensors also detected trace of ammonia vapor that is lower than the human nose detection limit (< 0.04 *ppm*).

Due to the simple design and very low power consumption, our sensors are compatible with wearable integrated circuit devices. By further study, we expect that our work on DWCNTs sensors could provide robust and high performance product to the world in future.

Bibliography

[1] J. Kong, N. R. Franklin, C. Zhou, M. G. Chapline, S. Peng, K. Cho, and H. Dai, "Nanotube molecular wires as chemical sensors," *science*, vol. 287, no. 5453, pp. 622–625, 2000.

[2] G. A. Jamal, M. R. Islam, M. A. Rahman, J. F. Meem, and R. A. Sathi, "Chirality dependence of single wall carbon nanotube based gas sensor," in *Region 10 Conference (TENCON), 2016 IEEE*, pp. 2771–2774, IEEE, 2016.

Partie I : Introduction

Chapter 1

Introduction to Carbon Nanotubes

This chapter introduces the blooming domain of Carbon Nanotubes (CNTs) in general, physics of CNTs, synthesis methods and application of CNTs. The Catalytic Chemical Vapor Deposition (CCVD) synthesis method and electronic nose application of CNTs are highlighted in the relevant sections.

1.1 Physics of Carbon Nanotubes

1.1.1 Carbon Nanotubes Structure

Carbon nanotubes (CNTs) are considered as one of most promising and the representative of one dimension nano materials. Since the discovery by Iijima [1], studies have proved that CNTs exhibit many outstanding electronic, mechanical and optical properties, due to the special electronic structure and high aspect ratio. The simplest structure of CNTs is single-wall carbon nanotube (SWCNT) with diameter of ca. $0.7 - 3nm$. SWCNT is theoretically considered as rolled up from graphene which contains a single layer of carbon atoms.

In graphene, one carbon atom is evenly linked to three neighbor carbon atoms through covalent bonds. In this structure, sp^2 hybridization between carbon atoms happen according to valence bond theory. The electrons of p_z orbitals are delocalized and freely move along graphene surface within p_z orbitals cloud, which is the origin of high conductivity for graphene, graphite and CNTs. While diamond has valence electrons that are localized in sp^3 hybridization framework, thereby, making it an insulator.

Graphene sheet resembles two dimensional honeycomb structure as depicted in Fig. 1.1. The vectors $\boldsymbol{a_1}$ and $\boldsymbol{a_2}$ in Fig. 1.1 represent the two primitive lattice vectors of graphene. An arbitrary carbon atom in the graphene sheet, $\boldsymbol{C_h}$, $(h = 1, 2...)$, can be described by the linear combination of primitive vectors, $n\boldsymbol{a_1} + m\boldsymbol{a_2}$ from an origin site in lattice.

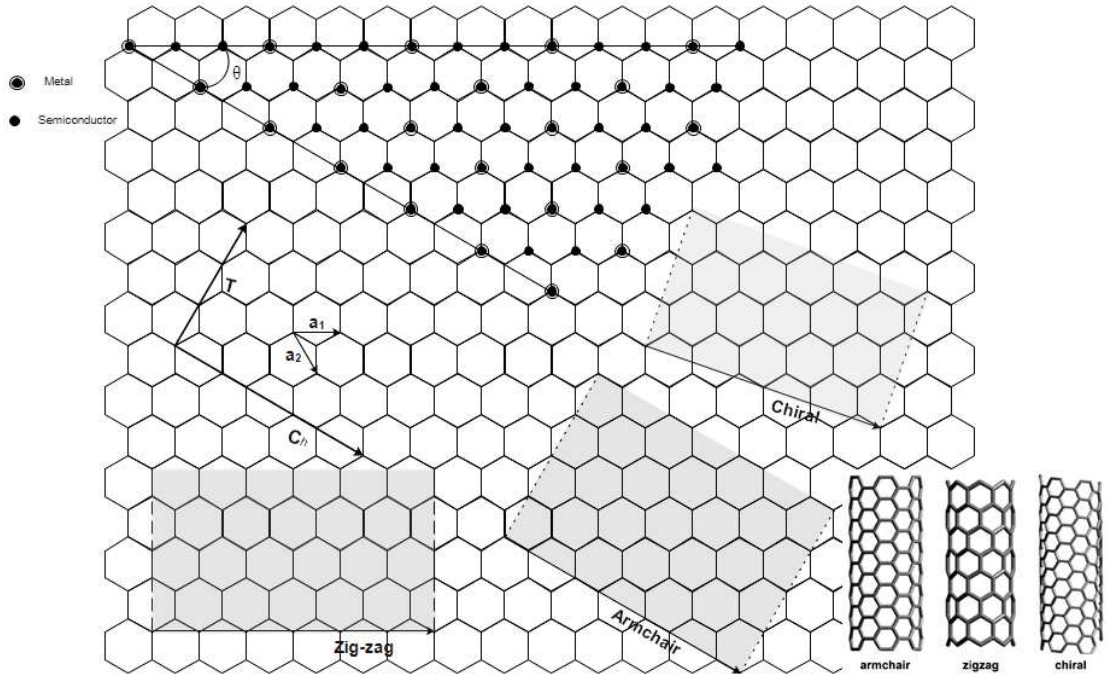


Figure 1.1: Diagram of two-dimensional graphene sheet. $\boldsymbol{a_1}$ and $\boldsymbol{a_2}$ are the lattice vectors. $\boldsymbol{C_h}$ and $\boldsymbol{T}$ are chiral vector and translation vector, respectively. $\boldsymbol{C_h}$ specifies the chirality of nanotube, which is uniquely defined by (n, m). Three types of chirality of CNTs, armchair, zig-zag and chiral, are outlined with chiral vector in graphene sheet.

Carbon nanotubes' properties are specifically determined by integers (n, m), i.e. $\boldsymbol{C_h}$. Thereby CNTs are classified depending on the direction in which graphene rolls up, which defines the chirality of CNTs. CNTs with three different typical structure, named armchair, zig-zag, and chiral are illustrated in Fig 1.1. The physical, mechanical and chemical properties thereby differ from each other with respect to (n, m).

1.1.2 Electronic Properties of CNTs

A SWCNT is formed by rolling graphene up along $\boldsymbol{C_h}$. The circumference of the tube is the scalar of $\boldsymbol{C_h}$. The chirality and the chiral angle 'θ', as defined in Figure .1.1, is uniquely determined by (n, m). The electronic conductivity of SWCNTs is also ruled by (n, m): SWCNTs are metallic with $n = m$[2][3][4]; SWCNTs with $n - m = 3l$, where l is a nonzero integer, are semiconducting with small band-gap[4]; other SWCNTs are semiconducting with large band-gap[2][3][4]. The (n, n) tubes ($\theta = 0°$) are known as armchair SWCNTs, of which the metallic conductivity is curvature independent owing to the symmetry. The band-gaps of tubes with large-gap and small-gap decrease in accordance with $1/R$ and $1/R^2$, respectively. For practical purposes, the small-gap SWCNTs are accounted as metallic at room temperature, since the band gaps experimentally observed

are very small. The SWCNTs with $m = 0$ ($\theta = 30°$) are called 'Zig-zag'. They can be either metallic or semiconducting based on discussion above.

As one member of CNTs family, SWCNTs have received intense interests in academia and industry since this simplest structure makes it easy to model. However, the other members of the family, multi-wall carbon nanotubes (MWCNTs) which were the first discovered CNTs[1] in history, have also drew great research attention. A MWCNT is a CNT formed by a number of concentric SWCNTs of different diameters. The chiral vectors $\boldsymbol{C_h}$ differ from each layer, thereby the chirality differs from each layer. Studies[5][6] show that the adjacent layers are generally non-commensurate. As a consequence, the electronic coupling between adjoining layers is decreased compared to graphite. Unlike SWCNTs of which the electronic properties have been well studied, MWCNTs preserve much complicated electronic properties because of the complex structure. Nevertheless, MWCNTs are generally considered to be metallic in practice as a result of large diameter induced zero-gap between valence band and conduction band. The metallic CNTs have long mean free path of electron and phonon scattering at room temperature. If the physical length of conductor is shorter than the mean free path, ballistic electron transport occurs when electric field is applied. Nano electronic components have been fabricated based on ballistic transport, like ballistic field effect transistors[7][8], quantum resistors[9], and logic circuits[10].

As C-C bond in CNTs is sp^2 type, CNTs exhibit high stability under aggressive mechanical, chemical and thermal treatment. Only the hemispherical ends and defects have a moderate activity. Because of this reason, CNTs are good candidates for extreme condition usage. Such as electron filed emission source[11][12], provided that the atmosphere does not contain oxygen.

1.1.3 Double Wall Carbon Nanotubes

Double-wall carbon nanotubes (DWCNTs), as shown in Fig. 1.2, are the simplest MWCNTs. As between SWCNTs and more complicated MWCNTs (I will use MWCNTs to refer to those which have more than two layers if it is not specified since here), DWCNTs preserve many properties that are close to both SWCNTs and MWCNTs but also different from them.

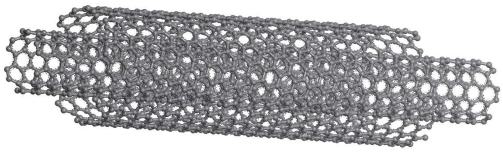


Figure 1.2: Schematic of double-wall carbon nanotubes

The study of DWCNTs sheds light on inter-planar interaction effect on MWCNTs'

physical and chemical properties. DWCNTs have small diameter, less defects compared to MWCNTs with three and more layers. Wu et al.[13] theoretically investigated the transport properties of particular DWCNTs, which shows a dramatic variation in conductance corresponding to variation of chirality of inner and outer walls. The outer wall also plays a role of protection on inner wall. The work from Poklonski et al.[14] shows that the conductance of inner wall is temperature ($T \leqslant 500K$) independent. DWCNTs also have higher thermal stability than SWCNTs[15] and comparable to that of MWCNTs. As a consequence, DWCNTs can endure high current and high temperature for particular application. Recently, a team has evidenced some strong coupling between the two layers which may favors the growth of some specific structures[16].

1.2 Synthesis of CNTs

Because different structures grant different properties to each carbon nanotube, the synthesis of controlled CNTs is an important goal, which has been widely studied. So far, there are three popular approaches to produce CNTs.

In 1991, arc-discharge was utilized when CNTs were first discovered[1]. In 1992 year, gram scale synthesis of MWCNTs of high-quality was achieved by Ebbesen and Ajayan by the same state-of-the-art[17]. In 1993, substantial amounts of SWCNTs were first synthesized by arc discharge[18]. Although it has been developed very early and gram level production was achieved, arc discharge method has high demand of equipment and requires large amount of energy, which reciprocates prohibition of its popularization for mass production. Besides, arc discharge can only produce powdered samples of bundled nanotubes, typically with a low purity. It is not reported, to the extent of my knowledge, that structural ordered CNTs are produced by arc discharge method. The Laser ablation method has the same disadvantages as arc discharge in terms of cost and maintenance, although the produced CNTs are much cleaner.

1.2.1 Catalytic Chemical Vapor Deposition

Among the main utilized methods for CNTs synthesis, catalytic chemical vapor deposition (CCVD) is the most widely used method. CCVD allows production at low-cost and high-yield. It is able to produce highly ordered CNTs. The history of CCVD can be traced back to 1890 when formation of carbon filaments was observed by French scientists. After being developed for more than one century, the CCVD has become the most popular method for producing carbon nanomaterials (carbon filaments, carbon fibers, carbon nanotubes, graphene and nanodiamond). In this work, the DWCNTs we used were synthesized by means of CCVD. The DWCNTs are selectively produced in gram scale and have low residual catalyst components. The CCVD process typically involves catalysts which are mostly supported on refractory oxides, protection/carrier gas, argon for instance, source of carbon, e.g. hydrocarbon, heating and cooling procedure throughout whole process and of course metal nanoparticles (transition metals, most often). Each of them has evident influences on the final products, such as the

number of layers, chirality, diameter, length, yields and so on. But catalysts have drawn attention the most as it is the key for nucleation of carbon and, thereby, forming carbon nanotubes. The catalysts' components, size, interaction with catalyst-support directly determine the morphology of CNTs grown on them.

A typical CCVD setup for carbon nanotubes (CNTs) synthesis can be seen in Fig. 1.3. An electrical tube furnace is used for temperature control. Inside the furnace, the substrate (e.g. graphite, quartz, silicon, alumina) supported catalyst (metal nanoparticles, Fe, Co, Ni for instance) is placed in a quartz boat within a quartz tube. Then with the protection of argon (eg. Ar) gas, the sample is heated to a set temperature. It is reported that low-temperature and high-temperature CCVD generally produce MWCNTs and SWCNTs, respectively. For example, in our DWCNTs synthesis, a high temperature is required. Then carbon precursor (e.g. methane, carbon dioxide, benzene) is injected into the quartz tube at a controlled flow-rate. The carbon precursor gas flow injection rates are different according to different research work. It is injected into the furnace for a period of reaction time as needed. At the end, the reaction is flushed with the carrier gas and the furnace is then cooled down. This method is capable of producing gram scale CNTs. The reaction product is made up of nano carbon and catalyst compounds and, thereby, needs purification process for further use.

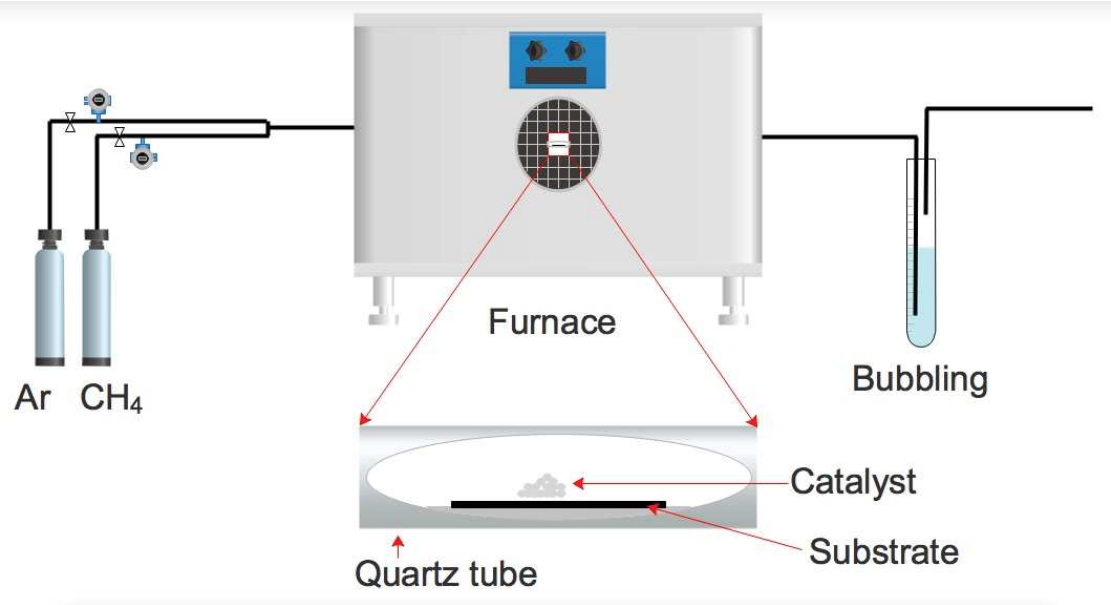


Figure 1.3: Illustration of a typical catalyst vapor deposition process of SWCNTs fabrication as described in the work of A. M. Cassell et. al[19].

1.2.2 CNTs Growth Mechanism

There are two simplified growth models for CNTs: base-growth and tip-growth. The base-growth model was first proposed by J. Kong. et al.[20] originating from carbon

fiber growth mechanism [21][22][23]. In this case, the catalyst particles have a strong contact with the substrate. There is obtuse contact angle between catalyst particle and substrate[24]. The hydrocarbon, such as methane in ref.[20], molecules are absorbed on catalyst particles. The surface of catalyst particle is first saturated by decomposition of methane. Carbon atoms, then, diffuse into catalyst particle. The precipitation of carbon atoms fails to push catalyst particle up off the substrate because of the strong contact. As a consequence, the carbon atoms are obliged to promote out of catalyst particle through its vertex where least interaction exists between catalyst particle and substrate. A hemisphere of carbon is first formed. With continue feeding of carbon from methane, it grows to be a cylinder tube as it can be seen in Fig. 1.4.

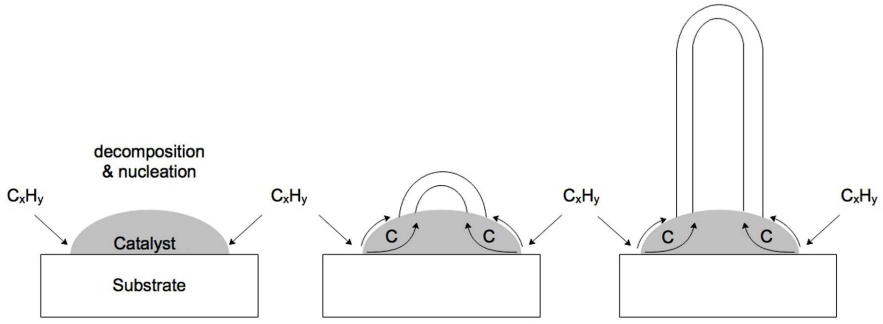


Figure 1.4: Base-growth model. C_xH_y represents hydrocarbon as carbon precursor. The scheme is inspired by the Ref.[25] and depicts the growth of DWCNTs.

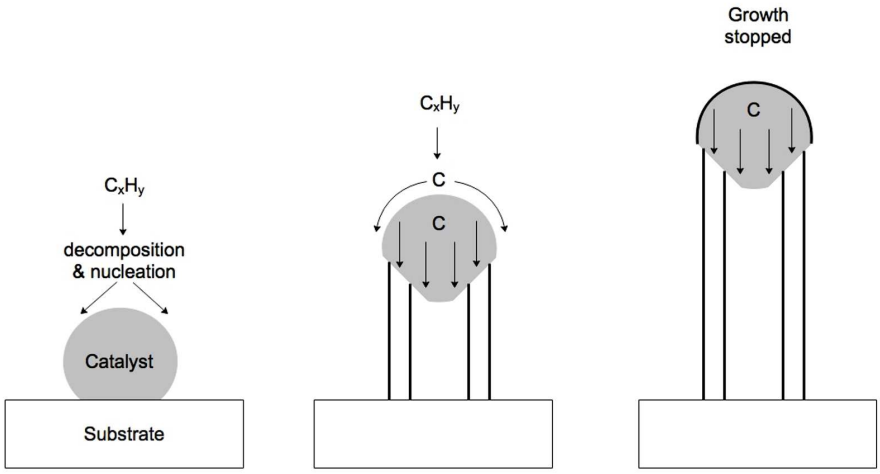


Figure 1.5: Tip-growth model. C_xH_y represents hydrocarbon as carbon precursor. The scheme is inspired by Ref.[26] and depicts the growth of DWCNTs.

In the Tip-growth model, the interaction between the catalyst particle and the substrate is weaker. The catalyst particle has an acute contact angle with the substrate.

Therefore, carbon atoms from decomposition of hydrocarbon diffuse through catalyst particle from top surface to the bottom surface where carbon atoms, nucleation push catalyst particles up off the substrate. As long as the top surface is opened to carbon precursor to decompose, the diffusion and nucleation keep on going and, thereby, the CNT is formed and grows longer and longer. Unless the catalyst particle is fully cover with excess carbon, the growth continues. This model is illustrated in Fig. 1.5

1.3 CNTs Functionalization

Individual carbon nanotubes have unique and superior electronic, mechanical, thermal and optical properties compared to conventional materials. However, due to van der Waals attraction, CNTs tend to pack together and form bundles and ropes. The high aspect ratio enhances this effect. Correspondingly, the properties are strongly affected and performances in any aspects are thereby altered. As discussed in Juan G. D. et al.,s work[27], the best way to reach CNTs, properties is individualize them. To fulfill mono-dispersed CNTs suspensions, much effort has been taken into research. In general, two approaches have been widely used, which are covalent and non-covalent functionalization. Non-covalent functionalization is a nondestructive approach by which the π-conjugation of outer surface of CNTs is preserved. It can be realized by tuning the interfacial properties of CNTs with aromatic compounds, surfactants and polymers through π stacking or hydrophobic interaction. On the other side, covalent functionalization is a method in which chemical entities are bonded to CNTs surface via covalent bonds and, therefore, much more stable.

Non-covalent Functionalization

The surfactant molecules can be noncovalently absorbed on surface of CNTs by which the CNTs are separated individually. Thereby, noncovalent treatment with surfactant or polymers has been appreciably utilized as pre-treatment for further investigation of CNTs research. In noncovalent functionalization of CNTs, applying ultra-sonication is considered helping surfactant molecules to separate individual CNT from bundles.

In Ref.[28], Strano and coworkers have studied the mechanism of dispersing CNTs with surfactant and ultra-sonication. Ultra-sonication provides high shear which splits CNTs at the ends of bundles, Fig. 1.6. It gives small space between the ends of CNTS. The gap is then propagated with adsorption of surfactant molecules, Fig. 1.6 (iii). An individual CNT is separated from bundle, Fig. 1.6(iv), as a consequence of combination of ultra-sonication and surfactant. When given sufficient surfactant and ultra-sonication duration, the CNTs should be ideally dispersed individually. Notwithstanding, such mechanical method usually leads to fragmenting CNTs. It reduces the aspect ratio. This side effect increases as ultra-sonication prolonged. Thus, optimized duration of ultra-sonication is suspension quality dependent

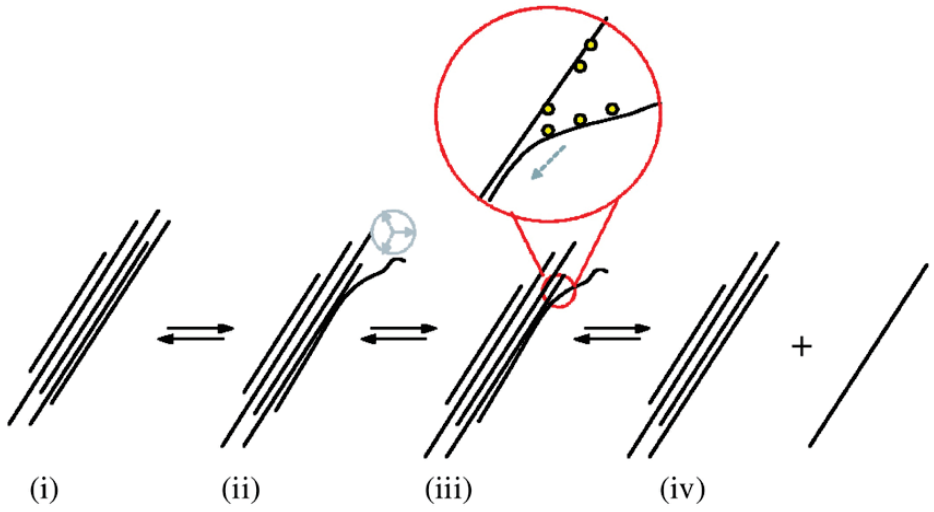


Figure 1.6: The non-covalent functionalization mechanism of nanotube isolation proposed by Strano et al.[28]. Ultrasonic processing exfoliates the bundle end (ii), which then becomes a site for additional surfactant adsorption. This later process continues in an "unzippering" fashion (iii) that terminates with the release of an isolated, surfactant-coated nanotube in solution (iv).

This strategy can also be used to progressively replace one surfactant by another one in order to get a better dispersion, or to replace a toxic surfactant by a non-toxic one[29] Surfactant selection for CNTs suspension is solvent dependent. In general, non-polar surfactants are superior choice for organic solvent. Yet, polar surfactants, for instant ionic surfactants, are preferable for aqueous solution.

Covalent Functionalization

Functionalization is significantly meaningful for sensor research in terms of specificity and selectivity. Covalent functionalization is a chemical functionalization method. It is accomplished based on the covalent bonding between functional groups and carbon atoms on CNTs. The reactive carbon atoms are mainly from two parts of CNT cylinder. First, it is the fullerene-like end caps. Because graphene layer is highly curved in hemispherical form some carbon atoms form pentagon rings, the caps carbon atoms are highly reactive comparable to fullerenes[30][31][32]. The second source is the sidewalls which usually exhibit structural defects. The direct covalent sidewall functionalization is associated with a change of hybridization from sp^2 to sp^3 and a simultaneous loss of π-conjugation system on graphene layer[33]. This process happens in reaction with compounds of high chemical reactivity, such as F_2[34] and strong oxidants in general.

Functionalization through defect sites is an additional method for covalent functionalization. Notwithstanding that reported proportion are small and different[35], defect sites are preferable to covalent functionalization compared to sites without defects on

side wall. These defect sites include pentagon-heptagon pairs, sp^3-hybridized defects and vacancies in nanotube lattice which are called Stone-Wales defects as it is shown in Fig. 1.7[30]. Compared to carbon atoms with sp^2 hybridized bonds, these defect sites are more reactive.

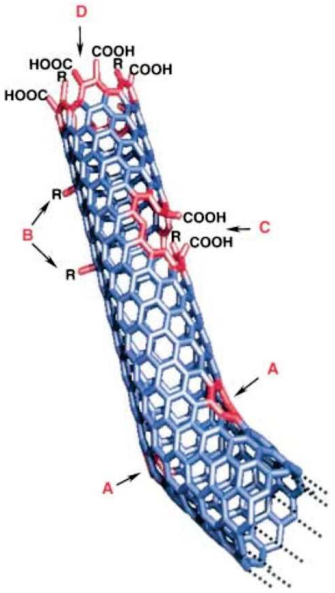


Figure 1.7: Defects of CNTs[30]: A) five- or seven-membered rings in the C framework, instead of the normal six-membered ring B) sp^3-hybridized defects, C) C framework damaged by oxidative conditions, and D) open end of CNT, terminated with -COOH groups.

Besides of improvement in solubility, CNTs can gain new electrical and/or mechanical properties by covalent functionalization. For example, oxidation brings carboxyl groups onto CNTs surface which increases CNT's solubility remarkably. Additionally, carboxyl groups provide substitution sites for additional functionalization.

Based on mechanisms above, DWCNTs have been functionalized by oxidation and amination[36] and fluorination[37] in our work.

Bibliography

[1] S. Iijima, "Helical microtubules of graphitic carbon," *nature*, vol. 354, no. 6348, p. 56, 1991.

[2] R. Saito, G. Dresselhaus, and M. S. Dresselhaus, *Physical properties of carbon nanotubes*. World scientific, 1998.

[3] K. Tanaka, K. Okahara, M. Okada, and T. Yamabe, "Electronic properties of buckytube model," *Chemical Physics Letters*, vol. 191, no. 5, pp. 469–472, 1992.

[4] N. Hamada, S.-i. Sawada, and A. Oshiyama, "New one-dimensional conductors: graphitic microtubules," *Physical Review Letters*, vol. 68, no. 10, p. 1579, 1992.

[5] N. B. Brandt, S. M. Chudinov, and Y. G. Ponomarev, *Semimetals: 1. Graphite and its Compounds*, vol. 20. Elsevier, 1988.

[6] M. Dresselhaus and M. Endo, "Relation of carbon nanotubes to other carbon materials," in *Carbon Nanotubes* (P. A. Mildred S. Dresselhaus, Gene Dresselhaus, ed.), ch. 2, pp. 11–28, Springer, 2011.

[7] A. Javey, J. Guo, Q. Wang, M. Lundstrom, and H. Dai, "Ballistic carbon nanotube field-effect transistors," *nature*, vol. 424, no. 6949, pp. 654–657, 2003.

[8] R. Martel, T. Schmidt, H. Shea, T. Hertel, and P. Avouris, "Single-and multi-wall carbon nanotube field-effect transistors," *Applied Physics Letters*, vol. 73, no. 17, pp. 2447–2449, 1998.

[9] S. Frank, P. Poncharal, Z. Wang, and W. A. de Heer, "Carbon nanotube quantum resistors," *Science*, vol. 280, no. 5370, pp. 1744–1746, 1998.

[10] Z. Chen, J. Appenzeller, Y.-M. Lin, J. Sippel-Oakley, A. G. Rinzler, J. Tang, S. J. Wind, P. M. Solomon, and P. Avouris, "An integrated logic circuit assembled on a single carbon nanotube," *Science*, vol. 311, no. 5768, pp. 1735–1735, 2006.

[11] Y. Cheng and O. Zhou, "Electron field emission from carbon nanotubes," *Comptes Rendus Physique*, vol. 4, no. 9, pp. 1021–1033, 2003.

[12] N. De Jonge, Y. Lamy, K. Schoots, and T. H. Oosterkamp, "High brightness electron beam from a multi-walled carbon nanotube," *Nature*, vol. 420, no. 6914, pp. 393–395, 2002.

[13] Y. Wu, P. Cheng, H. Zhu, Y. Huang, K. Zhang, and R. Liao, "Transport properties of double-walled carbon nanotubes and carbon boronitride heteronanotubes," *Carbon*, vol. 95, pp. 220–227, 2015.

[14] N. A. Poklonski, N. N. Hieu, E. F. Kislyakov, S. A. Vyrko, A. I. Siahlo, A. M. Popov, and Y. E. Lozovik, "Interwall conductance in double-walled armchair carbon nanotubes," *Physics Letters A*, vol. 372, no. 35, pp. 5706–5711, 2008.

[15] Y. Kim, H. Muramatsu, T. Hayashi, M. Endo, M. Terrones, and M. Dresselhaus, "Thermal stability and structural changes of double-walled carbon nanotubes by heat treatment," *Chemical Physics Letters*, vol. 398, no. 1, pp. 87–92, 2004.

[16] A. Ghedjatti, Y. Magnin, F. Fossard, G. Wang, H. Amara, E. Flahaut, J.-S. Lauret, and A. Loiseau, "Structural properties of double-walled carbon nanotubes driven by mechanical interlayer coupling," *ACS nano*, vol. 11, no. 5, pp. 4840–4847, 2017.

[17] T. Ebbesen and A. P M, "Large-scale synthesis of carbon," *Nature*, vol. 358, p. 16, 1992.

[18] D. Bethune, C. Klang, M. De Vries, G. Gorman, R. Savoy, J. Vazquez, and R. Beyers, "Cobalt-catalysed growth of carbon nanotubes with single-atomic-layer walls," *Nature*, vol. 363, no. 6430, pp. 605–607, 1993.

[19] A. M. Cassell, J. A. Raymakers, J. Kong, and H. Dai, "Large scale cvd synthesis of single-walled carbon nanotubes," *The Journal of Physical Chemistry B*, vol. 103, no. 31, pp. 6484–6492, 1999.

[20] J. Kong, A. M. Cassell, and H. Dai, "Chemical vapor deposition of methane for single-walled carbon nanotubes," *Chemical Physics Letters*, vol. 292, no. 4, pp. 567–574, 1998.

[21] R. Baker, "Catalytic growth of carbon filaments," *Carbon*, vol. 27, no. 3, pp. 315–323, 1989.

[22] G. G. Tibbetts, "Why are carbon filaments tubular?," *Journal of crystal growth*, vol. 66, no. 3, pp. 632–638, 1984.

[23] G. Tibbetts, M. Devour, and E. Rodda, "An adsorption-diffusion isotherm and its application to the growth of carbon filaments on iron catalyst particles," *Carbon*, vol. 25, no. 3, pp. 367–375, 1987.

[24] M. Kumar and Y. Ando, *Carbon Nanotube Synthesis and Growth Mechanism*. INTECH Open Access Publisher, 2011.

[25] R. Baker, M. Barber, P. Harris, F. Feates, and R. Waite, "Nucleation and growth of carbon deposits from the nickel catalyzed decomposition of acetylene," *Journal of catalysis*, vol. 26, no. 1, pp. 51–62, 1972.

[26] R. Baker and R. Waite, "Formation of carbonaceous deposits from the platinum-iron catalyzed decomposition of acetylene," *Journal of Catalysis*, vol. 37, no. 1, pp. 101–105, 1975.

[27] J. G. Duque, A. N. G. Parra-Vasquez, N. Behabtu, M. J. Green, A. L. Higginbotham, B. K. Price, A. D. Leonard, H. K. Schmidt, B. Lounis, J. M. Tour, *et al.*, "Diameter-dependent solubility of single-walled carbon nanotubes," *ACS nano*, vol. 4, no. 6, pp. 3063–3072, 2010.

[28] M. S. Strano, V. C. Moore, M. K. Miller, M. J. Allen, E. H. Haroz, C. Kittrell, R. H. Hauge, and R. Smalley, "The role of surfactant adsorption during ultrasonication in the dispersion of single-walled carbon nanotubes," *Journal of Nanoscience and Nanotechnology*, vol. 3, no. 1-1, pp. 81–86, 2003.

[29] V. Datsyuk, P. Landois, J. Fitremann, A. Peigney, A. M. Galibert, B. Soula, and E. Flahaut, "Double-walled carbon nanotube dispersion via surfactant substitution," *Journal of Materials Chemistry*, vol. 19, no. 18, pp. 2729–2736, 2009.

[30] A. Hirsch, "Functionalization of single-walled carbon nanotubes," *Angewandte Chemie International Edition*, vol. 41, no. 11, pp. 1853–1859, 2002.

[31] S. B. Sinnott, "Chemical functionalization of carbon nanotubes," *Journal of Nanoscience and Nanotechnology*, vol. 2, no. 2, pp. 113–123, 2002.

[32] E. V. Basiuk, M. Monroy-Peláez, I. Puente-Lee, and V. A. Basiuk, "Direct solvent-free amination of closed-cap carbon nanotubes: a link to fullerene chemistry," *Nano Letters*, vol. 4, no. 5, pp. 863–866, 2004.

[33] P.-C. Ma, N. A. Siddiqui, G. Marom, and J.-K. Kim, "Dispersion and functionalization of carbon nanotubes for polymer-based nanocomposites: a review," *Composites Part A: Applied Science and Manufacturing*, vol. 41, no. 10, pp. 1345–1367, 2010.

[34] E. Mickelson, C. Huffman, A. Rinzler, R. Smalley, R. Hauge, and J. Margrave, "Fluorination of single-wall carbon nanotubes," *Chemical physics letters*, vol. 296, no. 1, pp. 188–194, 1998.

[35] D. B. Mawhinney, V. Naumenko, A. Kuznetsova, J. T. Yates, J. Liu, and R. Smalley, "Surface defect site density on single walled carbon nanotubes by titration," *Chemical Physics Letters*, vol. 324, no. 1, pp. 213–216, 2000.

[36] T. Lorne, M. Jiménez-Ruiz, S. Rols, J.-M. Escudier, J. Rubio-Zuazo, M. Zbiri, A.-M. Galibert, B. Soula, and E. Flahaut, "Competition between covalent and non-covalent grafting of fluorescein isothiocyanate on double-walled carbon nanotubes: A quantitative approach," *Carbon*, 2017.

[37] L. G. Bulusheva, P. N. Gevko, A. V. Okotrub, Y. V. Lavskaya, N. F. Yudanov, L. I. Yudanova, O. G. Abrosimov, E. M. Pazhetnov, A. I. Boronin, and E. Flahaut, "Thermal behavior of fluorinated double-walled carbon nanotubes," *Chemistry of materials*, vol. 18, no. 20, pp. 4967–4971, 2006.

Chapter 2

Carbon Nanotubes Based Gas Sensors

2.1 Why is Gas Sensing Important?

The air does not only protect life from cosmic radiation, but also supports life in many other ways. The oxygen in air keeps human metabolism working. However, the air is not purely constituted by gases that are vital to life, there are many other species that are harmful and toxic or even deadly to life, such as CO, NO, NO_2, SO_2, NH_3 and volatile organic compounds. In the natural ecosystem, the toxic gases normally remain at low concentration. The amount of some species may be suddenly increased in a natural event like SO_2, H_2S, CO,HCl released from volcanic eruption. Nowadays, the impact of human's activities on atmosphere is more and more significant. Fossil combustion, degradation of industrial and living wastes, industrial accident, chemical fertilizer and many other modernization activities release and create more and more hazard gases into air. In industrial production, more and more hazard substances are used, many of them are toxic gases, which increases the risk of workers' health or/and life. In many cases the substances used are also combustible. As a consequence, the products often contain different volatile and noxious substances. Secondary harm could occur to family members, especially children and elders. Therefore, gas detection is important and meaningful in various areas such as gases analysis and control, air quality monitoring. From chemical to petrochemical industry, scientific research to engineering , environmental monitoring to security censorship, food industry to medical diagnosis and many other manufacturing industry and agriculture field, gas sensors have been widely used. Thus, research on highly sensitive, selective, low cost, long lifetime novel gas sensors for different purpose has attracted intense interests.

2.2 Materials for Gas Sensing

2.2.1 Conventional Materials

There are variety of materials that have been used for developing gas sensors. Conventional materials include metal oxides, polymers, thin metal films, solid electrolytes as debriefed in the book *Handbook of Gas Sensor Materials* Volume 1[1]. These materials have been deeply studied and widely used in gas sensors development, especially metal oxides, which have been used in every type of gas sensor, see Ref.[1] on page 50. However, as pointed out in Ref.[2], there are shortages in the application of metal oxides, like high power consumption and noise compared to other materials. Moreover, the miniaturization of metal oxides sensors is hindered by the high power consumption. Besides, there are other shortcomings of metal oxides in gas sensors application, for example, low chemical stability, low mechanical strength, high operating temperature. Conducting polymers (CPs) are the most promising polymers for gas sensors application according to study[3]. CPs based sensors have been developed for various gases detection, such as NH_3, NO_2 and O_2. However, the high power consumption and high noise[2] drawback their popularization. In addition, CPs based gas sensors are vulnerable to water vapor[4][5][6]. Thin metal films based sensors are easy to be miniaturized and are compatible with Si electronic devices, which make the thin metal films based sensors promising in portable and wearable devices. However the thin metal films are fragile to the ambience[7][8][9]. Water vapor also strongly affects the sensing performance[10]. The solid electrolytes based gas sensors are highly selective. But due to the detection mechanism related to mobile ions in the bulk solid phase[11], it is a challenge for their miniaturization. Besides, to obtain high concentration of ions, it often requires high operating temperature, which, thereby, demand high energy consumption. There are also many other materials for gas sensing that use acoustic or optical method to detect gases, such as piezoelelctric crystals and optical fibers. Due to the method utilized, these kind of gas sensors are limited for miniaturization

2.2.2 Nano Carbon Materials for Gas Sensing

As pointed out by G. Korotcenkov[1], there are no ideal sensing materials that meet all requirements. Research continues to find new materials that have new characteristics to develop novel gas sensors. Following development of nanotechnology, recent research is focusing on nanomaterials based gas sensors. One that is mostly studied is nano carbon materials based gas sensors. There are many members in the nano carbon family, carbon black, fullerenes, carbon nanotubes (CNTs), graphene, nanodiamond particles and their functionalized materials. Among many carbon materials, most researches have been focusing on CNTs due to their extraordinary chemical, mechanical and electrical properties. The mature of CNTs synthesis methods have reduced the cost of production, especially the CCVD method which is considered as the most economic method while providing high quality CNTs[12].

2.3 CNTs Gas Sensors

In 2000, Dai and co-workers[13] first time demonstrated that CNTs based field effect transistor (FET) can be used as gas sensor. Since then, various CNTs based gas sensors have been developed by different approaches, such as semiconducting CNTs based FETs (NTFETs)[14][15][16][17][18][19][20], chemiresistors[21][22][23][24][25][26][27], capacitors [28][29][30], resonators/optical gas sensors[31][32][33][34][35] and so on. Some gas sensors based on CNTs have been reported that utilize different approaches to detect gases, such as CNTs based resonator or optical gas sensors,

NTFETs and CNTs-chemiresistors based gas sensors are the most promising CNTs based gas sensors due to their integrability in Si based electronics, simple configuration and low measurement requirement. NTFETs have been reported by a large number of literatures in the field of CNTs based gas sensor. Typically, a NTFET does not have the body terminal as schemed in Figure 2.1. And in CNTs chemiresistor configuration, there is only a constant source-drain voltage or a constant current through source-CNT(s)-drain applied. Though the configuration of NTFET and CNTs chemiresistor are simple, there are many different mechanisms that have been discussed for each type of CNTs based gas sensor.

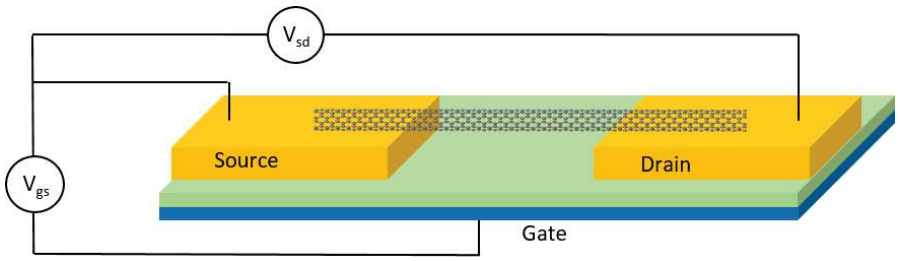


Figure 2.1: Scheme of NTFET based gas sensor.

2.3.1 Mechanisms of CNTs Gas Sensing

For the NTFETs and chemiresistors, the basic principle is the modulation of conductivity of devices by absorbing gas molecules. For pristine semiconducting CNTs based FETs or chemiresistors, two elemental mechanism are in charge of sensors' response to the gas exposure. The first one is modulation of Schotkky Barrier (SB) that exist between semiconducting CNTs and metal electrodes. Taking p-type semiconducting CNTs based FET as an example. The Jablonski diagram of such device is schemed in Figure 2.2. As it has been discussed[36][37], the SB is sensitive to the workfunction of metal. When the sensor is exposed to analyte gases, such as NH_3, the work function of metal is reduced[38].

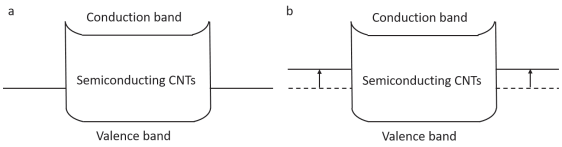


Figure 2.2: The band diagram of p-type NTFET (a) before and (b) after NH_3 exposure when gate-source voltage is zero at room temperature[38].

This mechanism has been described dominating the NTFET based NH_3 sensor[38]. While when the junctions of metal electrode and CNT are insulated from NH_3 molecules, the adsorption of NH_3 molecules in the middle of CNT has minim impact on the source-drain current.

The SB modulation mechanism has been reported and utilized in many CNT based gas sensors[39][37][40][41]. Other mechanisms have been also discussed for NTFET based gas sensors. Such as direct charge transfer induced by gas molecules adsorption[16], indirect interaction could lead to change in CNTs' electrical properties[13]. In many reports, the CNTs are usually decorated with metal nanoparticles/clusters, such as Pd[14], Al[42], Au[43]. Kauffman and Star have studied metal (Ag, Au, Pd and Pt) decorated SWCNT based FETs for NO detection[43]. By comparing different metal decorated NTFETs, they have found that the sensitivity of their devices depend on the workfunction of the decorated metal. NO exposure changes the potential barrier which is related to the workfunction of metal at the interface between metal nanoparticles and SWCNTs. While in another study by Khalap et al.[44], the defects in CNTs play an important role. When defects exist, the semiconducting and metallic SWCNTs are no different in the detection of H_2. The Pd-decorated defects make SWCNTs sensitive to H_2 at low pressures as a result of additional interaction between defect and atomic H generated by Pd nanoparticles. In either way, the metal nanoparticles facilitate the interaction between CNTs and gas molecules, thereby, the performance of pristine CNTs as gas sensor is improved by decorating the CNTs with metal nanoparticles.

For CNTs chemiresistor based gas sensor, the main gas sensing mechanism is charge transfer induced charge carrier density variation in CNTs. This effect causes conductance changes. Many mechanisms can cause charge transfer, such as physisorption of gas molecules, dipole-dipole interaction between gas molecules and CNTs. Another sensing mechanism is modulation of contact resistance (CR). CR exists in the connection of CNT-CNT and CNT-metal electrode. For the CNT-polymer composites, it can be changed by the swelling of polymer networks which is induced by absorption of gas molecules[45]. Since our sensors are in resistor configuration, we will discuss the mechanisms in Chapter 2 (Section 2.4) of Part II that can possibly explain our detection results.

The CNTs based capacitive gas sensors have also been developed for humidity sensing[30] chemical vapor and gas sensing[46][28][29][47]. For a conventional capacitor of two face-to-face plates configuration the capacitance is proportional to the area of plates. Thereby, by depositing CNTs onto the plate, one can increase the effective area as the network of

CNTs is mesoporous. However, the CNTs are sensitive to the ambient condition. When exposed to gases, the CNTs' electrical properties are changed *via* physisorption or chemical bonding. Therefore the dielectric constant, modified by the interaction with gas molecules, induces a measurable change of the capacitance of the device[30]. For a interdigital capacitor as described in Ref.[47], the SWCNTs are deposited onto electrodes and form a thin film which as a whole constructs one plate of capacitor with the substrate, SiO_2 in the reference, serving as the second plate. In this configuration, the capacitance consists two parts, one is so called gate capacitance which depends on the thickness of SWCNTs film and the SiO_2; the second is quantum capacitance which is determined by the Fermi level of SWCNTs. Thus, the adsorbates in SWCNTs networks affect both gate capacitance and quantum capacitance. Thereby, a net change of capacitance is observed when the device is exposed to gases or vapors.

2.3.2 State of the Art for Integrating CNTs

The first CNT based gas sensor was a FET that used an individual semiconducting single-walled carbon nanotube. Latterly, NTFET gas sensors were developed based on CNTs networks. Ever since, the NTFET and resistor configuration have been widely utilized for CNTs based gas sensor. As FET and resistor are the most utilized configuration for CNTs based gas sensor research, we will mainly review the state-of-the-art of CNTs based FET and resistor for gas sensing.

There are two types of CNTs FET and/or resistor based gas sensors: one type mainly use an individual semiconducting SWCNT for fabricating NTFET or diode; the second one rather use a film of CNTs in the devices. We will take the NTFET based gas sensor as an example to discuss the fabrication procedure. For an individual semiconducting SWCNT based FET (ISNTFET), the single CNT is either deposited onto substrate[48] or directly grows on the substrate[49][50][51][52].

For the deposition method, SWCNTs are first suspended in water with the help of surfactant or organic solvent. The suspension must be highly diluted in order to have very low concentration of individually separated CNTs. One out of many devices that have been deposited a drop of suspension may be found an individual SWCNT on selected areas. This method requires less procedures and has low complexity. However, it really takes lucky to successfully integrate an individual SWCNT. The order of fabricating electrodes and deposition of SWCNT can be exchanged. One can deposit an individual semiconducting SWCNT on substrate and fabricate metal electrodes later above the SWCNT or one SWCNT is directly deposited onto substrate to bridge the electrodes. The first approach ensures a better electrical contact between SWCNT and electrodes.

Because of the low efficiency of deposition method, the method of direct growing SWCNT on substrate is more popular for fabricating ISNTFET. In 1998, Kong[49] et al. reported the synthesis of individual CNT on silicon wafer. The catalyst islands are first loaded onto substrate by patterning PMMA film in which holes were fabricated by electron beam lithography. Once the PMMA film is removed, CNTs are synthesized *via* CCVD method. After the growth of CNTs, electrodes are fabricated on the substrate and are bridged by CNT(s). By controlling the condition of CCVD process, one can

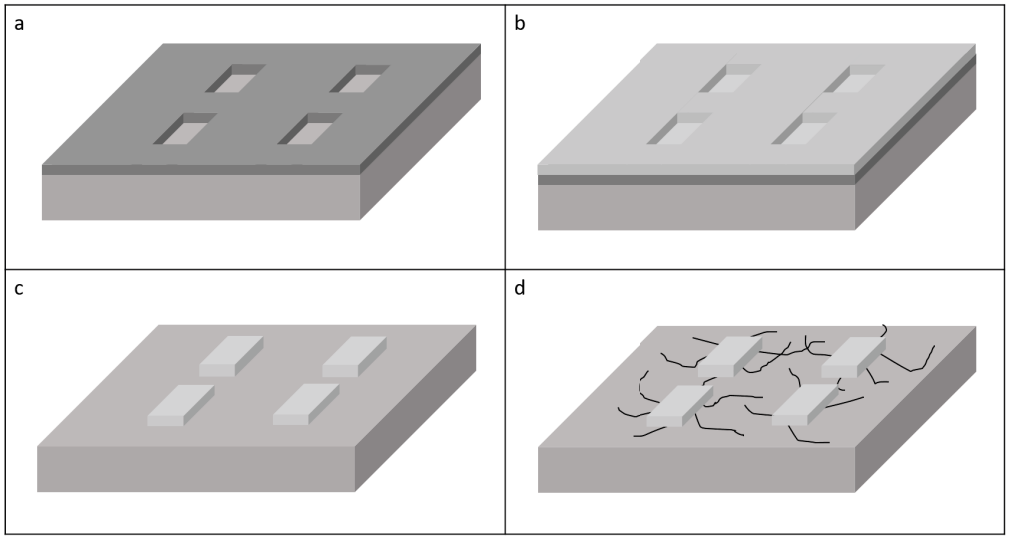


Figure 2.3: Scheme of direct growth of SWCNTs on substrate. a) Holes are fabricated in PMMA layer *via* electron beam lithography. b) Catalyst nanoparticles suspension is dropped onto PMMA layer. c) Catalyst islands are formed by removing PMMA *via* lift-off. d) SWCNTs are synthesized *via* CCVD method.

synthesize the SWCNTs on the substrate. This method is widely utilized due to the fact that it defines the CNTs on substrate with a much higher efficiency. The direct growing method is suitable for mass production despite it requires much more energy input. In fact, many SWCNTs can be found between two catalyst islands above which electrodes will be defined. Thereby, extra work is required to remove undesired nanotubes.

Whether the deposition method or direct growth method, both have their advantage and drawbacks. The deposition method is easy to conduct, costs much less energy. It is still being improved with new techniques. For example, by applying electrophoresis, the CNT can be firmly aligned and, thereby, connect the two electrodes which prevent defective products.

Besides, there is a fundamental concern in fabrication of ISNTFET based gas sensor that the sensitivity and selectivity of the device not only depends on the SB mechanism but also on the chirality of the semiconducting SWCNT. Recently, Jamal and co-workers[53] used first principle simulation to study the density of states (DOS) variation near Fermi level of individual SWCNT based gas sensors upon different vapor exposures. They studied two types of chirality for semiconducting SWCNTs ((7,0) and (8,0)) and one type of chirality for metallic SWCNTs ((9,0)) based FETs. The simulation shows very interesting results. Between two types of semiconducting SWCNTs, there are clear differences in the change of DOS upon each chemical vapor exposure. The (8,0) semiconducting SWCNTs based FET shows highest change in DOS near Fermi level. A distinct selectivity to NO_2 can be found in their results compared to other two types of SWCNTs. Thus, for design ISNTFET based gas sensors, one must also takes account of

their precise chirality. Otherwise the sensitivity and selectivity of ISNTFETs disparate from one to another with same gas detection condition.

Though synthesis of SWCNTs of random and narrow chirality distribution has been reported[54][55][56][57][58], it remains a challenge to control the synthesis of SWCNTs of specified/selective chirality. An alternative approach is chirality dependent separation of SWCNTs[59]. Despite low time efficiency, this method[59] can gradually obtain each type of SWCNTs. It is depending on the strength of interaction between SWCNTs and gel which is chirality dependent. But this method is only suitable for fabricating ISNTFETs *via* deposition method of which the low efficiency is a great concern.

Therefore, the ISNTFET based gas sensors are theoretically highly selective and sensitive to different gases based on the SB mechanism and CNTs chirality. However, it is generally of low efficiency and consumes high power in some cases. Besides, recent research reveals that the factor of SWCNTs' chirality hinders the generalization of result from each ISNTFET based gas sensor research that omits chiral factor.

Due to the difficulties in fabrication of ISNTFET, many researches of NTFET based gas sensor turn to use the CNTs networks rather than an individual semiconducting SWCNT. It is very easy to integrate a thin film of CNTs onto substrate simply by dropping CNTs suspension on the substrate or spin coating for large area deposition. The chance is much higher to successfully fabricate a CNTs networks based sensor than an individual CNT based sensor. It has been used for variety of sensors, such as NO_2[60][61][62], NH_3[31][21][63], humidity[64][65][66] and organic compound vapor detection[67][68].

The CNTs networks not only increases the number of CNTs but also the number of junctions that are formed between nanotubes. The existence of junctions is argued as the reason of sensitivity increase along with the increase of density of the networks[69](a ratio that is proportional to the number of junctions and inversely proportional to the number of CNTs that connect both electrodes). From the work of Boyd et al., one can find that the increase in density of the CNTs networks increases the sensitivity of the sensors and weaken the SB mechanism. The sensors of high density of CNTs networks remain sensitive while single CNT sensor's sensitivity reduced dramatically when the contacts between CNT(s) and metal electrodes are covered, because SB mechanism is responsible for sensitivity of individual CNT based gas sensor. The high sensitivity of the sensors based on CNTs networks is at the cost of certain degree of loss of selectivity. However, to increase the CNTs film based sensors' selectivity, functionalized CNTs have been developed, such as, with polymer composite[45], chemical functional groups[70], and metal nanoparticles[71].

Thereby, in terms of cost, simplicity of procedure, power saving, we consider the integration of CNTs based networks as a superior choice compared to that of individual semiconducting SWCNTs. There are many options of CNTs networks, such as aligned CNTs film, vertically aligned CNTs forest and random oriented CNTs networks. Because our objective in this work is to develop a very simple fabrication method, we have not selected vertically aligned networks because their electrical connection requires several additional levels of lithography steps. Furthermore, as there is not really consisting

arguments to claim that aligned CNTs based gas sensor exhibit better performance than disordered CNTs networks, we have investigated in our work, randomly oriented CNTs networks.

There are many ways to integrate random oriented CNTs film, such as spray-coating, which can achieve homogeneous deposition of CNTs films. However, in wafer-based micro/nano electronics, integration of CNTs is requested only on small selected area. Most area of the substrate are for the electrodes or wires. When spray-coating is used, the substrate is covered by a stencil or mask which leave the selected area exposed to the spray. Thus, it is at the expense of great amount of CNTs to integrate CNTs by spray-coating, and the wasted CNTs are difficult to recycle.

2.4 Objectives of this Research

Taking into account the various constraints and issues pointed out in the previous description of the state of the art, we have made a set of choices at the starting of this research work that we are summarizing now.

The ambition were the following:

- Produce at a lab scale, CNTs based gas sensors, with a low cost and easy to implement method, potentially scalable at an industrial level and compatible with many substrate including flexible ones.

- Elaborate gas sensors working at room temperature and under ambient air, requiring to find conditions for which temperature fluctuations and humidity are not a concern.

The main technical orientation of the work presented in this thesis report have emerged at the end of my first year of research, after the investigation of alternative routes that will not be mentioned for a better concision. Our gas sensors will integrate DWCNTs synthesized by CCVD. After purification and chemical functionalization, they will form a disordered network bridging two metal electrodes, by using a simple and low cost integration process based on liquid-stencil lithography. This set of parameters enables us to match closely to the pre-cited ambition of this work. My work was thus dedicated to the optimization of the fabrication process and the gas sensing characterization of the devices in order to prove their robustness in temperature and under water vapor, their easy fabrication with good reproducibility, their low consumption and adaptation to real-life sensing conditions.

Bibliography

[1] G. Korotcenkov, "Handbook of gas sensor materials," vol. 1.

[2] S. Lakkis, R. Younes, Y. Alayli, and M. Sawan, "Review of recent trends in gas sensing technologies and their miniaturization potential," *Sensor Review*, vol. 34, no. 1, pp. 24–35, 2014.

[3] J. Janata and M. Josowicz, "Conducting polymers in electronic chemical sensors," *Nature materials*, vol. 2, no. 1, p. 19, 2003.

[4] K. Liu, Y. Li, L. Hong, and M. Yang, "Humidity sensitive properties of an anionic conjugated polyelectrolyte," *Sensors and Actuators B: Chemical*, vol. 129, no. 1, pp. 24–29, 2008.

[5] S. Christie, E. Scorsone, K. Persaud, and F. Kvasnik, "Remote detection of gaseous ammonia using the near infrared transmission properties of polyaniline," *Sensors and Actuators B: Chemical*, vol. 90, no. 1, pp. 163–169, 2003.

[6] M. G. Buehler and M. A. Ryan, "Temperature and humidity dependence of a polymer-based gas sensor," *Proc. Electro-Optical Technology Remote Chemical Detection Identification II*, pp. 40–48, 1997.

[7] R. Pitts, P. Liu, S. Lee, E. Tracy, R. Smith, and C. Salter, "Interfacial stability of thin film hydrogen sensors," in *Proceedings of the DOE Hydrogen Program Review*, 2001.

[8] D. Baselt, B. Fruhberger, E. Klaassen, S. Cemalovic, C. Britton, S. Patel, T. Mlsna, D. McCorkle, and B. Warmack, "Design and performance of a microcantilever-based hydrogen sensor," *Sensors and Actuators B: Chemical*, vol. 88, no. 2, pp. 120–131, 2003.

[9] P. Fedtke, M. Wienecke, M.-C. Bunescu, M. Pietrzak, K. Deistung, and E. Borchardt, "Hydrogen sensor based on optical and electrical switching," *Sensors and Actuators B: Chemical*, vol. 100, no. 1, pp. 151–157, 2004.

[10] K. Skucha, Z. Fan, K. Jeon, A. Javey, and B. Boser, "Palladium/silicon nanowire schottky barrier-based hydrogen sensors," *Sensors and Actuators B: Chemical*, vol. 145, no. 1, pp. 232–238, 2010.

[11] G. Alberti and M. Casciola, "Solid state protonic conductors, present main applications and future prospects," *Solid State Ionics*, vol. 145, no. 1, pp. 3–16, 2001.

[12] M. Paradise and T. Goswami, "Carbon nanotubes–production and industrial applications," *Materials & Design*, vol. 28, no. 5, pp. 1477–1489, 2007.

[13] J. Kong, N. R. Franklin, C. Zhou, M. G. Chapline, S. Peng, K. Cho, and H. Dai, "Nanotube molecular wires as chemical sensors," *science*, vol. 287, no. 5453, pp. 622–625, 2000.

[14] J. Kong, M. G. Chapline, H. Dai, *et al.*, "Functionalized carbon nanotubes for molecular hydrogen sensors," *Advanced Materials*, vol. 13, no. 18, p. 1384, 2001.

[15] K. Bradley, J.-C. P. Gabriel, A. Star, and G. Grüner, "Short-channel effects in contact-passivated nanotube chemical sensors," *Applied Physics Letters*, vol. 83, no. 18, pp. 3821–3823, 2003.

[16] T. Someya, J. Small, P. Kim, C. Nuckolls, and J. T. Yardley, "Alcohol vapor sensors based on single-walled carbon nanotube field effect transistors," *Nano letters*, vol. 3, no. 7, pp. 877–881, 2003.

[17] J. Zhang, A. Boyd, A. Tselev, M. Paranjape, and P. Barbara, "Mechanism of no 2 detection in carbon nanotube field effect transistor chemical sensors," *Applied Physics Letters*, vol. 88, no. 12, p. 123112, 2006.

[18] W.-D. Zhang and W.-H. Zhang, "Carbon nanotubes as active components for gas sensors," *Journal of Sensors*, vol. 2009, 2009.

[19] T. Sarkar, S. Srinives, S. Sarkar, R. C. Haddon, and A. Mulchandani, "Single-walled carbon nanotube–poly (porphyrin) hybrid for volatile organic compounds detection," *The Journal of Physical Chemistry C*, vol. 118, no. 3, pp. 1602–1610, 2014.

[20] S. Badhulika, N. V. Myung, and A. Mulchandani, "Conducting polymer coated single-walled carbon nanotube gas sensors for the detection of volatile organic compounds," *Talanta*, vol. 123, pp. 109–114, 2014.

[21] S. Wang, Q. Zhang, D. Yang, P. Sellin, and G. Zhong, "Multi-walled carbon nanotube-based gas sensors for nh 3 detection," *Diamond and Related Materials*, vol. 13, no. 4, pp. 1327–1332, 2004.

[22] L. Niu, Y. Luo, and Z. Li, "A highly selective chemical gas sensor based on functionalization of multi-walled carbon nanotubes with poly (ethylene glycol)," *Sensors and Actuators B: Chemical*, vol. 126, no. 2, pp. 361–367, 2007.

[23] A. Kaniyoor, R. I. Jafri, T. Arockiadoss, and S. Ramaprabhu, "Nanostructured pt decorated graphene and multi walled carbon nanotube based room temperature hydrogen gas sensor," *Nanoscale*, vol. 1, no. 3, pp. 382–386, 2009.

[24] F. Rigoni, G. Drera, S. Pagliara, A. Goldoni, and L. Sangaletti, "High sensitivity, moisture selective, ammonia gas sensors based on single-walled carbon nanotubes functionalized with indium tin oxide nanoparticles," *Carbon*, vol. 80, pp. 356–363, 2014.

[25] D. Jung, M. Han, and G. S. Lee, "Gas sensor using a multi-walled carbon nanotube sheet to detect hydrogen molecules," *Sensors and Actuators A: Physical*, vol. 211, pp. 51–54, 2014.

[26] A. Abdelhalim, M. Winkler, F. Loghin, C. Zeiser, P. Lugli, and A. Abdellah, "Highly sensitive and selective carbon nanotube-based gas sensor arrays functionalized with different metallic nanoparticles," *Sensors and Actuators B: Chemical*, vol. 220, pp. 1288–1296, 2015.

[27] S. F. Liu, A. R. Petty, G. T. Sazama, and T. M. Swager, "Single-walled carbon nanotube/metalloporphyrin composites for the chemiresistive detection of amines and meat spoilage," *Angewandte Chemie International Edition*, vol. 54, no. 22, pp. 6554–6557, 2015.

[28] K. G. Ong, K. Zeng, and C. A. Grimes, "A wireless, passive carbon nanotube-based gas sensor," *IEEE Sensors Journal*, vol. 2, no. 2, pp. 82–88, 2002.

[29] E. Snow, F. Perkins, E. Houser, S. Badescu, and T. Reinecke, "Chemical detection with a single-walled carbon nanotube capacitor," *Science*, vol. 307, no. 5717, pp. 1942–1945, 2005.

[30] J. Yeow and J. She, "Carbon nanotube-enhanced capillary condensation for a capacitive humidity sensor," *Nanotechnology*, vol. 17, no. 21, p. 5441, 2006.

[31] S. Chopra, A. Pham, J. Gaillard, A. Parker, and A. Rao, "Carbon-nanotube-based resonant-circuit sensor for ammonia," *Applied Physics Letters*, vol. 80, no. 24, pp. 4632–4634, 2002.

[32] S. Chopra, K. McGuire, N. Gothard, A. Rao, and A. Pham, "Selective gas detection using a carbon nanotube sensor," *Applied Physics Letters*, vol. 83, no. 11, pp. 2280–2282, 2003.

[33] F. Picaud, R. Langlet, M. Arab, M. Devel, C. Girardet, S. Natarajan, S. Chopra, and A. Rao, "Gas-induced variation in the dielectric properties of carbon nanotube bundles for selective sensing," *Journal of applied physics*, vol. 97, no. 11, p. 114316, 2005.

[34] A. Zribi, A. Knobloch, and R. Rao, "Co 2 detection using carbon nanotube networks and micromachined resonant transducers," *Applied Physics Letters*, vol. 86, no. 20, p. 203112, 2005.

[35] M. McGrath and A. Pham, "Carbon nanotube based microwave resonator gas sensors," *International journal of high speed electronics and systems*, vol. 16, no. 04, pp. 913–935, 2006.

[36] Z. Chen, J. Appenzeller, J. Knoch, Y.-m. Lin, and P. Avouris, "The role of metal-nanotube contact in the performance of carbon nanotube field-effect transistors," *Nano letters*, vol. 5, no. 7, pp. 1497–1502, 2005.

[37] J. Suehiro, H. Imakiire, S.-i. Hidaka, W. Ding, G. Zhou, K. Imasaka, and M. Hara, "Schottky-type response of carbon nanotube no 2 gas sensor fabricated onto aluminum electrodes by dielectrophoresis," *Sensors and Actuators B: Chemical*, vol. 114, no. 2, pp. 943–949, 2006.

[38] N. Peng, Q. Zhang, C. L. Chow, O. K. Tan, and N. Marzari, "Sensing mechanisms for carbon nanotube based nh3 gas detection," *Nano letters*, vol. 9, no. 4, pp. 1626–1630, 2009.

[39] Y. Wong, W. Kang, J. Davidson, A. Wisitsora-At, and K. Soh, "A novel microelectronic gas sensor utilizing carbon nanotubes for hydrogen gas detection," *Sensors and actuators B: chemical*, vol. 93, no. 1, pp. 327–332, 2003.

[40] T. Yamada, "Equivalent circuit model for carbon nanotube schottky barrier: Influence of neutral polarized gas molecules," *Applied physics letters*, vol. 88, no. 8, p. 083106, 2006.

[41] T.-C. Lin and B.-R. Huang, "Palladium nanoparticles modified carbon nanotube/nickel composite rods (pd/cnt/ni) for hydrogen sensing," *Sensors and Actuators B: Chemical*, vol. 162, no. 1, pp. 108–113, 2012.

[42] R. Wang, D. Zhang, W. Sun, Z. Han, and C. Liu, "A novel aluminum-doped carbon nanotubes sensor for carbon monoxide," *Journal of Molecular Structure: THEOCHEM*, vol. 806, no. 1, pp. 93–97, 2007.

[43] D. R. Kauffman and A. Star, "Chemically induced potential barriers at the carbon nanotube- metal nanoparticle interface," *Nano letters*, vol. 7, no. 7, pp. 1863–1868, 2007.

[44] V. R. Khalap, T. Sheps, A. A. Kane, and P. G. Collins, "Hydrogen sensing and sensitivity of palladium-decorated single-walled carbon nanotubes with defects," *Nano letters*, vol. 10, no. 3, pp. 896–901, 2010.

[45] B. Philip, J. K. Abraham, A. Chandrasekhar, and V. K. Varadan, "Carbon nanotube/pmma composite thin films for gas-sensing applications," *Smart materials and structures*, vol. 12, no. 6, p. 935, 2003.

[46] K. G. Ong and C. A. Grimes, "A carbon nanotube-based sensor for co2 monitoring," *Sensors*, vol. 1, no. 6, pp. 193–205, 2001.

[47] E. S. Snow and F. K. Perkins, "Capacitance and conductance of single-walled carbon nanotubes in the presence of chemical vapors," *Nano Letters*, vol. 5, no. 12, pp. 2414–2417, 2005.

[48] X. Guo, L. Huang, S. O'Brien, P. Kim, and C. Nuckolls, "Directing and sensing changes in molecular conformation on individual carbon nanotube field effect transistors," *Journal of the American Chemical Society*, vol. 127, no. 43, pp. 15045–15047, 2005.

[49] J. Kong, H. T. Soh, A. M. Cassell, C. F. Quate, and H. Dai, "Synthesis of individual single-walled carbon nanotubes on patterned silicon wafers," *Nature*, vol. 395, no. 6705, p. 878, 1998.

[50] J. Kong, C. Zhou, A. Morpurgo, H. Soh, C. Quate, C. Marcus, and H. Dai, "Synthesis, integration, and electrical properties of individual single-walled carbon nanotubes," *Applied Physics A: Materials Science & Processing*, vol. 69, no. 3, pp. 305–308, 1999.

[51] H. T. Soh, C. F. Quate, A. F. Morpurgo, C. M. Marcus, J. Kong, and H. Dai, "Integrated nanotube circuits: Controlled growth and ohmic contacting of single-walled carbon nanotubes," *Applied Physics Letters*, vol. 75, no. 5, pp. 627–629, 1999.

[52] T. Someya, P. Kim, and C. Nuckolls, "Conductance measurement of single-walled carbon nanotubes in aqueous environment," *Applied physics letters*, vol. 82, no. 14, pp. 2338–2340, 2003.

[53] G. A. Jamal, M. R. Islam, M. A. Rahman, J. F. Meem, and R. A. Sathi, "Chirality dependence of single wall carbon nanotube based gas sensor," in *Region 10 Conference (TENCON), 2016 IEEE*, pp. 2771–2774, IEEE, 2016.

[54] S. Reich, L. Li, and J. Robertson, "Control the chirality of carbon nanotubes by epitaxial growth," *Chemical physics letters*, vol. 421, no. 4, pp. 469–472, 2006.

[55] X. Li, X. Tu, S. Zaric, K. Welsher, W. S. Seo, W. Zhao, and H. Dai, "Selective synthesis combined with chemical separation of single-walled carbon nanotubes for chirality selection," *Journal of the American Chemical Society*, vol. 129, no. 51, pp. 15770–15771, 2007.

[56] M. Fouquet, B. C. Bayer, S. Esconjauregui, R. Blume, J. Warner, S. Hofmann, R. Schlögl, C. Thomsen, and J. Robertson, "Highly chiral-selective growth of single-walled carbon nanotubes with a simple monometallic co catalyst," *Physical Review B*, vol. 85, no. 23, p. 235411, 2012.

[57] M. He, H. Jiang, B. Liu, P. V. Fedotov, A. I. Chernov, E. D. Obraztsova, F. Cavalca, J. B. Wagner, T. W. Hansen, I. V. Anoshkin, *et al.*, "Chiral-selective growth of single-walled carbon nanotubes on lattice-mismatched epitaxial cobalt nanoparticles," *Scientific reports*, vol. 3, p. 1460, 2013.

[58] F. Yang, X. Wang, D. Zhang, J. Yang, D. Luo, Z. Xu, J. Wei, J.-Q. Wang, Z. Xu, F. Peng, *et al.*, "Chirality-specific growth of single-walled carbon nanotubes on solid alloy catalysts," *Nature*, vol. 510, no. 7506, p. 522, 2014.

[59] H. Liu, D. Nishide, T. Tanaka, and H. Kataura, "Large-scale single-chirality separation of single-wall carbon nanotubes by simple gel chromatography," *Nature communications*, vol. 2, p. 309, 2011.

[60] L. Valentini, I. Armentano, J. Kenny, C. Cantalini, L. Lozzi, and S. Santucci, "Sensors for sub-ppm no 2 gas detection based on carbon nanotube thin films," *Applied Physics Letters*, vol. 82, no. 6, pp. 961–963, 2003.

[61] C. Cantalini, L. Valentini, L. Lozzi, I. Armentano, J. Kenny, and S. Santucci, "No 2 gas sensitivity of carbon nanotubes obtained by plasma enhanced chemical vapor deposition," *Sensors and Actuators B: Chemical*, vol. 93, no. 1, pp. 333–337, 2003.

[62] H. Y. Jeong, D.-S. Lee, H. K. Choi, D. H. Lee, J.-E. Kim, J. Y. Lee, W. J. Lee, S. O. Kim, and S.-Y. Choi, "Flexible room-temperature no 2 gas sensors based on carbon nanotubes/reduced graphene hybrid films," *Applied physics letters*, vol. 96, no. 21, p. 213105, 2010.

[63] E. Bekyarova, M. Davis, T. Burch, M. Itkis, B. Zhao, S. Sunshine, and R. Haddon, "Chemically functionalized single-walled carbon nanotubes as ammonia sensors," *The Journal of Physical Chemistry B*, vol. 108, no. 51, pp. 19717–19720, 2004.

[64] P.-G. Su, Y.-L. Sun, and C.-C. Lin, "A low humidity sensor made of quartz crystal microbalance coated with multi-walled carbon nanotubes/nafion composite material films," *Sensors and Actuators B: Chemical*, vol. 115, no. 1, pp. 338–343, 2006.

[65] K.-P. Yoo, L.-T. Lim, N.-K. Min, M. J. Lee, C. J. Lee, and C.-W. Park, "Novel resistive-type humidity sensor based on multiwall carbon nanotube/polyimide composite films," *Sensors and Actuators B: Chemical*, vol. 145, no. 1, pp. 120–125, 2010.

[66] J.-W. Han, B. Kim, J. Li, and M. Meyyappan, "Carbon nanotube based humidity sensor on cellulose paper," *The Journal of Physical Chemistry C*, vol. 116, no. 41, pp. 22094–22097, 2012.

[67] L. Valentini, C. Cantalini, I. Armentano, J. Kenny, L. Lozzi, and S. Santucci, "Highly sensitive and selective sensors based on carbon nanotubes thin films for molecular detection," *Diamond and Related Materials*, vol. 13, no. 4, pp. 1301–1305, 2004.

[68] K. Parikh, K. Cattanach, R. Rao, D.-S. Suh, A. Wu, and S. K. Manohar, "Flexible vapour sensors using single walled carbon nanotubes," *Sensors and Actuators B: Chemical*, vol. 113, no. 1, pp. 55–63, 2006.

[69] A. Boyd, I. Dube, G. Fedorov, M. Paranjape, and P. Barbara, "Gas sensing mechanism of carbon nanotubes: from single tubes to high-density networks," *Carbon*, vol. 69, pp. 417–423, 2014.

[70] P. Slobodian, P. Riha, A. Lengálová, P. Svoboda, and P. Sáha, "Multi-wall carbon nanotube networks as potential resistive gas sensors for organic vapor detection," *Carbon*, vol. 49, no. 7, pp. 2499–2507, 2011.

[71] B.-Y. Wei, M.-C. Hsu, P.-G. Su, H.-M. Lin, R.-J. Wu, and H.-J. Lai, "A novel sno 2 gas sensor doped with carbon nanotubes operating at room temperature," *Sensors and Actuators B: Chemical*, vol. 101, no. 1, pp. 81–89, 2004.

Partie II : Experiments

Chapter 1

Synthesis and Functionalization of Double wall Carbon Nanotubes and Fabrication of DWCNTs Gas Sensor

This chapter presents the techniques that are utilized in this thesis for synthesizing double-walled carbon nanotubes (DWCNTs), further functionalization, and for the fabrication of double-walled carbon nanotubes gas sensors. Sections 1 and 2 introduce CNTs synthesis and functionalization approaches; section 3 presents the CNTs integration approaches for sensor fabrication and Section 1.4 describes characterization of the fabricated sensors.

1.1 Double-walled Carbon Nanotubes Synthesis

1.1.1 DWCNTs synthesis *via* CCVD

In previous work of our group[1], when solid solution of cobalt oxide in magnesium oxide were used as catalysts, DWCNTs were observed with a large proportion. With further research and modifications, DWCNTs can then be produced in gram scale with very high proportion ca. 80% of the reaction products[2].

In DWCNTs synthesis process, the catalyst was prepared by combustion process[3] except that $(NH_4)_6Mo_7O_24 \bullet 4H_2O$ of required quantity was first mixed with a solution of magnesium and cobalt nitrates, and equivalent amount of citric acid was used as fuel instead of urea. A powder of $Mg_{1-x}Co_xO$ and MoO_y mixture was prepared as catalyst for DWCNTs synthesis. 6 g of catalyst powder were then placed in furnace and heated to 1000 $°C$ under a flow of H_2 and CH_4 mixture (18%mol CH_4, 250 $sccm$). The decomposition of CH_4 happened during this procedure. After the temperature reached 1000 $°C$, the furnace was cooled down under H_2 and CH_4 flow to the room

temperature. The heating and cooling rates are 5 $°C/min$. By this approach, the obtained powder consists of carbon nanotubes and MgO, Co and Mo carbides. Further treatment in HCl was carried out to extract carbon nanotubes by removal of unreacted catalytic material and unprotected catalytic nanoparticles. HRTEM characterization utilized later revealed that the products comprises 80% of DWCNTs. Figure 1.1 depicts the DWCNTs synthesis process. Figure 1.2[2] shows the HRTEM image of DWCNTs and the quality of DWCNTs in terms of proportion of DWCNTs, diameter of inner (d_i) and outside (d_o)walls of DWCNTs.

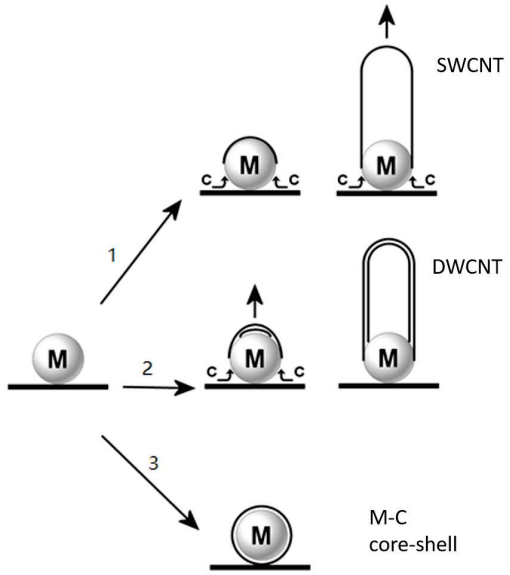


Figure 1.1: DWCNTs synthesis *via* CCVD method under metal nanoparticles (M). The process described in the text mainly produces DWCNTs according to the process depicted in rout 2.

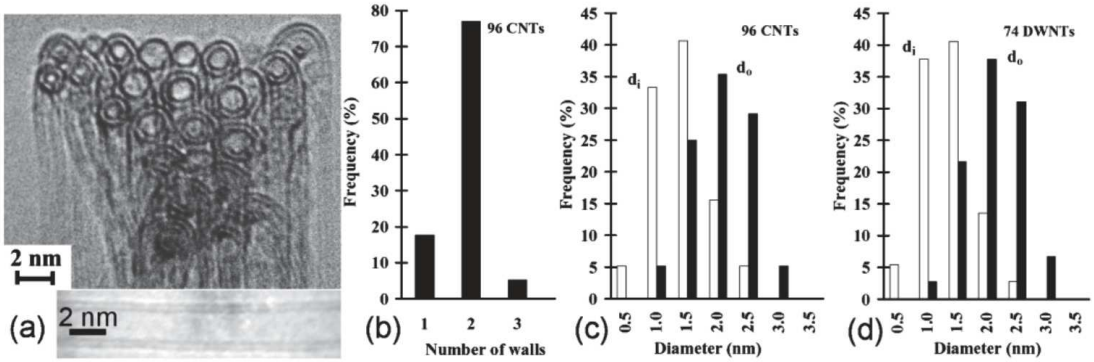


Figure 1.2: (a) HRTEM image of DWCNTs and (b) distribution of the numbers of walls for the whole population (established from 96 individual CNTs). Distribution of inner (d_i) and outer (d_o) diameter for the whole population of (c) CNTs and for (d) DWCNTs only.

1.1.2 DWCNTs Extraction and Purification

The DWCNTs composite powders synthesized by CCVD are CNTs mixed with partially transformed catalyst. To purify DWCNTs, the composite powder is treated with acid (HCl). The extraction procedure is described as follow.

DWCNTs composite powder is first weighed, 5 g for instance, and placed in an erlenmeyer flask. 20 g of deionized water is added into erlenmeyer.

75 mL of concentrated hydrochloric acid (HCl, concentration 37%)are then added dropwise to the DWCNTs composites with Pasteur pipette. Meanwhile, erlenmeyer flask is put in a crystallizing dish with water inside to dissipate heat from ionization of HCl.

The DWCNTs suspension is then magnetically stirred overnight before filtration. On the next day, the solution is filtered with 0.45 μm Cellulose nitrate filter and washed with deionized water until neutrality. A humid 'paste' of DWCNTs is collected for further processing.

At the end of this process, the population of DWCNTs that will be available for the next of the work is composed by nanotubes of different length, generally assembled in small bundles. According to electron microscopy inspection, we estimate the length of DWCNTs to be around 10 μm.

1.2 Double-walled Carbon Nanotubes Functionalization

1.2.1 Non-covalent Functionalization: Carboxymethyl Cellulose Surfactant Assisted-DWCNTs Suspension

Like other types of CNTs, raw DWCNTs are hard to be dispersed in deionized (DI) water. To suspend DWCNTs in DI water, sodium carboxymethyl cellulose (CMC) surfactant is used as dispersing agent. DWCNTs suspension is prepared by mixing DWCNTs with CMC in DI water (DWCNTs : CMC : $H_2O = 1 : 10 : 1000$). DWCNTs are agglomerated in CMC solution at first. The suspension is submitted to probe ultra-sonication (30 min) to separate individual nanotube. DWCNTs are then highly dispersed in form of individual nanotubes. To eliminate DWCNTs that are not separated by surfactant and ultra-sonication, the suspension is then subjected to high speed centrifugation (16000 rpm, 10 min). The undebundled DWCNTs are then sedimented at the bottom. The supernatant, contains well dispersed DWCNTs, it is collected as DWCNTs suspension for further deposition.

1.2.2 Covalent Functionalization

Oxidation of DWCNTs

The oxidation of DWCNTs procedure starts with extraction of DWCNTs composites as describe in the Section 1.1.2, because it limits agglomeration of CNTs by using freshly prepared wet samples. To have, for example, 10 mg oxidized DWCNTs, 98 mg of composite powder are needed.

Following the purification process, once filtrate becomes neutral, the humid DWCNTs material is transferred into a round bottom flask with a magnetic stirring bar into which 12.7 mL of 3 **M** nitric acid are added. The flask is then stirred at 750 rpm and maintained at 130 $°C$ in reflux conditions for 24 h.

24 h later, the mixture of nitric acid and oxidized DWCNTs is filtered with DI water by using 0.45 μm polypropylene filtration membrane.

When the filtrate is neutral, oxidized DWCNTs are then dispersed in DI water with a mass of 10 g in total. The dispersion is then submitted to probe sonication and centrifugation afterward. Oxidized DWCNTs suspension is obtained from the collected supernatant.

Amination of DWCNTs

Activation of Carboxylic Functions In order to make possible an amination reaction (Fig. 1.3), two functional groups are required: a carboxylic group and an amine group. The carboxylic group in our situation originates from oxidized DWCNTs (O-DWCNTs) as previously described while the amine group is brought into O-DWCNTs by coupling reaction with selected chemical coupler.

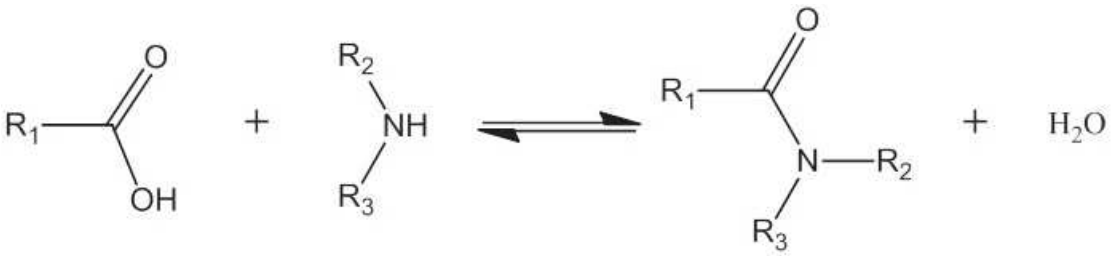


Figure 1.3: Scheme of amination reaction

As the coupling reaction is an equilibrium reaction, it is rather displaced in the direction of the formation of the carboxylic function or the amine function (Fig. 1.3). For the purpose of substitution with amine group, the carboxylic group is "activated" precedingly and thus converted to acyl chloride group (-CO-Cl) which is a more reactive moiety. The DWCNTs-COOH were activated by an acyl chloride compound, in our case oxalyl chloride is selected, according to the mechanism depicted in Fig. 1.4.

Fixation of a diamine: 1,4-diaminobutane When all the oxalyl chloride has been removed, the activated DWCNTs are dispersed in THF by an ultrasonic treatment (ultrasonic bath, 10 min). The attachment of the diamine to the DWCNTs-COCl uses the nucleophilic substitution grafting mechanism and leads to the creation of an amide bond between the activated nanotubes and the diamine as described in Figure 1.5

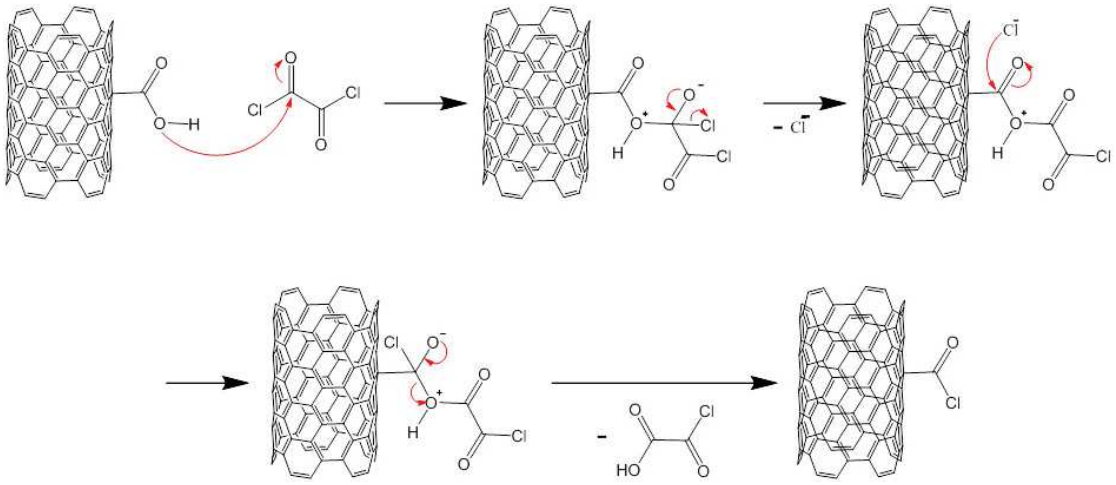


Figure 1.4: Mechanism of activation of the carboxylic function by oxalyl chloride.

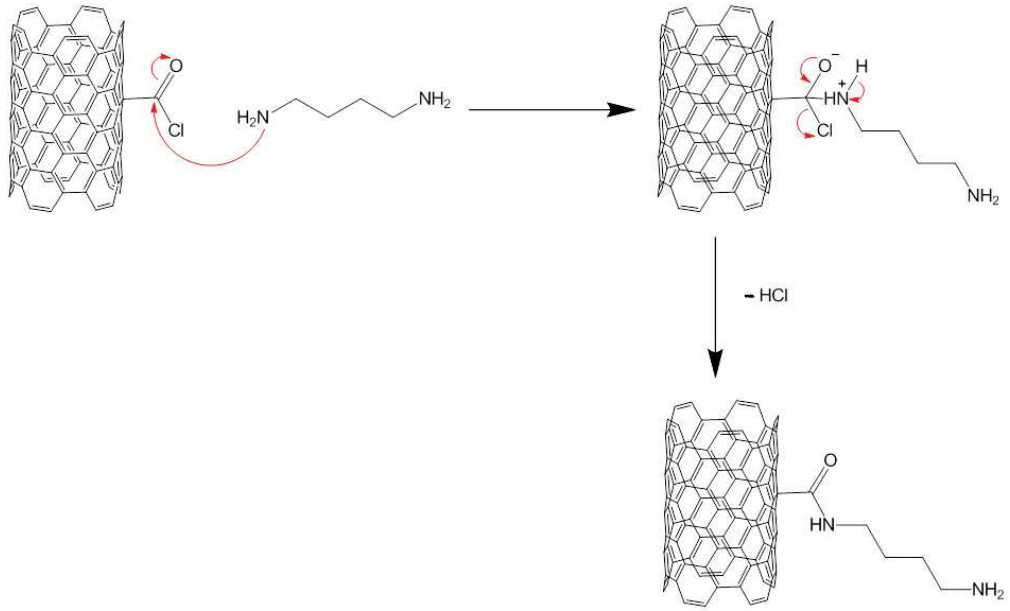


Figure 1.5: Mechanism of the grafting of 1,4-diaminobutane by forming an amide bond.

A typical procedure of amination of DWCNTs is as follow: 100 *mg* of oxalyl chloride activated DWCNTs are dispersed in 100 *ml* of THF into which 22.7 *mmol* of 1,4-diaminobutane and 22.7 *mmol* of N, N-diisopropylethylamine (DIEA) are added. The DIEA is a rather strong base (pKa = 10,1) and weakly nucleophilic, commonly used in organic chemistry. Its use makes it possible to both increase the pH of the medium in order to promote the -NH_2, the form of the primary amine functional group (and not the form -NH_3^+ which is not favorable to nucleophilic substitution), and to trap hydrochloric

acid formed during the reaction (Figure 1.6).

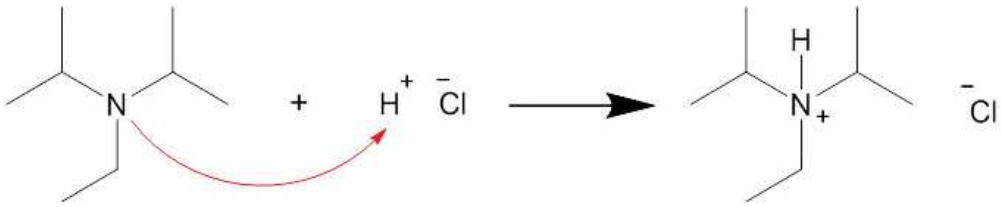


Figure 1.6: Role of N, N-diisopropylethylamine: trapping the hydrochloric acid released during the reaction.

The mixture is sonicated for 10 minutes in an ultrasonic bath and then magnetically stirred at 30 $°C$ for 96 h. It is important to work with an excess of amine in order first to be sure to be able to functionalize all the acyl groups present on the DWCNTs and, secondly, to avoid the risk of bridging by fixing the diamine on two close carboxylic groups, on the same DWNT or between two DWCNTs.

Furthermore, by using organic solvent, such as THF instead of the reagent that constitutes 1,4-diaminobutane, it makes it possible, on one hand, to gain better homogenization and stir of the reaction medium, and on the other hand, to run the experiment nearly at room temperature. We preferred to use THF rather than DMF (general selection) in order to avoid the introduction of nitrogen other than that present in the diamine, and thus to be able to hope to carry out a quantification of grafting by elemental analysis and XPS. After stirring for 96 h, the mixture is filtered through a polypropylene membrane, thus removing THF, resulting in a portion of the unreacted diamine. The amino DWCNTs are thus obtained. It is then washed with THF and filtered 10 times, in order to remove any trace of residual diamine. Finally, the aminated DWCNTs are dispersed in H_2O for further use by the same means to suspend DWCNTs while utilizing Sodium dodecyl sulfate (SDS) instead of CMC as surfactant.

Fluorination of DWCNTs

The fluorinated DWCNTs are received from *Nikolaev Institute of Inorganic Chemistry SB RAS, Russia*. The details of the process are preserved. But the general protocol of fluorination is as follow[4]: Purified DWCNTs are first placed in a Teflon flask which is kept in a vapor over a solution of BrF_3 in Br_2. 7 days later, the sample is dried by nitrogen flow which is replaced by Br_2 in the end.

1.3 Sensor Fabrication

The DWCNTs gas sensors are fabricated in resistor configuration. Figure 1.7 illustrates the scheme of the sensor. In one sensor, DWCNTs film is integrated between source and drain electrodes made from Gold/Titanium.

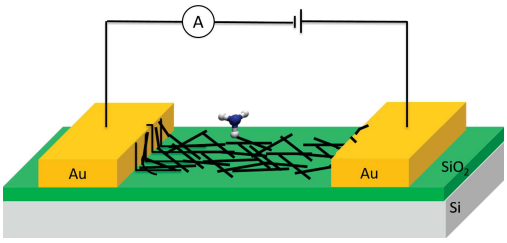


Figure 1.7: DWCNTs gas sensor schematic.

The DWCNTs gas sensors are fabricated based on stencil lithography technique. By stencil patterning, DWCNTs films are integrated onto SiO_2/Si substrates on which an array of gold electrodes are pre-defined.

A wafer scale of chips is fabricated by standard photolithography, lift-off and metal evaporation technique. Gold/Titanium are used for creating electrodes by metalization. A plan view of substrate is shown in Figure 1.8. An DWCNTs film should be integrated only to bridge the gap between upside drain and downside source electrodes. There is no cross connection by DWCNTs film between adjacent electrodes pairs. To achieve localized integration, a stencil with cavities of size that is restricted to match with electrode is utilized (Figure 1.8).

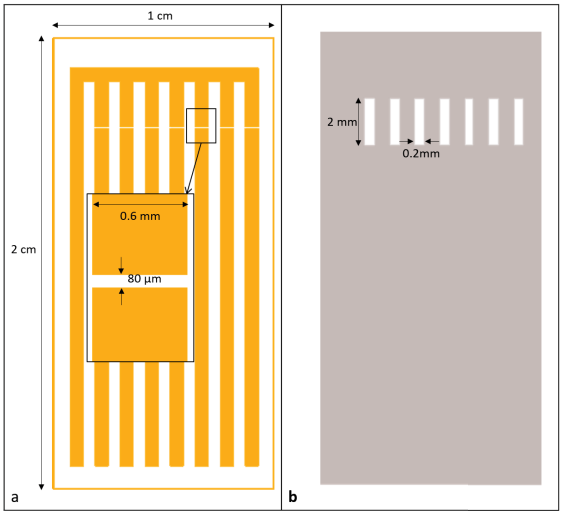


Figure 1.8: a) Schematic of top view of electrodes array. The DWCNTs films are integrated to bridge the gap of each electrode pair. b) Scheme of stencil mask made from PDMS.

The substrate is pre-processed with air plasma, because the substrate surface is not enough hydrophilic which makes it difficult to integrate and maintain DWCNTs film. By air plasma, hydroxyl groups are generated and thereby improve hydrophilic character on SiO_2 surface.

Parallel to plasma processing on substrate, DWCNTs suspension as prepared are ultrasonicated by probe sonication to re-disperse DWCNTs immediately before use since

with time some DWCNTs sediment during storage. After sonication, DWCNTs suspension are ready for deposition.

1.3.1 Electrodes Array Fabrication on SiO_2/Si Wafers

Organic or inorganic contamination on SiO_2/Si wafer are removed by oxygen plasma stripping. Absorbed water is removed by dehydration bake at 200 $°C$ for 10 min. Negative photo-resist of thickness of 5 μm is spin coated automatically (EVG 120). Annealing and development of photo-resist are also accomplished in EVG 120. The wafer along with the mask are then submitted to mask aligner, Karl Suss MA 150. The photo-resist is exposed to UV light while the wafer is in contact with the mask. The patterned wafer is developed and cleaned in EVG 120 for hard-baking to harden the photo-resist and improve adhesion of the photo-resist to the wafer surface. The recipe for photolithography created by *Techniques et Équipements Appliqués à la Microélectronique* (TEAM) of LAAS in cleaning room of LAAS is attached in Appendix.

A uniform layer of Gold/Titanium (Au/Ti, 100 nm/3 nm) film is deposited by metal vapor deposition. Ti layer is first deposited on the surface of substrate, which is used for improving Au adhesion on substrate. The unexposed photoresist with metal film on its surface are removed by DMSO. Then arrays of Au/Ti electrodes are left on the substrate using this lift-off process in our devices, the electrode width is 600 μm and the gap is 80 μm, which is very large compared to the average length of DWCNTs (ca. 10 μm). The investigated configuration is thus such that nanotubes cannot connect the two electrodes directly at the same time. There is only one or zero ends of nanotubes touching the electrodes.

The substrate is then cut by the size of each electrode array. Before cutting, a thin layer of photoresist is spin coated on surface of substrate to prevent contamination from cutting. Substrate are finally cleaned immediately after cutting.

1.3.2 PDMS Stencils Fabrication

PDMS stencils are obtained by a molding process. The mold of stencil is fabricated by photolithography with pattern as illustrated in Figure 1.8. It is an inversed pattern of stencil in which pillars in the mold transform into cavities. The position of each pillar, as the position of each cavity in stencil, is corresponding to each intra gap of each pair of electrodes of the sensor substrate.

To prepare PDMS stencil, PDMS prepolymer and curing agent are mixed at a ratio of 10:1 by mass. The mixture is then stirred to let prepolymer and curing agent being fully mixed. The mixture is degassed by eliminating bubbles created during mixing by placing it in a dessicator at low vacuum. It is then cast on mold. Flatting and removal of excess PDMS is performed till a thin layer of PDMS left on the mold. Bubbles created by flatting are eliminated in the dessicator. Breaking and repeating the vacuum several times speeds up bubbles elimination. The mold is then placed in a oven which is pre-heated to and kept at 60 $°C$. After 4 hours, the PDMS is polymerized. After thermalization at room temperature, the PDMS stencil can be unmolded by hand.

1.3.3 Integration of DWCNTs

First, raw DWCNTs suspension is sonicated by probe ultra-sonication in intermittent mode for 10 min. The intermittent pulses are set at 5 s 'ON' and 5 s 'OFF'. The power of 150 W is selected for sonication. No ice is used for cooling during the sonication. The substrate is covered by stencil and then placed in plasma oven. After 5 min in air plasma at maximum power, localized functionalization is created. Air bubbles between stencil and substrate, especially those around cavities, should be eliminated before air plasma treatment to avoid liquid leaking from cavities and, thereby, deployment of DWCNTs between electrodes pairs.

Then each cavity is filled up with 0.6 μL of well-dispersed DWCNTs suspension. DWCNTs film are formed on substrate when water evaporates. The water evaporation rate is boosted by heating the substrate to 60 $°C$ for 3 min on a hot plate. The 60 $°C$ thermal treatment is sufficiently low to avoid degradation of raw and functionalized DWCNTs. Repeating the process allows to increase the quantity of deposited raw DWCNTs.

For the integration of oxidized, aminated and fluorinated DWCNTs lower concentration of DWCNTs suspension was used. Because the functionalized DWCNTs can easily attach onto the substrate due to the interaction between the functional group and the hydroxyl group on substrate. For example, the concentration of oxidized DWCNTs suspension is $0.01wt\%$.

1.4 Characterization

1.4.1 Optimization of the Integration Process

A lot of my work was dedicated to optimizing the quantity of DWCNTs suspension to be deposited in the stencil cavities in order to equip each set of electrodes with an adequate networks of disordered DWCNTs, giving rise to resistors with electrical resistance below 100 $k\Omega$, that turned out to be efficient for gas sensing purpose. This optimization took some efforts and was not dictated by any theory but by an iterative method guided by experimental observations. One of the main result of this work was the observation that multiple cycles of deposition/evaporation in the cavities were necessary to reach the optimal DWCNT network between the electrodes *via* a reproducible way. The following section tries to give an overview of this optimization work insisting on the dispersed volumes, DWCNTs concentration, importance of rinsing and numbers of cycles.

The substrate's surface is activated during the deposition process as described above, hydrophilicity is improved only on selected areas of substrate's surface. This requires the substrate to be covered by the stencil prior to air plasma. It makes it possible for raw DWCNTs to attach onto the walls of the cavities. This is verified when enough raw DWCNTs are deposited. From Figure 1.9, one can see that with increasing of deposited raw DWCNTs suspension, blocks of carbon nanotubes are formed and expanded at the end of cavity. From this point of view, the optimal amount of suspension for deposition should be restricted depending on the concentration of DWCNTs. But it is not only

determined by this factor, since the integration requires further treatments to improve the electrical performance.

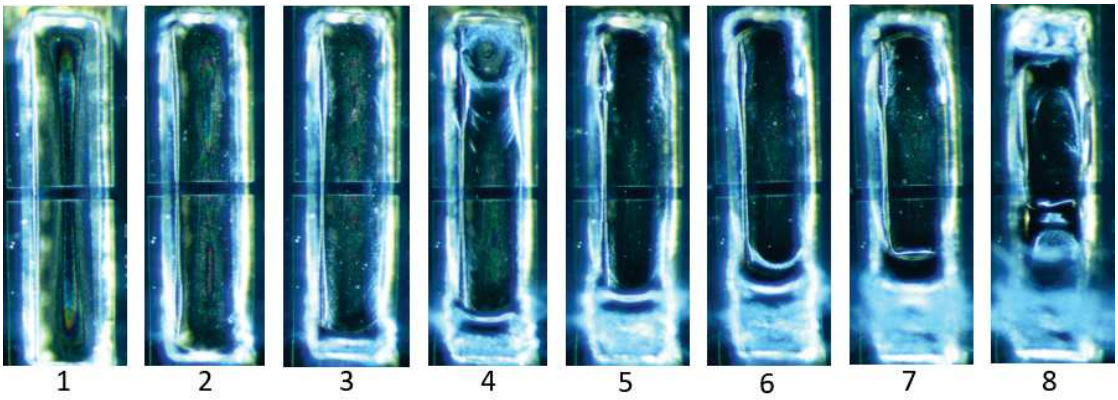


Figure 1.9: Optical observation of raw DWCNTs deposition process. The number of order of images corresponds to the number of repeats of deposition cycle i.e. the number of deposited droplets of 0.6 μL of raw DWCNTs suspension.

After deposition, the stencil is strongly attached onto the substrate at the edges of cavities and DWCNTs films. It results in jagged stencil around DWCNTs films when stencil is peeled off. It also leads to DWCNTs films being peeled off together with the stencil, which results in a failed fabrication of sensor, if the connection is too strong.

It is essential to integrate DWCNTs without introducing new substances. Thereby substrate should be treated by air plasma alone prior to being covered by stencil as optimization. Interaction between DWCNTs and stencil is weakened as non plasma stripped PDMS stencil surface keeps a low hydrophilicity. By this way, the size of block of DWCNTs, as shown in Figure 1.9, is dramatically reduced when same amount of DWCNTs deposited. PDMS stencil is no long binding to substrate and DWCNTs film. After rinsing, DWCNTs films are deposited without PDMS stencil residual.

The conductance of deposited DWCNTs is measured using a Keithley 2450 equipment. As Au electrodes provide sufficiently low resistance, the high resistance measured is mainly from the DWCNTs film and contact between DWCNTs film and Au electrodes, as shown in Figure 1.10. It can vary in a large range of magnitude. Two reasons may cause this result. First, it is the contact resistance (R_c) between DWCNTs and Au electrodes, which is the first reasonable explanation of high resistance and variation. Because the two materials, Au and DWCNTs, have different work functions. The second reason is the junction resistances between DWCNTs (R_f in Figure 1.10. Surfactant molecules can be attached on DWCNTs' surface. They offer an energy barrier which impedes the charger carriers transfer between nanotubes and results in large electrical resistances. In order to decrease the various resistance, electrical annealing can be performed.

As discussed in the work of Lifeng Dong and coworkers[5] and Dr. Florent Seichepine's thesis[6], Joule heating process reduces contact resistance between CNTs and metal

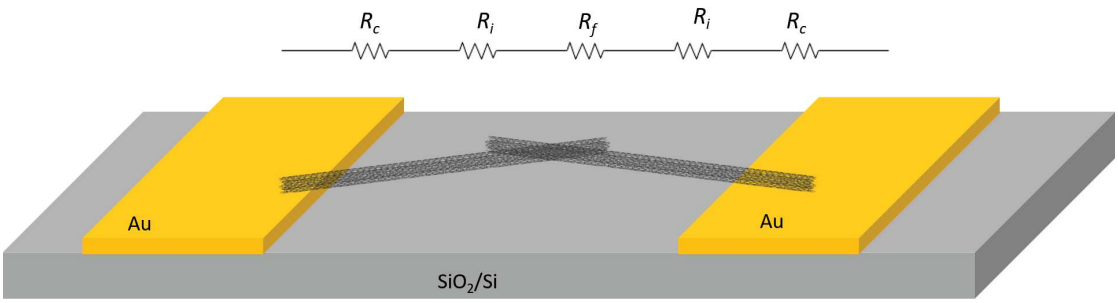


Figure 1.10: Schematic of resistance origin in DWCNTs based sensor. The R_c, R_i and R_f represent the contact resistance, intrinsic resistance and junction resistance respectively.

electrodes.

The Joule heating treatment is achieved by continuously supplying a high current (100 μA) for 100 s to the device. Following Joule heating treatment, the I-V characteristic of device is measured. Figure 1.11 illustrates I-V characteristic of a device before and after Joule heating treatment; it can be seen that after second time of Joule heating treatment, this method can barely improve conductivity. One can conclude that Joule heating treatment reduces conductance of our devices, however, the improvement is moderate.

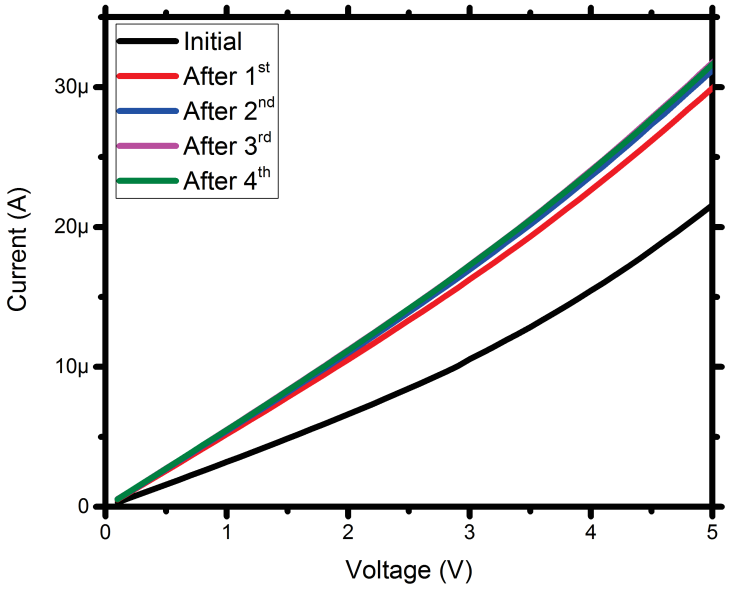


Figure 1.11: I-V characteristic before and after Joule heating treatment of a resistor equipped with raw DWCNTs.

Sodium carboxymethycellulose (CMC) surfactant is used as dispersing agent to suspend raw DWCNTs in DI water as described in Sections 1.2.1 and 1.3. CMC is easily dissolved in water at room temperature. Thus, it can be removed by washing in DI water. However, as DWCNTs film is integrated through a layer-by-layer deposition of DWCNTs and interconnection between DWCNTs is weak, most of DWCNTs will be removed from the film(Figure 1.13). As a consequence, it is highly possible to reduce the conductivity by removing surfactant in DI water. However, resistance measurement after removal of CMC shows high conductivity improvement. As it is shown in Figure 1.12, the device was submerged in DI water for 6 *min* and dried with nitrogen. Its resistance is decreased dramatically after rinsing.

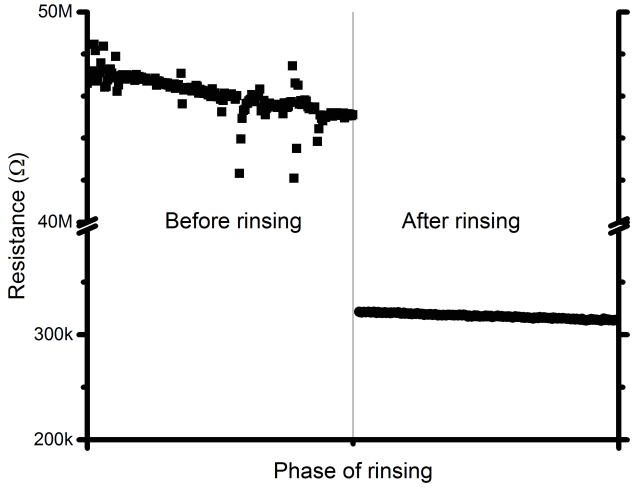


Figure 1.12: Rinsing effect on improving raw DWCNTs film conductivity

From optical observation, most DWCNTs are removed from the substrate along with CMC removal. Nevertheless the reverse change in resistance confirms that the removal of CMC reduce the contact resistance between DWCNTs. A better conductive DWCNTs film is thereby created. The rinsing duration in DI water was optimized by a careful study. First, for an individual rinsing, fabricated devices are immersed in DI water for different times. Resistance measurement shows that when immersion time increases, some devices become insulating. When immersing time is longer than 10 *min* nearly every device becomes insulating. Then, to find out optimal rinsing duration, the device is repeatedly rinsed in DI water for 3 *min* at a time and dried with nitrogen. By this approach, it is found that 15 *min* in total for rinsing is sufficient to improve conductivity while removing CMC surfactant. Figure 1.13 (a) shows resistance variation depending on the number of rinsing steps.

As rinsing process improves contact resistance between raw DWCNTs while removing

surfactant and excessive DWCNTs, a new question is raised: which amount of raw DWCNTs suspension should be consumed for fabricating one sensors? To answer this, devices were fabricated by depositing different amounts of DWCNTs' suspension ($0.1wt\%$) for each electrode, 0.6 μL, 1.2 μL, 1.8 μL, 2.4 μL, 3.0 μL, 3.6 μL and 4.2 μL. Then the devices were rinsed in DI water as presented above. The resistance of each circuit was measured after rinsing.

Figure 1.13 (b) shows the rinsing effect on different electrodes of different amount of deposited DWCNTs. Figure 1.13 c) and d) are scanning electron microscopy (SEM) images of raw DWCNTs film before and after rinsing, respectively. Though majority of raw DWCNTs are being removed, raw DWCNTs that are at the bottom of its film and closest to substrate are being 're-deposited' and better connected to Au electrode. Thereby conductance is improved every time after rinsing.

Three devices' resistance evolution are plotted in Figure 1.14 a), b), and c). They show the same variation of conductivity. There are only the initial resistance and final resistance plotted in figures for simplicity. In Figure 1.14 d), we summarise the trend. By repeatedly depositing raw DWCNTs, it increases the amount of raw DWCNTs in contact with the substrate. Due to the weak connection between raw DWCNTs and substrate,the conductance of the sensor is very low as the resistances shown in Figure 1.14 before rinsing. But the effect of increase of the amount of deposited raw DWCNTs becomes clear after rinsing. With adequate DWCNTs deposited, the resistance of the sensor can be sufficiently low. However, with excessive raw DWCNTs deposited, the resistances of sensors after rinsing were increased. The relationship between the resistance of the sensor after rinsing and adequate and excessive amount of raw DWCNTs deposited follows the schematic tendency depicted in Figure 1.14 (d). With less raw DWCNTs deposited, the resistances of the sensors after rinsing vary in a large range. This integration of DWCNTs corresponds to the 'Uncertainty Zone' in Figure 1.14 (d). As illustrated in Figure 1.13 (c) and (d), the rinsing process removes majority of raw DWCNTs. From the experimental observation, it is found that most raw DWCNTs were removed at the first cycle of rinsing. But, with increasing rinsing cycles, resistance of raw DWCNTs film continued decreasing. As the majority DWCNTs were removed in the first cycle of rinsing, the decrease of resistance in following cycles of rinsing is due to the removal of surfactant molecules. Thus the junction resistance is reduced (Figure 1.13).

According to characterization above, raw DWCNTs sensor's fabrication is optimized in terms of amount of deposited nanotubes (3.6 μL for $0.1wt\%$ raw DWCNTs DI water suspension with CMC surfactant, $1wt\%$) and rinsing with DI water (3 min per time for 5 times, dried with nitrogen each time)

A whole procedure of fabrication of raw DWCNTs sensor is attached in the Appendix.

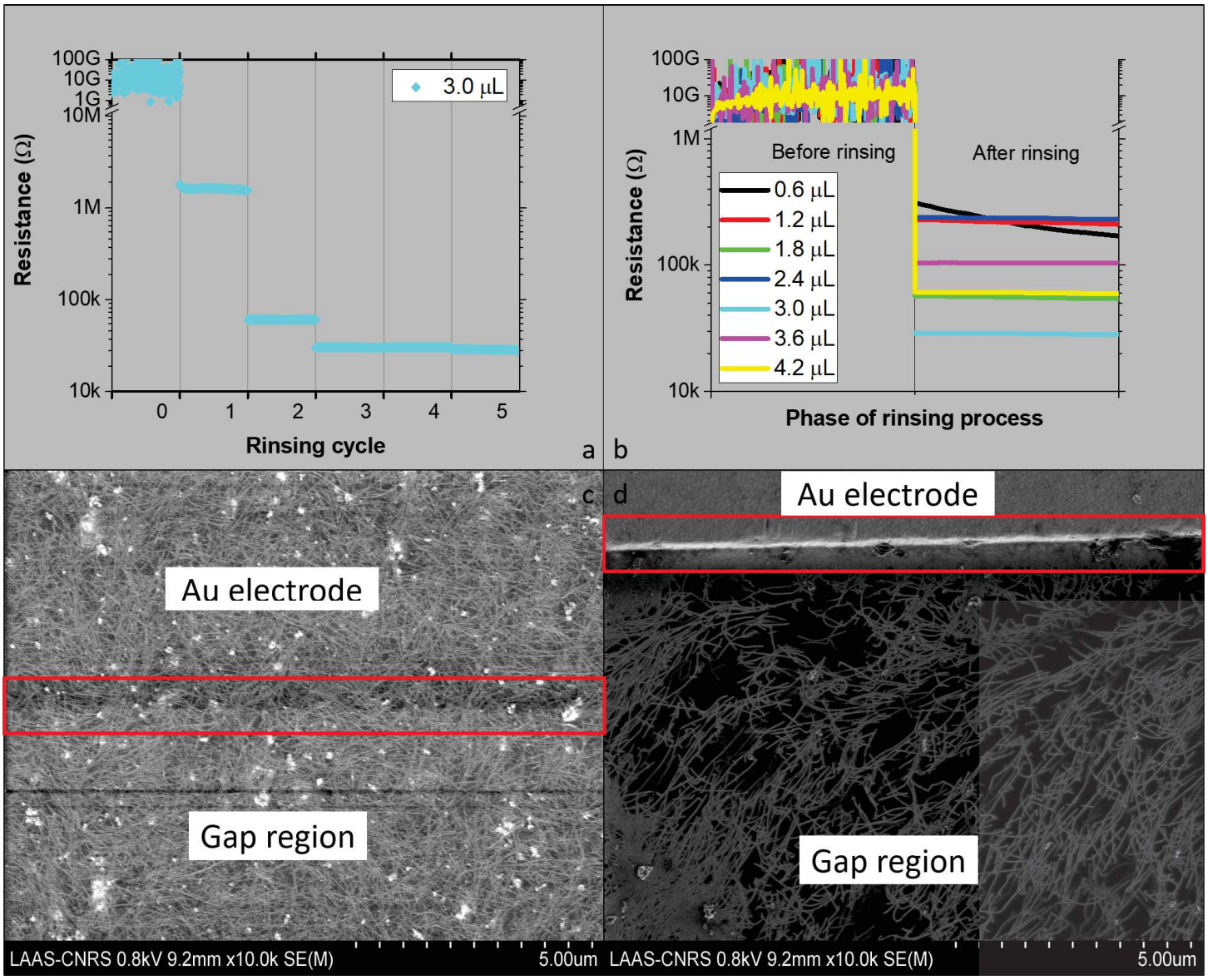


Figure 1.13: (a) Resistance evolution of raw DWCNTs sensor. X-axis is the cycle of rinsing, where '0' corresponds to no rinsing. Y-axis is the resistance measured after each rinsing cycle. (b) is the resistance comparison before and after rinsing of seven sensors integrating different volume of raw DWCNTs suspension. (c) and (d) are SEM images of deposited raw DWCNTs film before and after rinsing, respectively. The edge of one of the electrode is circled. The area below the edge is the gap between electrodes.

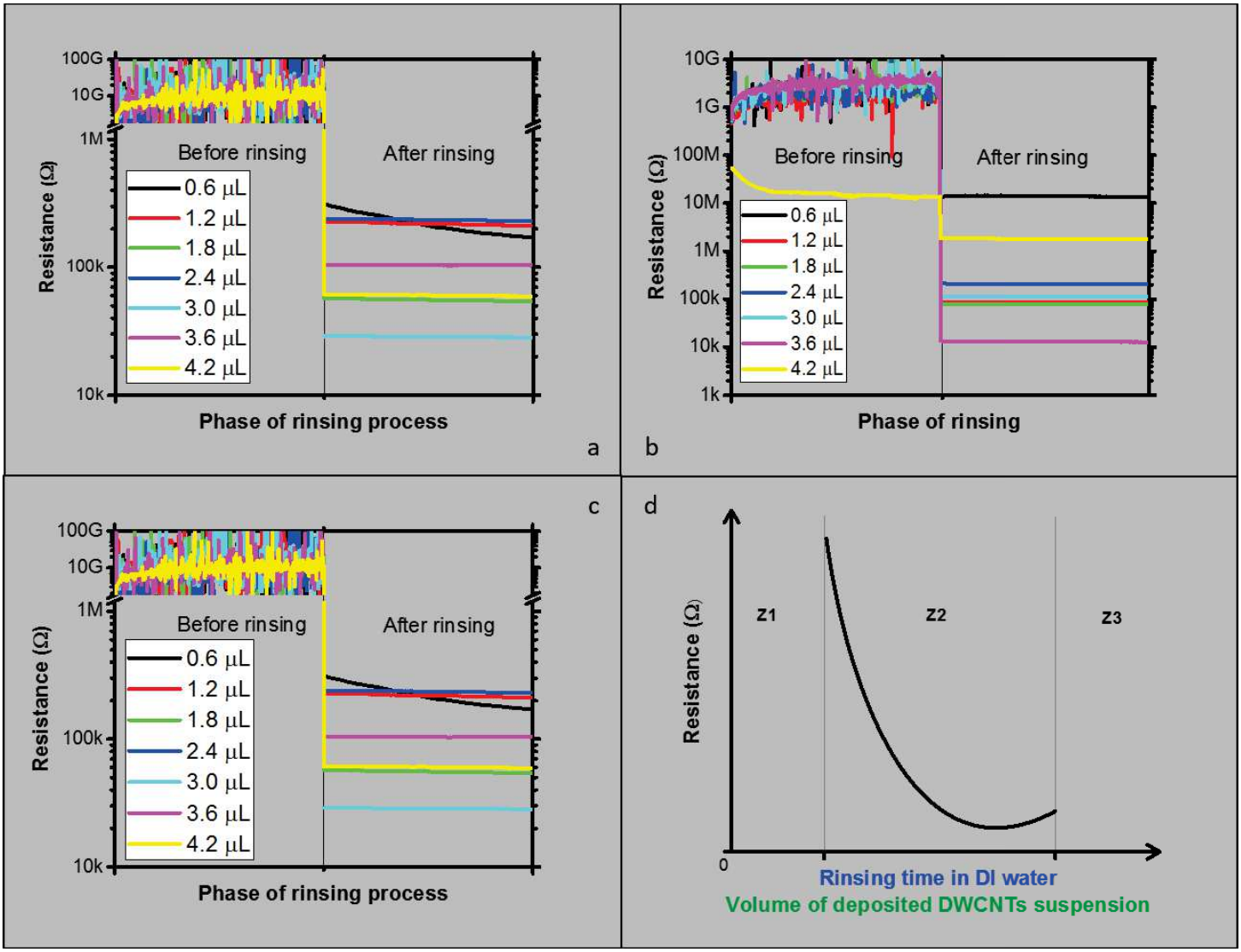


Figure 1.14: a), b), and c) are the resistance variation of 7 sensors of three different devices. d) shows a mode of resistance evolution with rinsing times and resistance differences between each electrode of one device after rinsing depending on the amount of deposited raw DWCNTs. Z1, Z2 and Z3 represent uncertainty zone, regular zone and undetermined zone, respectively, corresponding to the volume of deposited DWCNTs suspension axis label.

1.4.2 I/V Characterization

The ohmic characteristic of the contact between DWCNT films and the electrodes can be verified by corresponding I/V curves. For functionalized DWCNTs, it turned out that ohmic contacts with the electrodes are straight forward to obtain (Figure 1.16).

The question left is about the fabrication of ohmic contact between raw DWCNTs and Au electrode. Do raw DWCNTs form ohmic contact with Au electrodes? In what condition, do raw DWCNTs and Au electrodes form ohmic contact?

To answer the first question, we fabricated several devices made from raw DWCNTs with large variation of resistance and measured the current flowing through the devices while swapping voltage. Among all the devices tested, very few devices show ohmic contact. Other devices exhibited Schottky behaviour. The ohmic contact is only found when the resistance of device is not large. However, it is not vice versa. In Figure 1.15, devices (a) and (b) both have Schottky contact between raw DWCNTs film and Au electrodes. The resistance of the two devices are 6.5 $M\Omega$ and 1.5 $M\Omega$, respectively. The ones show ohmic contact are devices (c) and (d), of which the resistances are 540 $k\Omega$ and 7.7 $k\Omega$, respectively. It appears that with the decrease of resistance, the I-V characteristic is changing from Schottky contact to ohmic contact. When the resistance is within few kilo Ohm, the contact is ohmic. However, with raw DWCNTs, device of kilo Ohm is very difficult to fabricate. The resistance of fabricated device is large in general, several hundred kilo Ohm or larger.

Unlike raw DWCNTs sensors, oxidized DWCNTs sensors fabricated by the same protocol have small resistance in general, from few kilo Ohm to tens of kilo Ohm. This is due to strong interaction between carboxyl group and substrate which includes Au electrodes and SiO_2 that has been activated with hydroxyl group by air plasma. Sensor of resistance of hundreds kilo Ohm requires very small amount of oxidized DWCNTs. To integrate small amount of oxidized DWCNTs, it is generally achieved by using very low concentration suspension of oxidized DWCNTs. However, it is difficult to control integration of small amount of oxidized DWCNTs to fabricate desired resistance. Figure 1.16 shows I/V curves of four oxidized DWCNTs sensors of which the largest resistance is $ca.200\ k\Omega$. All the tested devices show ohmic conduction.

Like oxidized DWCNTs, aminated DWCNTs are also easy to attach to the Au electrodes. But the interaction between aminated DWCNTs and substrate is weaker than that between oxidized DWCNTs and substrate. More aminated DWCNTs are required to fabricate sensor of resistance in the same order of magnitude as oxidized DWCNTs sensor. Nevertheless, sensors with small resistances can be easily fabricated and all sensors of small resistance show ohmic conduction, Figure 1.17.

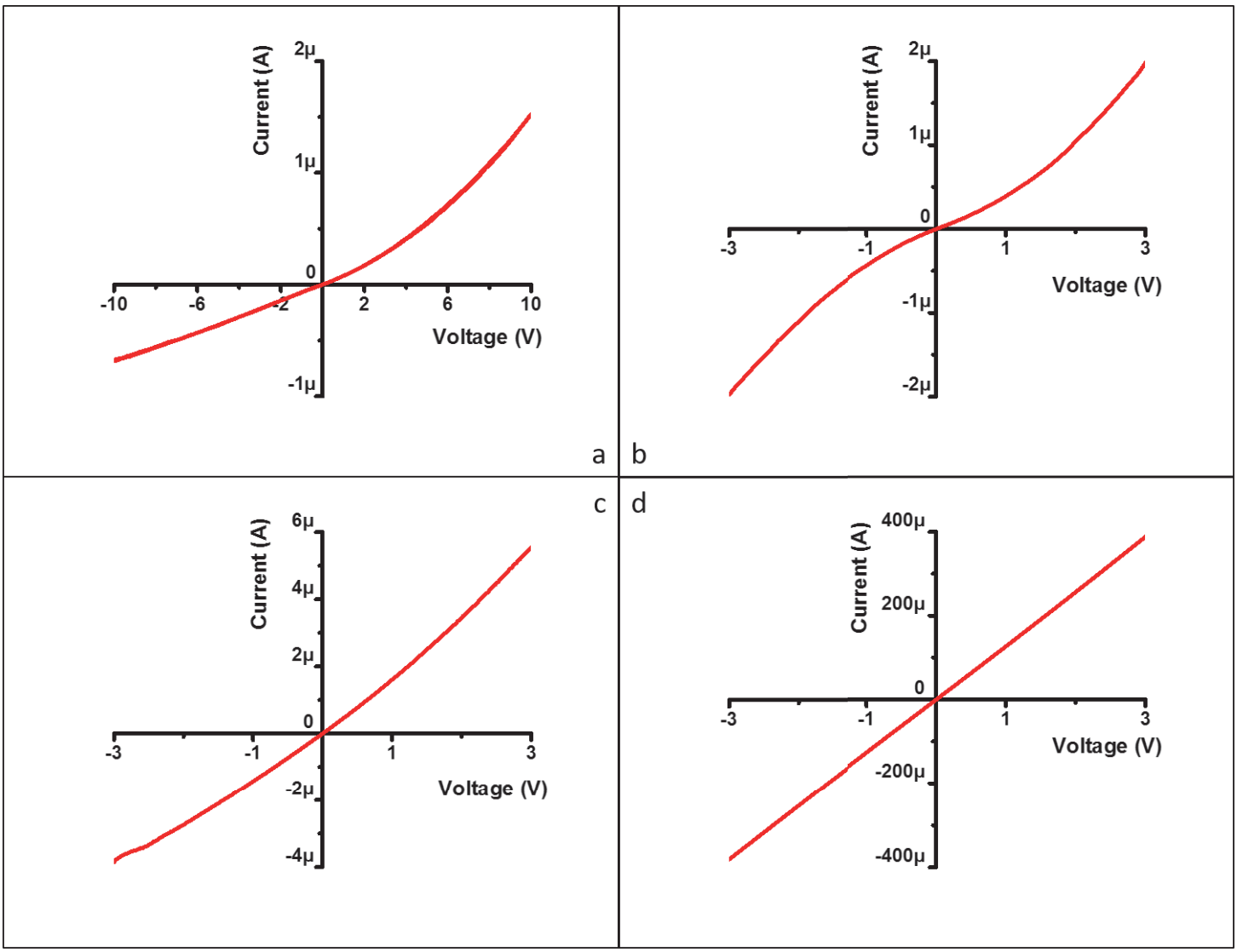


Figure 1.15: I-V characterization of raw DWCNTs based sensors. (a) and (b) sensors exhibit Schottky diode behaviour, while (c) and (d) show ohmic behaviour.

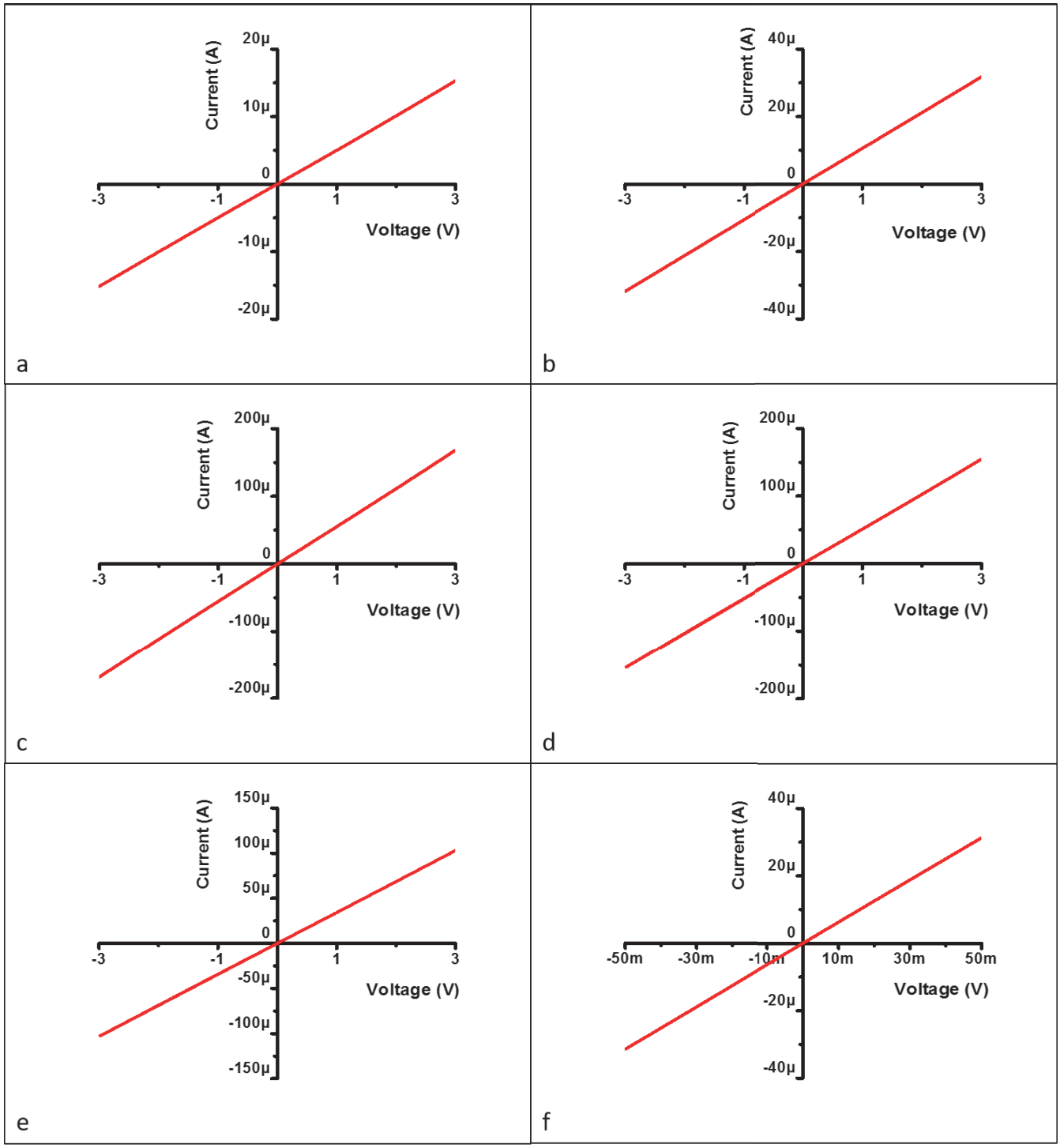


Figure 1.16: I-V characteristic curves of six sensors made by integrating different amount of oxidized DWCNTs suspension. The resistance of each one is 196 $k\Omega$, 94 $k\Omega$, 29 $k\Omega$, 19.4 $k\Omega$, 17.8 $k\Omega$ and 1.6 $k\Omega$, respectively.

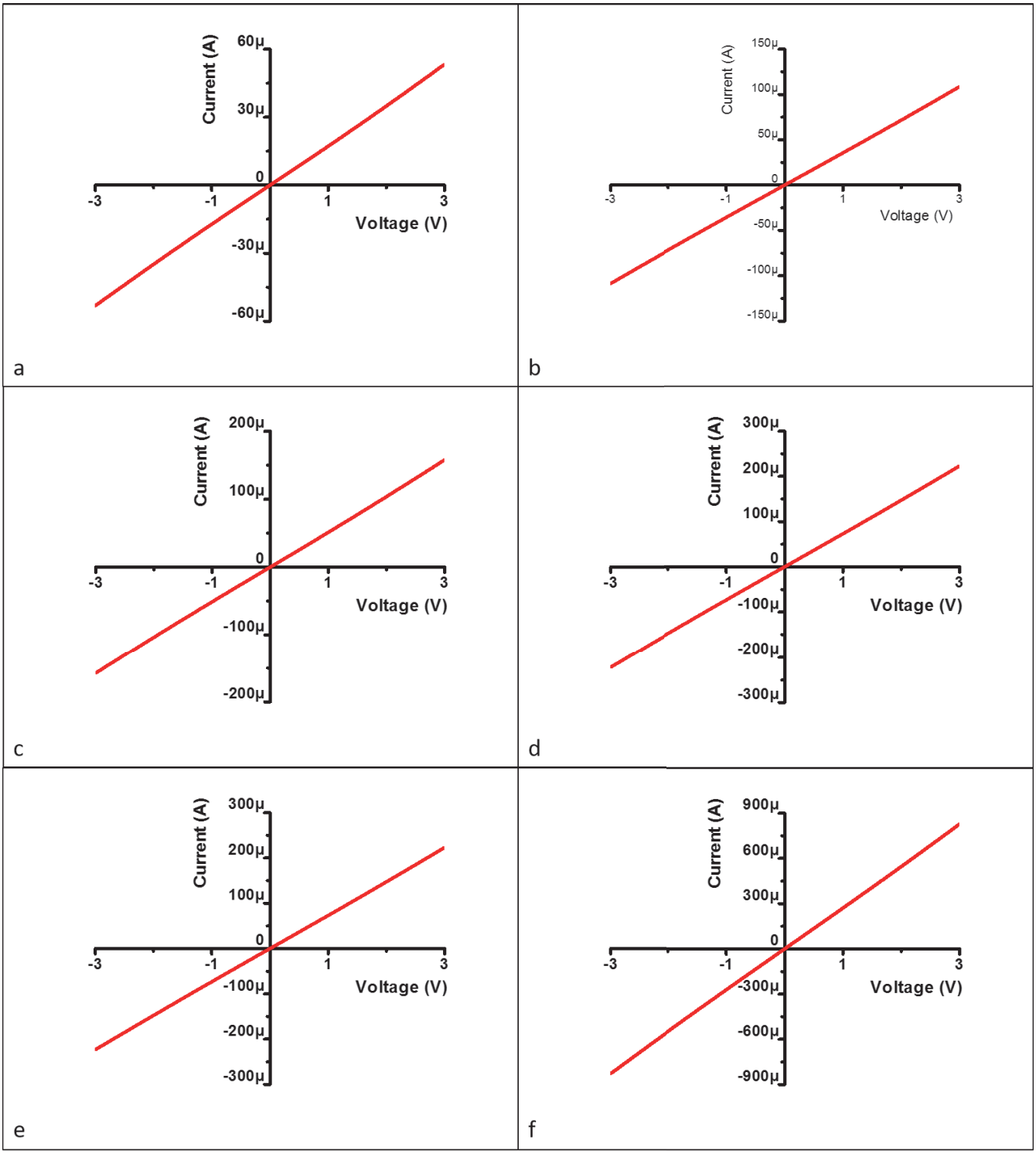


Figure 1.17: I-V characteristic curves of six sensors made by integrating different amount of aminated DWCNTs suspension. The resistance of each one is 56 $k\Omega$, 27.6 $k\Omega$, 19 $k\Omega$, 13 $k\Omega$, 7.3 $k\Omega$ and 3.6 $k\Omega$, respectively.

1.4.3 Mechanism of Electron Transport in DWCNTs Disordered Films

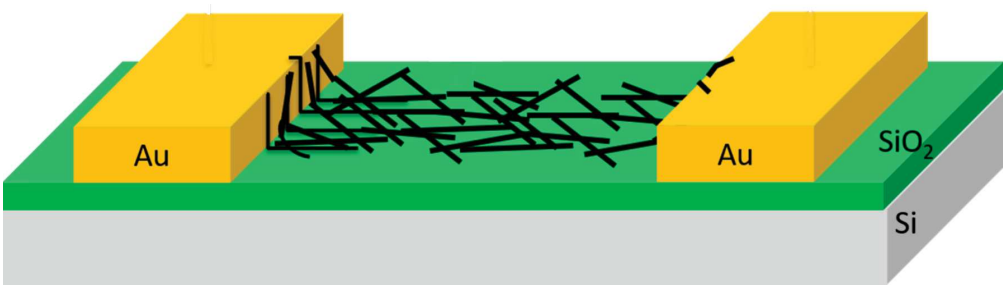


Figure 1.18: Schematic of disordered DWCNTs in the sensor.

As pointed previously, the electronic transport in CNT sensors made of an individual nanotube connecting two electrodes is dominated by: i) the Schottky barriers possibly formed between the electrodes and the CNT wall; ii) the band structure of the connecting CNT which drives the conductivity of this nano-object. Both elements are dependent on the structure of the CNT (number of walls, diameter, chirality). In the sensors investigated in this work, additional complexity arises due to the presence of a large number of DWCNTs in the gap region of the electrodes as can be seen in Figure 1.18. We are going to briefly discuss how the current flows from one electrode to the other through this disordered thin film made of randomly oriented DWCNTs. Several basic observations first enable us to set some starting hypothesis essential for drawing the main dominating parameters of the electrical conduction.

- Near room temperature, we consider that the DWCNTs conducting the electrons in the sensors are quasi-metallic. They can be described simply as conductors characterized by an intrinsic resistivity which depends on their free carriers density, Schottky barriers are not considered further.

- Our fabrication method has been optimized for depositing a large density of DWCNTs between the electrodes and because we select the devices exhibiting a low resistance ($< 100k\Omega$) we assume that the percolation threshold is attained in these devices, meaning that the current flows through a complex path of minimal resistance. Moreover, as surfactant molecules have been removed by successive rinsing step, we assume that there is not any molecules or polymeric matrix around the nanotubes.

- Comparing the average length of our DWCNTs (ca. 10 μm) and the size of the gap region (80 μm), we estimate that along the percolation path the conducting electrons need to jump several times from one DWCNTs to another. We thus need to include several junction in order to describe the transport properties of our sensors. Tunnel effect is thus involved in the conduction mechanism. The exact numbers of tunnel junctions encountered by the current flows is not known

and varies from one sensors to another, because the percolation path in disordered randomly oriented carpets of CNTs cannot be controlled by engineering. It is likely that along the conduction path 10 to 20 tunnel junctions are involved. We think that the observed dispersion of sensor resistances after fabrication reflects this variation of the numbers of tunnel junctions involved.

In summary, the transport is governed by the intrinsic conductivity of the DWCNTs and by the tunnel resistances of the junctions between DWCNTs, arranged in a complex network of connecting bundles.

We think that for describing the conduction in our devices, the theoretical frame work proposed by Ping Sheng in 1980[7] is very well adapted. For simplicity we will refer to this pioneering work that catches most of the physics involved in our sensors without considering the modifications, adaptation and improvements of this initial model that have been proposed later by other contributors. The model of P. Sheng describes the conduction into disordered materials characterized by large conducting regions separated by small insulating barriers. In our case, long "metallic" DWCNTs separated by tunnel junctions between the nanotubes.

In that case, thermal fluctuations turned out to govern the dependence of the conductance through a mechanism called fluctuation-induced tunneling. Indeed, thermal fluctuations (kT) generate voltage fluctuations across the tunnel barriers that result in-fine to a theoretical expression for the conductivity exhibiting a thermally activated characteristic at high temperature. According to Sheng's model, the sheet resistance of the disordered film is given by:

$$R \propto exp(\frac{T_1}{T + T_0}) \tag{1.1}$$

where T is the temperature, T_0 and T_1 are characteristics temperatures depending on the barrier height and thickness.

T_0 represent the temperature above which the fluctuation effects become significant. This temperature is generally small otherwise those effects vanish and the conductivity follows simple tunneling behaviour and does not exhibit any thermal activation. In our case, we will suppose that at room temperature $T \gg T_0$.

T_1 is the required temperature for thermal conduction over the energy barrier.

If $T \gg T_0$, we thus have $R \propto exp(\frac{T_1}{T})$, from this expression, we can write the resistance of our sensors as:

$$R = R_0 exp(\frac{E_{act}}{kT}) \tag{1.2}$$

where R_0 is a typical resistance that depends on the length of the percolation path and the intrinsic conductivity of the DWCNTs. E_{act} is an activation energy (in the theory of P. Sheng $E_{act} = kT_1$, with $T_1 = \frac{2SV_0}{\pi k e^2 \omega}$, where S is the junction surface, V_0 is the energy barrier height and w is junction thickness).

In order to prove that such a model enables to explain the sensitivity of our sensors to temperature, we have performed electrical measurements of the sensor resistance of

an oxidized DWCNTs based sensor whil sweeping the temperature from $T_i = 53°C$ to $T_f = 24°C$.

For $T = T_i$,

$$R = R_0 exp(\frac{E_{act}}{kT_i}) = R_i. \tag{1.3}$$

Thus

$$\ln\left(\frac{R(T)}{R_i}\right) = E_{act}(\frac{1}{kT} - \frac{1}{kT_i}) \tag{1.4}$$

Figure 1.19 presents such a logarithmic plot, clearly indicating a thermally activated behaviour with a typical activation energy of $0.02eV$

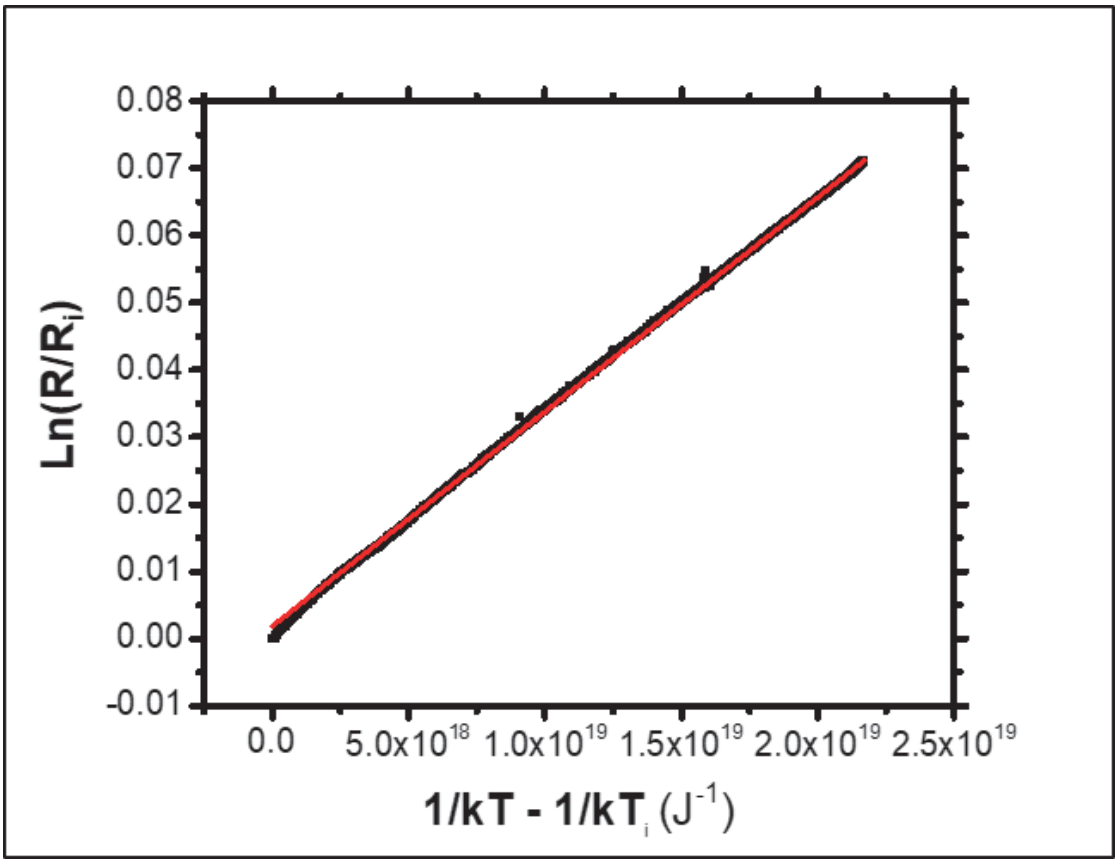


Figure 1.19: The electrical measurements of an oxidized DWCNTs sensor's resistance (black) which is plotted in the form of equation 1.4. The red curve is fitted with equation 1.4.

In summary, the resistance of our sensors at room temperature is governed by the intrinsic resistance of the involved DWCNTs (through R_0), and by the tunnel junctions

between DWCNTs (through $E_{act} = kT_1$). A model based on thermal induced tunneling accounts quite well for our experimental data and those tunnel junctions are responsible for the temperature dependence of the resistance of our sensors. Indeed, near RT, we assume that the intrinsic conductivity of the DWCNTs is not noticeably modified and thus R_0 in equation 1.2 is constant. Coming now to the numbers, we have measured that near RT, the relative variation of the resistance per degree Celsius is around 0.3%. This thermal behaviour could be obviously exploited for producing original temperature sensors, but in the context of this thesis, this characterization was necessary in order to compare the thermal sensitivity of the sensor to the sensitivity towards gas molecule adsorption. Indeed, under normal use at room temperature and ambient conditions, without any temperature regulation, the sensor temperature can drift during gas exposure. If this drift is larger than the effect of gas adsorption, then it will be impossible to detect the presence of the gas without including in the sensor a thermal regulation. As we will discover later in this thesis, the effect of ppm of gas molecules on the device induces resistance changes much larger than 0.3%, showing that our very simple sensors are quite immune to normal thermal drift.

1.4.4 Consequence for Gas Sensing Mechanisms

Upon gas exposure, the resistance of the sensor can be possibly changed according to two main possible mechanisms. The adsorption of gas molecules inside the gap region of the electrodes (physisorption or chemisorption) can induce some charge transfer capable to alter either the parameter R_0 or the parameter E_{act} of equation 1.2.

If the gas molecules interact directly with the surface of the DWCNTs (at defect sites or on their whole surface depending on surface functionalization), the induced charge transfer (if existing) will change the free carrier density of the DWCNTs and thus will change their intrinsic conductivity. In the end, this process will modify R_o and the final sensor resistance.

On the other hand, if the gas molecules interact at the junction sites, induced charge transfers (if any) can modify the energy barrier of the junction and thus will change the activation energy E_{act} and the end the sensor resistance.

We think that both mechanisms co-exist simultaneously. In the following we will mainly discussed the first one, because through chemical functionalization of the surface of the DWCNTs we can control the chemical interaction taking place at the DWCNTs' surface. Due to the impossibility to finely characterize the insulating material forming the tunnel junctions, it is not possible for us to discuss in detail the adsorption mechanism leading to a variation of E_{act}. However, the reader needs to remember that those mechanisms, even if not detailed in the following, are also governing the signal delivered by our resistive sensors during gas exposures.

1.5 Conclusion

Based on the liquid stencil lithography, we have successfully fabricated DWCNTs based resistor devices which are ready for gas detection test.

The fabrication process can be implemented on flexible substrates and is versatile to other substrates than Si/SiO_2.

The reproducible obtention of ohmic devices with raw DWCNTs is not really possible despite optimization of dispersed volumes, concentration, rinsing and electrical annealing.

Functionalized DWCNTs (oxidized and aminated) give rise to excellent ohmic characteristic with a very high yield.

In that case, the consumption of carbon nanotubes is very low. ca. 200 ng for oxidized DWCNTs sensors and ca. 1 μg for aminated DWCNTs sensors.

Inside a batch of fabrication, the final resistance of functionalized DWCNTs sensors is dispersed, from thousands of ohm to hundreds of ohm, but resistors with resistance lower than 100 $k\Omega$ that turned out to be suitable for gas sensing experiments are obtained with a typical success rate of ca. 80%.

Bibliography

[1] E. Flahaut, A. Peigney, C. Laurent, and A. Rousset, "Synthesis of single-walled carbon nanotube–co–mgo composite powders and extraction of the nanotubes," *Journal of Materials Chemistry*, vol. 10, no. 2, pp. 249–252, 2000.

[2] E. Flahaut, R. Bacsa, A. Peigney, and C. Laurent, "Gram-scale ccvd synthesis of double-walled carbon nanotubes," *Chemical Communications*, no. 12, pp. 1442–1443, 2003.

[3] K. Patil, "Advanced ceramics: combustion synthesis and properties," *Bulletin of Materials Science*, vol. 16, no. 6, pp. 533–541, 1993.

[4] L. G. Bulusheva, P. N. Gevko, A. V. Okotrub, Y. V. Lavskaya, N. F. Yudanov, L. I. Yudanova, O. G. Abrosimov, E. M. Pazhetnov, A. I. Boronin, and E. Flahaut, "Thermal behavior of fluorinated double-walled carbon nanotubes," *Chemistry of materials*, vol. 18, no. 20, pp. 4967–4971, 2006.

[5] L. Dong, S. Youkey, J. Bush, J. Jiao, V. M. Dubin, and R. V. Chebiam, "Effects of local joule heating on the reduction of contact resistance between carbon nanotubes and metal electrodes," *Journal of applied physics*, vol. 101, no. 2, p. 024320, 2007.

[6] F. Seichepine, *Réalisation d'interconnexions de faible résistivité à base de nanotubes de carbone biparois pour la microélectronique*. PhD thesis, Université de Toulouse, Université Toulouse III-Paul Sabatier, 2011.

[7] P. Sheng, "Fluctuation-induced tunneling conduction in disordered materials," *Physical Review B*, vol. 21, no. 6, p. 2180, 1980.

Chapter 2

Gas Detection and Results Analysis

This part of work describes the gas detection with sensors fabricated in Section 1.3. It begins with ethanol (EtOH) and acetone, the pure compound detection in Section 2.2. Then because water is always present in all environment and in order to investigate the ability of our sensors to discriminate between chemical compounds and water, aqueous solutions of ammonia and formaldehyde were tested.

EtOH, acetone and ammonia are selected for the gas detection experiments as they are commonly found in either domestic uses, agricultural uses, industrial uses or/and medical uses. EtOH is one of the most widely used organic compound, such as antiseptics, disinfectants, and antidote for medical usage, engine fuel for powering cars and rockets[1], and alcoholic beverages. It is also used as feedstock for synthesizing other organic materials. Acetone is mostly use in chemical industry, such as solvent, chemical intermediate, for synthesizing acetone cyanohydrin for instance. It is also found in domestic uses, like cleaning agents. It is also used for 3D-printing[2]. Ammonia is essentially used for fertilizers. There is ca. 88% of ammonia used as fertilizers worldwide as Ref.[3] reported in page 118. Ammonia is also found in daily necessaries, like cleaning agents and disinfectant. Ammonia is also used in food industry, production of lean finely textured beef for example.

EtOH is a flammable chemical and has low toxicity to human body. But it can cause some skin adverse effects, such as systemic dermatitis. It also aggravates the condition of patients who have peptic ulcer disease. Leakage of EtOH in storage can lead to fire or/and explosion.

Acetone is extremely flammable. Its flash point is $-20\ ^{\circ}C$. And the high volatility makes it easy to reach acetone's explosive concentration in the air. It is dangerous to be exposed to acetone of high vapor concentration. Since acetone can depress nervous system and cause coma and lower blood pressure.

Ammonia is highly toxic to human health. It is generally for human to be exposed to ammonia from inhaling its gas or vapor. It has pungent odor and irritates nose, eyes and throat. Exposure to high concentration ammonia vapor leads to facial and oral

burns and many breathing problems. Inhalation of excessive ammonia can also depress nervous system and cause loss of consciousness. Large use of ammonia in agriculture leads environmental concern. Overfertilization and runoff cause accumulation of nitrogen in watersheds. A direct consequence is the formation of hypoxic zone. It is reported[4] that the hypoxic zone in Gulf of Mexico is suspected to be caused by nitrogen in excess fertilizer runoff.

Thereby, since the wide use and their health and environmental impact, monitoring EtOH, acetone and ammonia are appealed to us as a good demonstrator to validate the functionality of our gas sensors.

In the following experiments, nitrogen is used as carrier gas for two reasons. One is that nitrogen is the first major component of atmosphere. Second is that nitrogen is less active compared to oxygen, while oxygen is a strong oxidizer.Thus, when it interacts with carbon nanotubes, nitrogen has less influence on their conductivity compared to oxygen and will be considered as inert.

2.1 Setup for Gas Exposure Experiments

Two setups were used for controlling gas atmosphere under the sensors. First setup controls the nitrogen flow by dial pressure gauge and flow rate meters. Two paths of nitrogen flow were generated with different flow rates. One path of higher flow rate was directly connected to a chamber where the sensor device was placed. The second path of lower flow rate passes through a bottle which contains ethanol or acetone of high purity. It is then merged with first path to dilute ethanol or acetone vapor. Due to the limitation of flow rate meters, very small concentration vapor of ethanol and acetone were could not be obtained. In the second setup, dial pressure gauges were replaced by a microfluidic flow control system (Fluigent MFCS^{TM} - EZ) in order to obtain an accurate control of the nitrogen flow. The resistance variation of sensors were measured by a source-meter (Keithley 2450). With this setup, low concentration of ammonia and formaldehyde vapor were generated from their aqueous solution. The concentration of each analyte in nitrogen was calibrated by mass loss rate from solution compared with the nitrogen mass flow rate. Figure 2.1 schematically illustrates the setup used for gas generation and detection.

2.2 Detection of Pure Compounds

DWCNTs gas sensors are exposed to ethanol or acetone vapor in nitrogen with the first setup, where ethanol and acetone vapors were generated by bubbling.

The device being tested was first kept in dry nitrogen for 10 *min* to remove H_2O molecules that are absorbed on the surface of DWCNTs films. When the resistance variation measured became stable, the device was exposed to ethanol or acetone vapor. After cut off vapor supply, the device was left in pure nitrogen to recover from exposure. The exhaust was filtered before being released into the atmosphere.

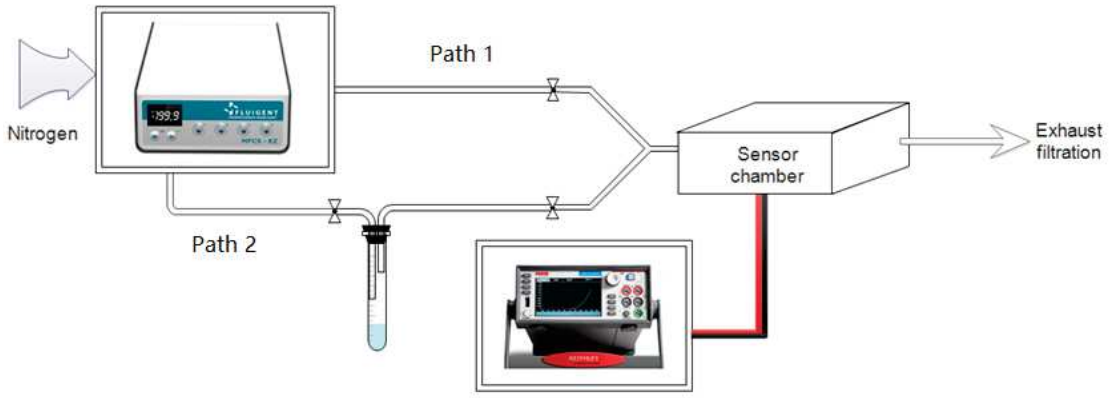


Figure 2.1: Schematic of gas exposure and detection setup.

The relative concentration of ethanol and acetone vapor are calculated by using equation 2.1 from Ref.[5]:

$$C = \frac{P_{vapor}}{\Delta P} \frac{f}{f+F} \tag{2.1}$$

Where C is the concentration of vapor, P_{vapor} is the vapor's partial pressure, ΔP is the input pressure of nitrogen flow. f is the flow rate of nitrogen flow that passes through ethanol or acetone, and F is the flow rate of the second nitrogen flow. The input pressure and flow rates are controlled and measured by gauge pressure meter and rotameters respectively. The partial pressure of ethanol or acetone is calculated by equation found in [6]. The relevant content can be found on pages [6, p. 5.30, p. 5.39 and p. 5.46].

$$P_{Eth} = 10^{8.32109 - \frac{1718.1}{237.52+T}} \, P_{Ace} = 10^{7.11714 - \frac{1210.595}{229.664+T}} \tag{2.2}$$

Where P_{Eth} and P_{Ace} are partial pressure of ethanol and acetone vapor respectively, and T term is the temperature in degree Celsius. $21 \deg C$ is used for calculation as the temperature condition of experiments was $21 \pm 1 \deg C$. It will be referred as room temperature(RT).

2.3 Detection of Compounds inside Water Vapor

Detecting a target analyte in a complex environment is a way to explore sensor's discrimination capability. With the second setup, ammonia and formaldehyde vapor were generated by evaporation from their aqueous solution by applying a constant nitrogen flow. The gas concentration was diluted by the second path of nitrogen. The exposure process is the same as in the previous section. However the concentration of vapor is

not calculated by the equations 2.1. It is calibrated by comparing the mass loss of solution with nitrogen mass flow. The mass loss in solution is measured with a balance and the nitrogen mass flow is calculated from its volumic flow rate. Since the input pressure of nitrogen, 1.027 atm, in this part is slightly higher than atmosphere, 1 atm, the calculation is carried out with ideal gas model.

The ammonia vapor concentration is calibrated with a low concentration aqueous solution. The low concentration ammonia aqueous solution (0.3wt%) is obtained by dilution of the high concentration solution (28-30%, Sigma-Aldrich). The mass loss in the low concentration ammonia aqueous solution is obtained by injecting a constant nitrogen flow. Vapor concentration of ammonia/water in nitrogen is then obtained by comparing the mass loss of ammonia solution with nitrogen flow, from which the ammonia vapor concentration is thereby generated by multiplying its mass ratio. Thus the ammonia vapor concentration excludes water mass which only causes fractional difference in ammonia vapor concentration. With the setup above, the ammonia vapor concentration was 17 ppm, and the water vapor concentration was 5690 ppm. The formaldehyde solution was prepared in the same way.

As discovered later, the oxidized, aminated and fluorinated DWCNTs gas sensor are all sensitive to ammonia (with water present in nitrogen). Oxidized DWCNTs sensor was selected for specifying its limit of detection in complex environments. For this purpose, an oxidized DWCNTs sensor was exposed to a set of ammonia vapor of different concentration.

2.4 Gas Detection Results

The signal delivered by our gas sensors is expressed in relative resistance variation, which is defined by the equation:

$$S(t) = \frac{\Delta R}{R_0} \times 100\% = \frac{R(t) - R_0}{R_0} \times 100\% \tag{2.3}$$

Where R_0 is the initial resistance of the device before exposure and $R(t)$ is the resistance of the device measured at time t during an exposure-recovery cycle. In the following context, the term 'signal' refers to the concept defined above.

2.4.1 Detection of pure Compounds

Raw DWCNTs Gas Sensor: It is known that pristine carbon nanotubes sensors are inert to ethanol detection, as presented in ref[7]. Our raw DWCNTs sensor shows a similar response to ethanol vapor exposure. As shown in Figure 2.2, three raw DWCNTs sensors of different resistances, 14.165 $k\Omega$, 17.385 $k\Omega$ and 75.35 $k\Omega$, were exposed to ethanol and acetone vapor at room temperature. The ethanol and acetone vapor generated by the same nitrogen pressure and flow rate had a concentration of 10000 ppm and 40000 ppm in nitrogen, respectively.

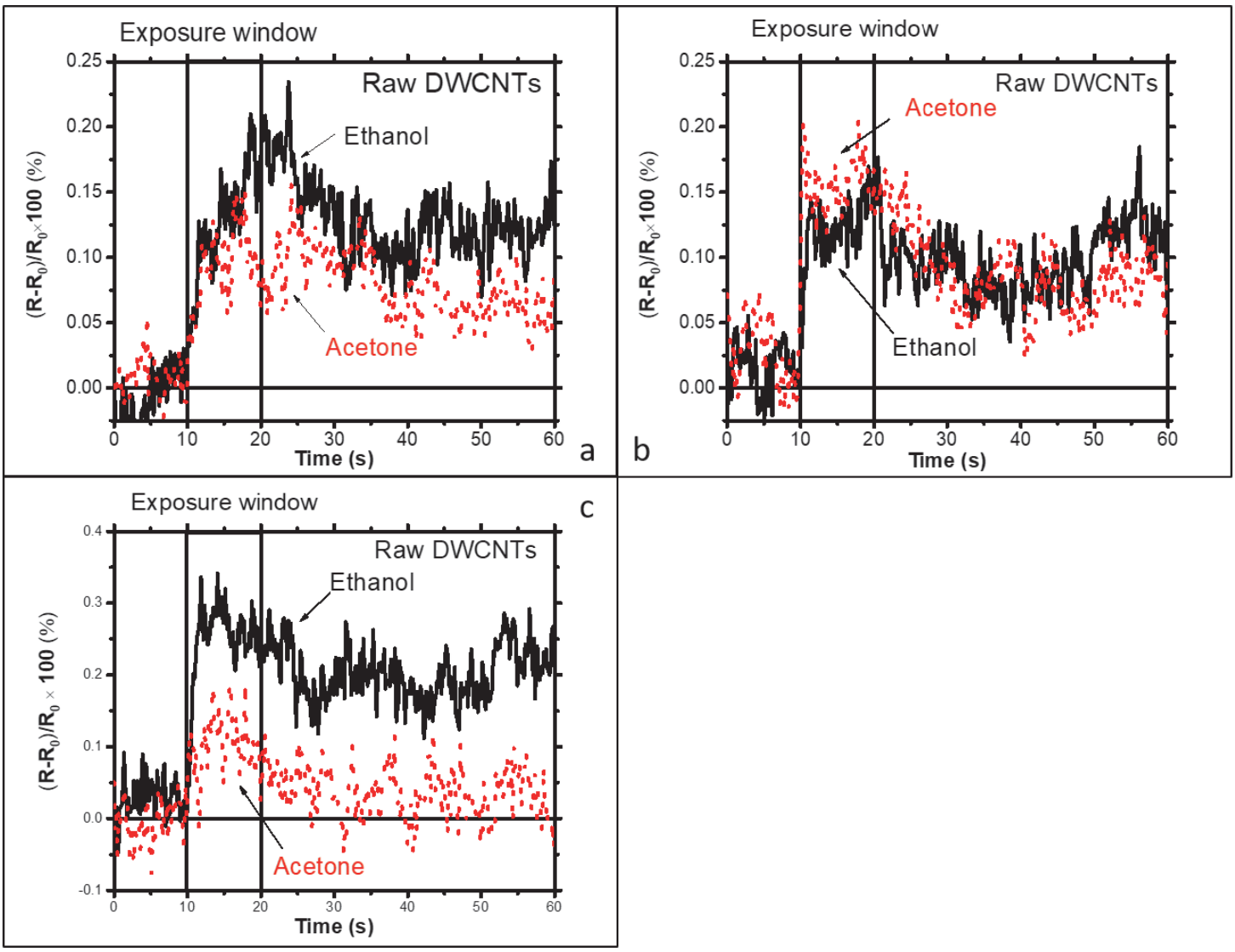


Figure 2.2: Three raw DWCNTs based sensors' response to ethanol and acetone vapor exposure.

From the response curve, it can be seen that the raw DWCNTs sensors exhibit a poor response to both kinds of vapors. The signals are merely distinguishable from noise. However, it is clear that the signals reach their maximum within exposure duration. In some case (Figure 2.2 (c)), the signal declined after reaching its maximum.

With our bench, not only the signal is minute, the recovery from exposure to ethanol back to initial is also a challenge, especially for acetone exposure.

Functionalized DWCNTs Gas Sensor: Aminated and oxidized DWCNTs gas sensors were exposed to ethanol and acetone vapor in the same exposure conditions, respectively. Since functionalization improves CNTs gas sensor's sensitivity, the aminated DWCNTs and oxidized DWCNTs gas sensors are expected to be more sensitive to ethanol and acetone vapor than raw DWCNTs sensors.

In Figure 2.3, two functionalized (amination and oxidation) DWCNTs gas sensors were exposed to 10000 *ppm* ethanol vapor and 40000 *ppm* acetone vapor, respectively. The resistance of the two sensors are 1.7 $k\Omega$ for aminated DWCNTs sensor and 2.2 $k\Omega$ for oxidized DWCNTs sensor.

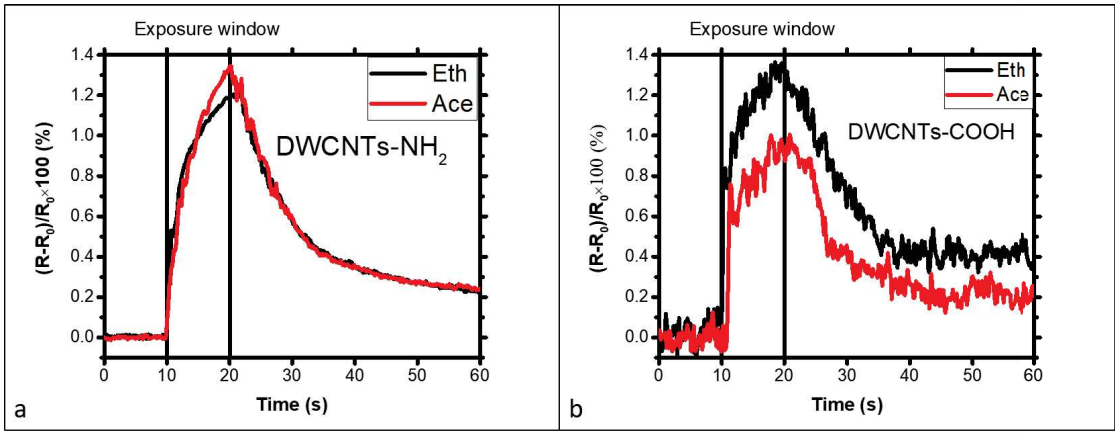


Figure 2.3: The signal of aminated (a) and oxidized (b) DWCNTs gas sensors to ethanol and acetone vapor exposure. The terms 'Eth' and 'Ace' in legend represent response to ethanol vapor and acetone vapor, respectively. R_0 is the initial resistance before exposure which is ca. 4 $k\Omega$ while R is the real-time resistance.

The two functionalized sensors give similar signal to Ethanol vapor (10000 *ppm*). The signal response is however quite weak with a relative resistance variation in the order of 1%. Oxidized DWCNTs sensor could discriminate ethanol vapor from acetone vapor. As oxidized DWCNTs sensor gives lower signal to acetone vapor exposure. However, this distinguishability of oxidized DWCNTs sensor is unfortunately not always so pronounced in repeated experiments.

To the conclusion, raw DWCNTs, oxidized and aminated DWCNTs exhibit poor sensitivity to ethanol and acetone vapor in our experiments. But it is obvious that chemical functionalization improves the sensitivity of DWCNTs gas sensors.

Gas Detection Mechanism

Raw DWCNTs Gas Sensor It has been studied that the modulation of Schottky barrier is the reason why CNTs field effect transistor (CNT-FET) based sensors are sensitive to alcohol[8][9][10][11][9][12]. However, that is for semiconductor CNTs. Since the DWCNTs we are using are metallic at room temperature, we rule out this mechanism in our case. We mention in the following two other possible mechanisms for explaining the weak resistance change observed upon ethanol and acetone exposure.

The first one is physisorption induced charge transfer. The ethanol or acetone molecules are trapped in interstitial space, junction between DWCNTs or/and pore of DWCNTs, or non chemical binded to surface of DWCNTs. And charge transfer is invoked from ethanol or acetone molecules to DWCNTs. As hole doped DWCNTs, the conductivity is reduced.

Another potential mechanism is that ethanol or acetone molecules interact with defect sites in DWCNTs. Especially those defect sites that are generated through purification process. As explained in Ref.[13], absorption of polar organic molecules on these defect sites induce charge transfer, because of polar nature of CNTs surface, as shown in Figure 2.4.

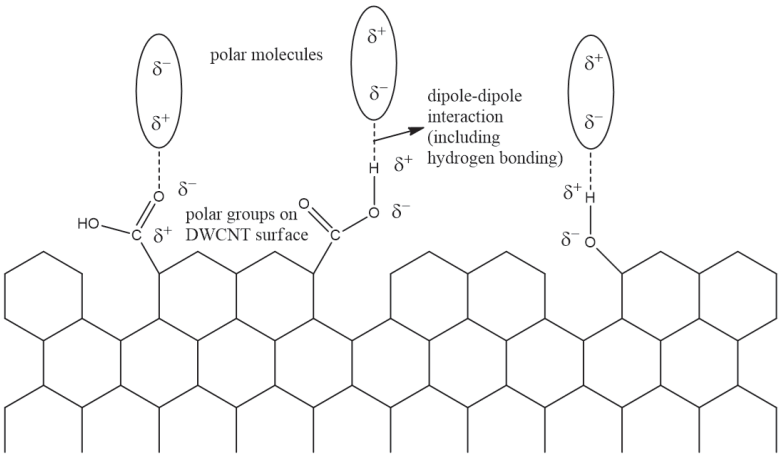


Figure 2.4: Dipole-dipole interaction between polar molecules and polar surface of DWCNT

In any case, these mechanisms are quite rare at room temperature, because the experimental variation of devices' resistance remain weak.

Functionalized DWCNTs Gas Sensor It is obvious from Figure 2.2 and Figure 2.3 that the functionalized DWCNTs gas sensors exhibit higher sensitivity to either ethanol or acetone vapor exposure compared to raw DWCNTs gas sensor. Therefore, besides the physisorption mechanism, we believe that the increased 'defect sites' by functionalization, i.e. the functional groups, is the main reason that improve DWCNTs sensitivity.

From Section 1.2.2, we know that the oxidized DWCNTs contain carboxyl groups on the surface. The carboxyl group can form hydrogen bonds with hydrogen bond donor or/and acceptor *via* its carbonyl oxygen and hydroxyl hydrogen, as illustrated in Figure 2.5. Depending on the charge transfer through two hydrogen bonds, the adsorbed molecules alter the charger carrier density of DWCNT. Consequently, the conductance of the sensor is changed.

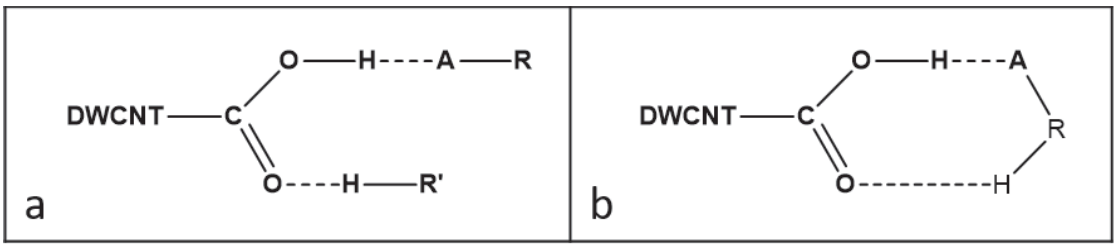


Figure 2.5: Schematic of hydrogen bonds. *A* represents atoms of strong electronegativity with lone pair(s) electrons.

Ethanol molecule has a hydroxyl group, which plays as both hydrogen bond donor and acceptor. As a donor, the hydrogen bond is formed between the hydrogen atom and carbonyl oxygen in carboxyl group on oxidized DWCNT. This type of bond improve the charger carrier density of oxidized DWCNTs as a positive charge transfer occur from ethanol molecule to oxidized DWCNT. When it is hydrogen bond acceptor, the oxygen atom of hydroxyl group connect with the hydroxyl hydrogen of carboxyl group on oxidized DWCNT. In this configuration, a positive charger transfer happen from oxidized DWCNT to ethanol molecule inducing a reduction of charge carrier density in the oxidized DWCNTs.

The two types of hydrogen bonds can be formed independently between one carboxyl group and two ethanol molecules, Figure 2.5 (a), or on carboxyl group and one ethanol group, Figure 2.5 (b). In Ref.[14], S. Aloisio et al. studied the hydration of formic acid with water molecule(s) in which there are three basic types of hydrogen bonds, Figure 2.6.

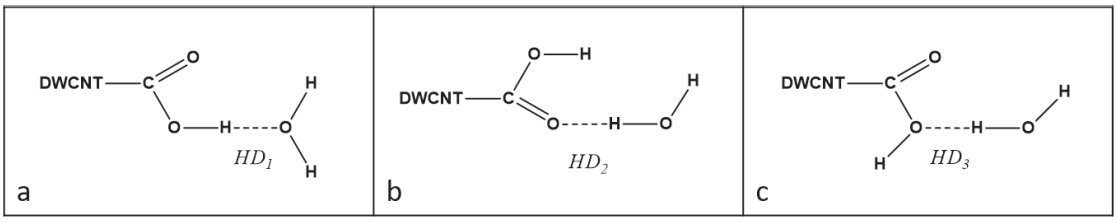


Figure 2.6: Three type of hydrogen bonds of carboxylic acid and water molecule.

Alexey B. Nadykto and Fangqun Yu have calculated the most stable configuration of hydrogen bonds between a formic (or acetic) acid molecule[15] and water molecule. Two

hydrogen bonds, HD_1 and HD_2, can be formed, one contains one formic (or acetic) acid molecule and one water molecule. In the second configuration, there are two hydrogen bonded water molecules of which one water molecule forms HD_1 bond and another one forms HD_2 bond with one formic (or acetic) molecule. Though two types of hydrogen bond induce different charge transfer between ethanol molecules and oxidized DWCNTs. As calculated in Ref.[14], the order of the length of hydrogen bonds is $HD_1 < HD_2 < HD_3$, which indicates the order of binding energies of three types of hydrogen bond. Meanwhile, in HD_1, oxygen of water acts as charge donor, while in HD_2, oxygen of carboxyl group acts as charge donor. As a result, there is a charge transfer from water to carboxyl group, thereby the nanotube. Consequently, the conductance of oxidized DWCNTs (film) reduced.

During ethanol vapor detection, between carboxyl group and ethanol, we hypothesize that hydrogen bond of configuration depicted as in Figure 2.7 is formed. From the discussion above, we expect a negative charge transfer occurring from ethanol to oxidized DWCNTs. Then, the conductance of oxidized DWCNTs is reduced from absorption of ethanol.

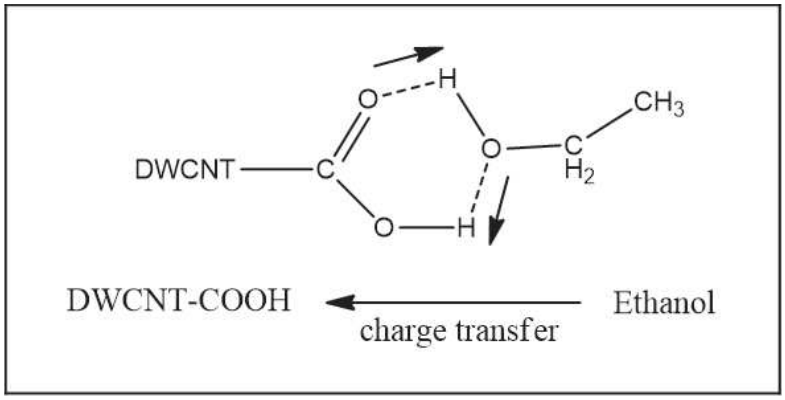


Figure 2.7: Hypotheses of hydrogen bond between ethanol and carboxyl group of oxidized DWCNTs. The arrows indicate negative charge transfer through hydrogen bond.

In the aminated DWCNTs, the hydroxyl group is replaced with $-\mathrm{N(H)-C(H_2)-}$ $-\mathrm{C(H_2)-C(H_2)-NH_2}$. Compared to the oxidized DWCNTs, we expect hydrogen bonds formed between ethanol molecules and the functional groups. Negative charge is transferred from ethanol to aminated DWCNTs. As a result, the p-type aminated DWCNTs' charge carrier density is reduced which also increases the resistance of aminated DWCNTs.

2.4.2 Complex Detection

Ammonia Vapor Detection

The DWCNTs sensors were first exposed to ammonia vapor. Since some water vapor is present in ammonia vapor exposure, a control experiment of water vapor exposure is

necessary. Because the ammonia concentration is very low, the amount of water vapor from ammonia solution approximates to it is from pure water in the same condition. In the following experiments we thus compare the signal of our devices when confronted to ammonia vapor or to the pure water vapor.

Raw DWCNTs Gas Sensor: When the raw DWCNTs sensor is exposed to ammonia and water, there are very distinct but low sensitivity as depicted in Figure 2.8. The black line is the response to water vapor and the red line is response to ammonia. This is one sensor expected to have high sensitivity, of which the resistance is ca. 91 $K\Omega$, and the raw DWCNTs film-Au electrode connection is metallic.

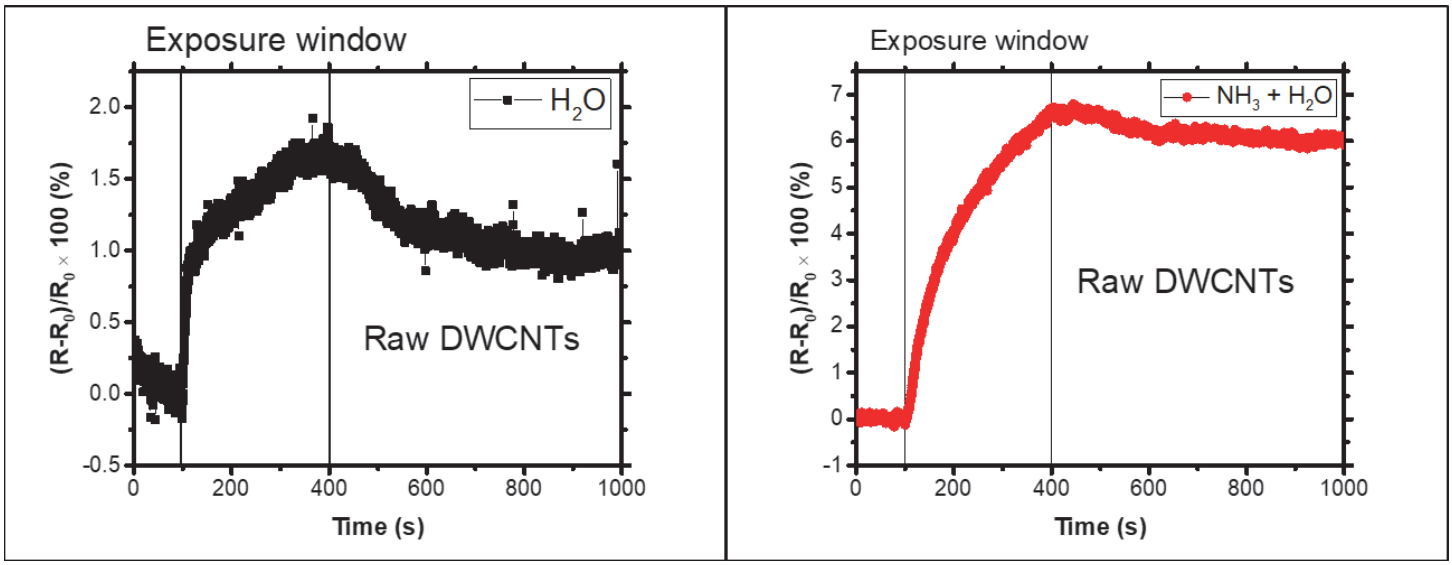


Figure 2.8: A raw DWCNTs sensor's response to water vapor (left)and ammonia solution vapor (right). R_0 is the initial resistance before exposure which is ca. 91 $k\Omega$ while R is the real-time resistance.

The relative resistance variation reaches less than 2% for pure water, while it reaches 7 % in the case of ammonia vapor.

There is thus a clear contrast in the signal between water vapor and ammonia solution vapor exposure. The ammonia detection mechanism has been explained in Ref.[16]. However, it is difficult for pristine carbon nanotube to adsorb ammonia. The interaction between pristine carbon nanotube and ammonia is weak and induce small amount of charge transfer[17][18][19]. As a consequence the resistance variation remains small. However, when exposed to the ammonia, the Schottky barrier at junction of raw DWCNTs film and Au electrode is also modulated by the ammonia molecules as explained in Ref.[16]. Therefor, a more significant signal appears. However, compared to functionalized DWCNTs sensors, the raw DWCNTs sensors have very small sensitivity to either water or ammonia vapor.

A striking observation can also be made in Figure 2.8, the recovery is rather poor within the time set. When there is only water vapor, it recovered ca. 40% of the resistance variation from exposure. And when ammonia is added, it recovered only ca. 9% of resistance variation from exposure. Compared to functionalized DWCNTs sensors (shown in following sections), the recovery of raw DWCNTs sensor from water vapor and ammonia vapor exposure is limited. No matter the gas is water vapor or water vapor with ammonia, the recovery is far from as good as oxidized DWCNTs sensors and close but less good to aminated DWCNTs sensor.

To the conclusion, the raw DWCNTs film is sensitive to ammonia. Even in the environment where there is water vapor of more than 300 times concentration to the ammonia, the raw DWCNTs film is capable of distinguishing ammonia from water. However, with the presence of ammonia, the recovery quality is reduced dramatically.

Oxidized DWCNTs Gas Sensor: The oxidized DWCNTs sensors are first exposed to ammonia vapor in the same condition then the same control experiment with pure DI water vapor is performed. As being functionalized with carboxyl group, we expect higher sensitivity from oxidized DWCNTs to both water and ammonia vapor.

Like it is plotted in Figure 2.9, an oxidized DWCNTs sensor shows relatively high sensitivity to ammonia and water compared to raw DWCNTs sensors.

Compared to raw DWCNTs sensor, (Figure 2.8), the sensitivity is improved more than 2 times for both ammonia and water vapor. The relative resistance variation now reaches 5 % for pure water vapor and 16 % for ammonia vapor. The response time is also improved. There are clear different resistance evolution when the two kinds of sensors are exposed to ammonia and/or water vapor, which will be discussed in an independent section later.

Besides the improvement of sensitivity, the recovery from exposure is also improved compared to the raw DWCNTs sensor. It recovers ca. 46% of resistance variation from ammonia exposure, and ca. 50 % from water exposure for the oxidized DWCNTs sensor within the time set. This indicates that the oxidation is not only a way to improve DWCNTs sensitivity towards some chemicals but also a mean to ameliorate DWCNTs self-recovery from these chemical exposures.

aminated DWCNTs Gas Sensor: In Figure 2.10, the typical response of aminated DWCNTs gas sensor exposed to ammonia vapor in the same condition is presented. It is clear that the aminated DWCNTs gas sensor exhibits same behaviour as oxidized DWCNTs gas sensor to the ammonia vapor exposure: the functionalization increases DWCNTs sensitivity to ammonia vapor. In this case, it is more than 3 times higher than raw DWCNTs sensor's sensitivity to ammonia vapor. The relative resistance variation reaches 23 % for ammonia vapor but remains as low as 3 % for pure water vapor.

This is a very interesting result that the amination improves DWCNTs sensitivity to ammonia while maintaining relative low sensitivity to water. From this point of view, this type of surface functionalization is an excellent candidate material for developing ammonia sensors.

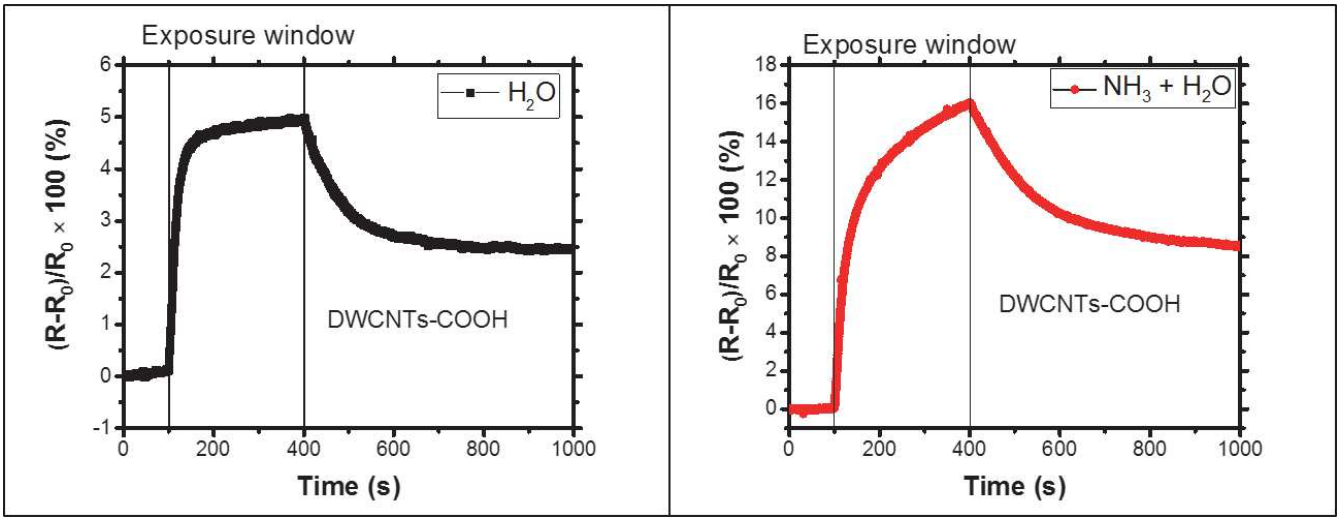


Figure 2.9: The signal of an oxidized DWCNTs sensor to water (left) and ammonia (right) vapor. R_0 is the initial resistance before exposure which is ca. 14 $k\Omega$ while R is the real-time resistance.

For the recovery of exposure, compared to raw DWCNTs sensor, there is 25% recovery of resistance variation from ammonia vapor exposure, and 48% recovery from water vapor exposure within the time set. Though it is improved compared to raw DWCNTs sensor, the time span is expected rather long from the recovery curve. The recovery from water vapor exposure is close to the one of oxidized DWCNTs sensor.

2.4.3 Gas Detection Mechanism Discussion

Ammonia Detection

Raw DWCNTs Gas Sensor: Sensing mechanisms for carbon nanotube based sensors have been discussed in the literature. It has been studied that the modulation of Schottky Barrier formed at CNT-metal contact dominates the sensing performance at room temperature[16] for semiconducting CNT based field effect transistor. But the DWCNTs used in this thesis are metallic conductor. Thereby, non Schottky barrier is expected at DWCNT-gold contact interface. Thus the signal is expected from other origins. I will propose two possible mechanisms.

The first one falls into debates is that the absorption of ammonia and/or water molecules are tracked into defects in raw DWCNTs. In Figure 1.7 of Section 1.3, among all the Stone-Wales defects, the carboxylic group ended sites, which are also the main yields of oxidation, have great attraction to ammonia and/or water molecules. Ammonia and/or water molecules are able to form hydrogen bonds with carboxyl group, which will be depicted in the next section. This interaction results in a electron doping of DWCNTs. Thus, the conductance of DWCNTs is reduced. The role of defects has already been studied by Joshua A. Robinson et al.[20]. With the condition set in the

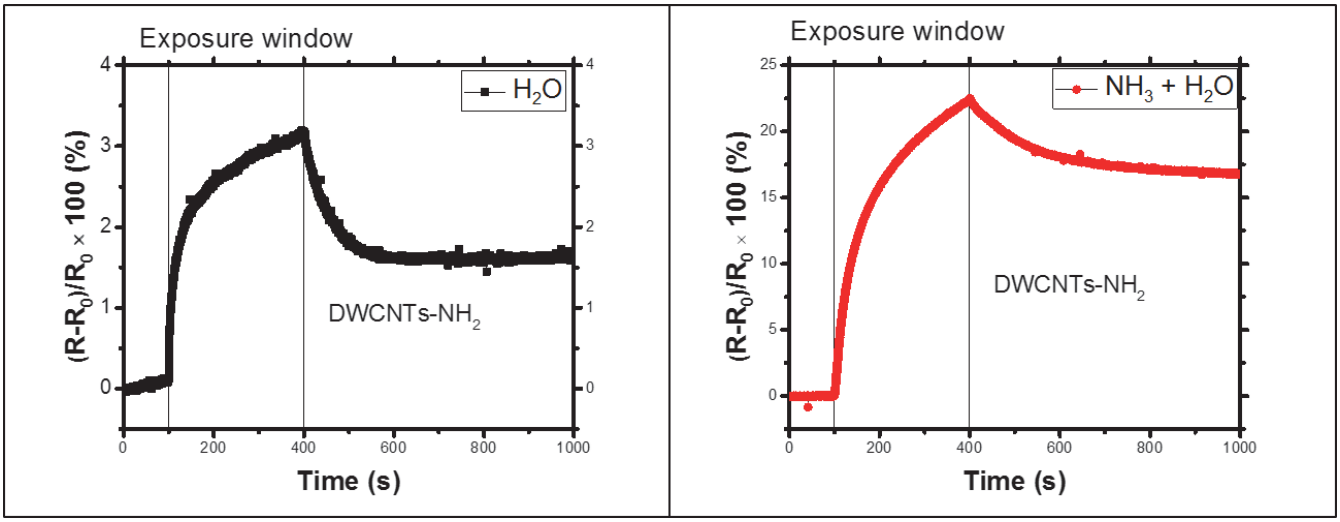


Figure 2.10: The signal of aminated DWCNTs sensor to the ammonia and water vapor exposure. R_0 is the initial resistance before exposure which is ca. 4 $k\Omega$ while R is the real-time resistance.

reference, the defect sites dominate the electrical response to the presence of chemical vapors.

The second possible mechanism is non chemical adsorption. The gas molecules are weakly binded on the surface or inside of nanotube, which is identified as physisorption. Since a film of DWCNTs is deposited, the gas molecules may also be absorbed in DWCNTs networks, the junction between DWCNTs or interstitial among DWCNTs. The physisorption induces charge transfer between DWCNTs and absorbed molecules. In Ref.[21], Jijun Zhao et al. have computed charge transfer between physical absorbed gas molecules and SWCNTs based on density functional theory. The computation shows that charge transfer occurs from absorbed ammonia and/or water molecules to SWCNTs. Thereby, the electrical conductance of SWCNT is reduced. The physisorption occurs for all types of molecules and for both metallic and semiconducting CNTs. Thus, the physisorption of ammonia and/or water molecules also leads to raw DWCNTs sensor's resistance increase. This inter-tube modulation plays a key role in nitrotoluene detection from work of Jing Li and co-workers[22]. As explained in the Section 1.4.3, our devices exhibit complex origin of resistance. The energy barrier between two contact DWCNTs creates the junction resistance. This energy barrier is tuned by the gas molecule(s) which is/are adsorbed at the interface of the junction. As a result, when ammonia/water molecules are adsorbed in our case, the junction resistance is increased.

In our case, these two mechanisms exist at the same time, because the purification results in defects inevitably and the physisorption occurs regardless of existence of defects. So, the resistance increases can be attributed to these two mechanisms.

Oxidized DWCNTs Gas Sensor: Same mechanisms can be considered for oxidized DWCNTs gas sensor. The first one is the same physisorption as discussed in previous section and will not be elaborated again. The second one is the charge transfer induced from interaction between functional groups and absorbed molecules.

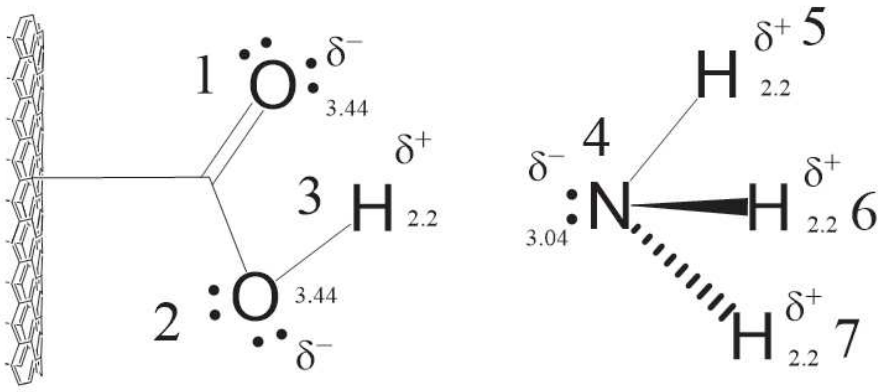


Figure 2.11: Polarization in carboxyl group and ammonia molecule. The integer is the index of atoms. Notes that the 5, 6 and 7 hydrogen atoms are equivalent to each other here. The decimal numbers next to atoms are corresponding element electronegativities. As oxygen and nitrogen have stronger electronegativity, they have negative potential in each dipole. δ with superscripts '+' and '−' denote the positive and negative partial charge.

Oxidized DWCNTs are the DWCNTs functionalized with carboxyl groups on the surface as described in Section 1.2.2. Because of differences in electronegativity between oxygen and hydrogen atoms, oxygen and carbon atoms, there is polarization in carboxyl group. Thereby oxygen atoms show partial negative charge and hydrogen shows partial positive charge (Figure 2.11). In addition, the ammonia is a polar molecule, (Figure 2.11). The nitrogen atom is the negative end of dipole in ammonia molecule.

The chemical adsorption occurs between ammonia molecules and carboxyl groups. From the configuration of partial charge in carboxyl group and ammonia molecule, as depicted in Figure 2.11, there are many possibilities of forming hydrogen bond(s) between carboxyl group and ammonia molecule. An investigation of thermodynamic stability of hydrogen-bonded complex of small carboxylic acids with ammonia has been done by Nadykto and Yu *via* quantum chemical calculations method[15]. In their work, they have performed density functional theory and Ab initio calculations on isomers formed between formic acid or acetic acid and ammonia. The most stable isomer configuration is presented in Figure 2.12. In another theoretical study from Zhao et al[23], Ab initio molecular orbital calculations were carried out on isomer, formic acid-ammonia, acetic acid-ammonia and benzoic acid-ammonia, which shows agreement on the most stable configuration with work of Nadykto et al.

The hyperconjugative interaction (i.e. charge transfer) occurs in accompany with hydrogen bonds formation from lone pair of hydrogen bond acceptor, nitrogen or oxygen,

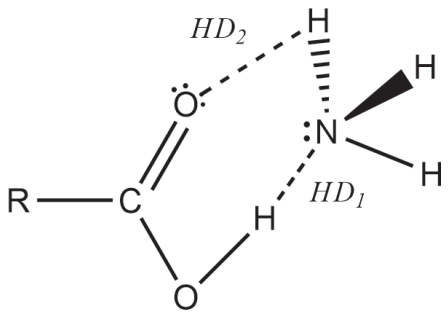


Figure 2.12: Most stable configuration isomer formed by carboxylic acids and ammonia. Two hydrogen bonds are formed, 'HD_1' and 'HD_2'.

to the antibonding σ^* orbital (O−H, N−H) of donor. This interaction begets a prolongation of the O−H or N−H bond, which are 0.04 and 0.01 Åin the benzoic acid-ammonia complex, respectively[23]. This means that the interaction of HD_1 hydrogen bond is stronger that it is of HD_2 hydrogen bond. It has also been shown that the lengths of two hydrogen bonds are very different, $HD_1 < HD_2$[23], which indicates that the HD_1 hydrogen bond energy is higher than it is of HD_2 bond energy. And as indicated in Ref.[23], the charge transfer interaction is 60 - 70 $kcal/mol$ for the short hydrogen bond and 20 - 30 $kcal/mol$ for the long hydrogen bond. Thereby, charge transfer occuring in the formation of HD_1 hydrogen bond is greater than it is in the formation of HD_2 hydrogen bond. The sum of two interactions results in a transfer of negative charge from ammonia to carboxylic acid. Similarly, there is a negative charge transfer from ammonia to the oxidized DWCNTs when exposed to ammonia vapor. Because our DWCNTs are p-type conducting, the adsorption of ammonia leads to a decrease of charge carrier, holes, density thereby resistivity is increased as observed during ammonia vapor exposure.

There are other possible configurations of hydrogen binding between DWCNT−COOH and NH_3. Figure 2.13 shows four hydrogen binding configurations. However, there are less stable than the one in Figure 2.12. So forth, only the most stable configuration is taken into account for analyzing charge transfer between oxidized DWCNTs and ammonia.

Aminated DWCNTs Gas Sensor: A functional entity of aminated DWCNTs consists in an amino group, a carbonyl oxygen, and four $-CH_2-$ and one N−H, Figure 1.5. The H−N(R)−C(R)=O linkage in the functional group is a model for the *cis* peptide linkages in protein and in the functional groups of nucleic acids. It has been studied[24][25][26] that the H−N(R)−C(R)=O linkage can form hydrogen bonds with water or ammonia molecules. From the research of Ref.[24] and Ref.[26], the two hydrogen bonds length are very close to each other with, no matter one or two water molecules. Though two references, [24] and [26], have contrary sign of the length difference between hydrogen bonds C=O$\cdots$H−O(H) and N−H$\cdots$O(H_2), it is extremely small, ca. 0.01 Å. Thereby the charge transfer between the linkage and one water molecule barely changes the charge density of nanotube. However it has clear shorter length of N−H$\cdots$N(H_3) than it is of C=O$\cdots$H−N(H_2) when ammonia molecule is bonded. Thus, a negative charge transfer from ammonia to nanotube is expected, which reduces the charge density

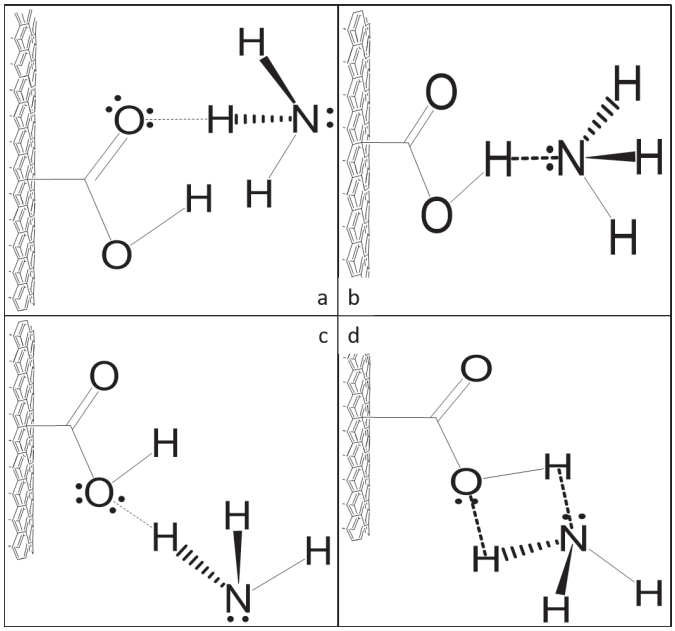


Figure 2.13: Other possible configuration hydrogen binding between carboxyl group and ammonia.

of nanotube as a consequence.

Furthermore, the existence of $-C(H_2)-C(H_2)-C(H_2)-$ provides three potential hydrogen bonds donor sites. Therefore, abundant hydrogen bonds, $-C-H\cdots O(H_2)$ or $-C-H\cdots N(H_3)$, lead to positive charge transfer from nanotube to absorbed molecules.

As mentioned in Section 1.4.3, between functionalized DWCNTs, the junction consist of physical contact and polar interaction through functional group (Figure 2.14 (a)). Figure 2.14 (b) illustrates a simple case in which an ammonia molecule is adsorbed at the interface of junction of oxidized DWCNTs. Because ammonia is polar molecule, it interacts with the polar functional groups. Thus, ammonia molecule tunes the shape of energy barrier, such as the distance between two DWCNTs and the height of the energy barrier, thereby, the charge carrier transfer through the polar interaction is weaken by the ammonia molecule. Because the improvement of conduction in the functionalized DWCNTs film is mainly due to the reduction of junction resistance, the influence of adsorbing ammonia molecules is more significant to functionalized DWCNTs film than it is to raw DWCNTs film. Thereby, we consider that the physisorption in the functionalized DWCNTs sensor also plays a key role to the gas detection.

More complex configuration of hydrogen bonds are possibly formed from the basic configurations above. In any case, for the chemical bonding and physisorption, the presence of water molecule(s) or ammonia molecule(s) leads to a decrease of conductivity of functionalized DWCNTs, and this effect is much stronger for ammonia adsorption.

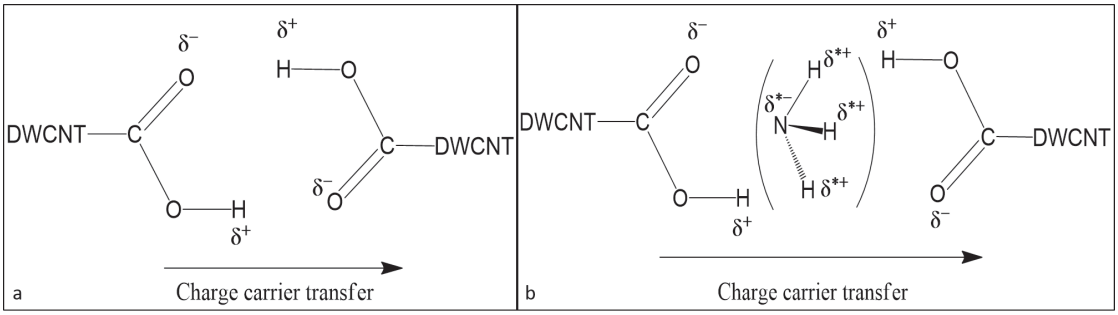


Figure 2.14: The junction of polar interaction before (a) and after (b) adsorbing an ammonia molecule. Assuming the charge carrier flow from left to right DWCNTs when electric field applied.

Water Detection

Raw DWCNTs Gas Sensor: Like ammonia, water molecules are absorbed *via* two paths: physisorption and defect binding. As modeled in Ref.[21], physically absorbed water molecules donate charges to CNTs, thereby, reduces the conductance of CNTs. As the effect of water molecules that are binded to defects, I will only consider the carboxyl group ended defect sites. This effect will be depicted in the following section, because it is similar to the situation where water molecules are adsorb on oxidized DWCNTs.

Functionalized DWCNTs Gas Sensor: Despite physisorption of water, the interaction between water molecules and functional groups raise significant effect on water detection. To discuss the functional groups effect, we first examine interaction between carboxyl group and water molecule(s).

In Ref.[15], A. B. Nadykto et al. have studied the hydrogen bonding between simple carboxylic acid and water or ammonia. In their work, formic acid and acetic acid have two most stable isomers configuration with water molecule(s) through hydrogen bonds, Figure 2.15.

Here, with oxidation, the carboxyl groups facilitate the adsorption of water molecules on the surface of DWCNTs. In Ref. [15], formic acid-ammonia and acetic acid-ammonia isomers have multiple stable configurations. Taking into account that carboxyl groups are grafted on DWCNTs surface, two of the most stable configuration as calculated in Ref. [15] can be formed in our case, where R denotes DWCNTs in Figure 2.15.

Like the discussion of ammonia adsorption by carboxyl group, there are charge transfer from water molecule to carboxyl group, thereby it reduces the hole density in DWCNTs and consequently reduces the conductivity. This model could explain explains our experimental observations.

In aminated DWCNTs, although hydroxyl group in carboxyl group is replaced by $-NH-CH_2-CH_2-CH_2-NH_2$ chain, the nitrogen of $-NH-$ plays same role as oxygen in hydroxyl group. Therefore, we assume similar hydrogen bonds configuration formed between water molecules and aminated DWCNTs. It results in a charge transfer from

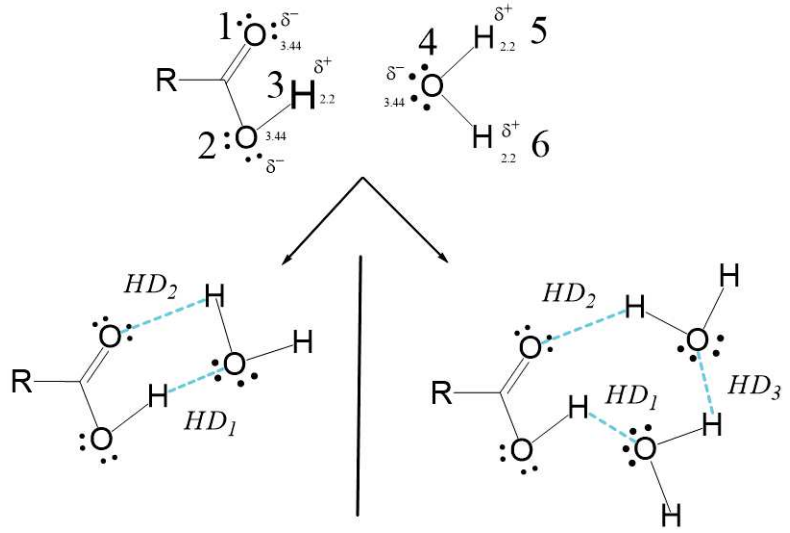


Figure 2.15: (a) The partial charge configuration of carboxyl group on DWCNT and water molecule. The integers are the index of atoms and the decimal are the electronegativity of corresponding element. δ with superscripts '+' and '−' denote the positive and negative partial charge. (b) and (c) are the hydrogen binding configurations of two of the most stable isomers as calculated in Ref. [15]

water molecule to aminated DWCNTs. Besides, water molecule can hydrogen bond to amino end of functional group, which also induces charge transfer from water to aminated DWCNTs.

2.4.4 Multiple exposure

To investigate the reproducibility to gas exposure, we tested our sensors with multiple, long duration and continuous gas exposures. Since we find that the functionalized DWCNTs sensors are highly sensitive to ammonia, we tested only oxidized and aminated DWCNTs sensors to ammonia vapor exposure. The control experiment remains DI water vapor exposure.

The test settings are described as follow: a device integrated with both aminated and oxidized DWCNTs is repeatedly exposed to 17 *ppm* ammonia vapor (in the presence of 5690 *ppm* water vapor), each exposure is ca. 1000 *s*. In this device, two sensors are fabricated from oxidized DWCNTs and two sensors are fabricated from aminated DWCNTs. Since the Keithley 2450 only allows one measurement at a time, one oxidized DWCNTs sensor is selected as the monitor of the whole exposure.

Figure 2.16 thus presents the response of an oxidized DWCNTs gas sensor exposed to ammonia vapor. It is similar to the previously presented exposure in Figure 2.9, except that now due to a large time window of exposure, the stabilization of the signal when gas molecule interacts is reached and an equilibrium state is observed. In the same way, the evolution of the recovery after gas exposure is now extended on a larger

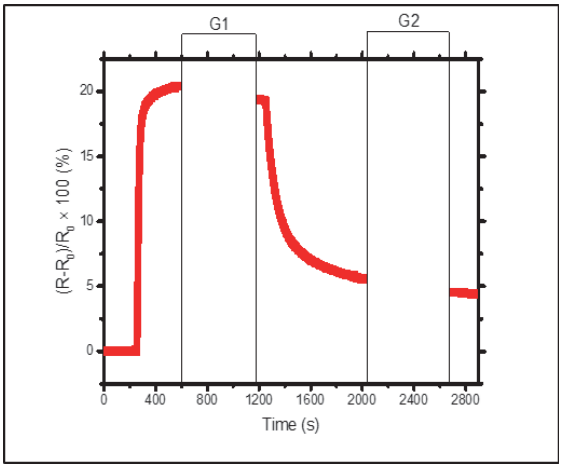


Figure 2.16: Intermittently measured signal of the an oxidized DWCNTs sensor to one cycle of ammonia vapor exposure. $G1$ and $G2$ gaps represent the time duration when measurement was taken on other sensors.

time scale. Figure 2.16 indicates that an equilibrium state is reached upon gas exposure in approximately 200 seconds (rising time), while after the end of the exposure, the recovery time before reaching a steady state is much larger ($> 1400\ s$).

With the exposure setting described, four cycles of ammonia vapor exposure were carried out. The results are plotted in Figure 2.17. The initial resistance of each sensor is ca. 1.6 $k\Omega$ (a), ca. $46k\Omega$ (b), ca. 360 Ω (c), ca. 10 $k\Omega$ (d). Sensors (a) and (c) contains oxidized DWCNTs, while sensors (b) and (c) contains aminated DWCNTs.

It can be seen that the oxidized DWCNTs sensors's (a, c) signals are "relatively" stable along the exposure cycle. All the sensors exhibited a poor recovery in first gas detection cycle. The main point is that starting from the second exposure, it takes less time for sensors to recover to the state that is close to what it was before exposure. The recovery from the forth exposure of the sensor (a) is not plotted, but also agrees with this conclusion.

It is clear that the aminated DWCNTs sensors exhibit the same response behaviour to ammonia compared to oxidized DWCNTs. However, by comparing the response of oxidized DWCNTs and aminated DWCNTs sensors to successive ammonia exposure, is is clearly shown that the recovery between successive exposure, i.e. the reversibility of the gas molecules adsorption, is much efficient and fast in the case of oxidized DWCNTs. We think that this reflects the differences in the strength of the interaction taking place in these two type of DWCNTs, as described in previous sections.

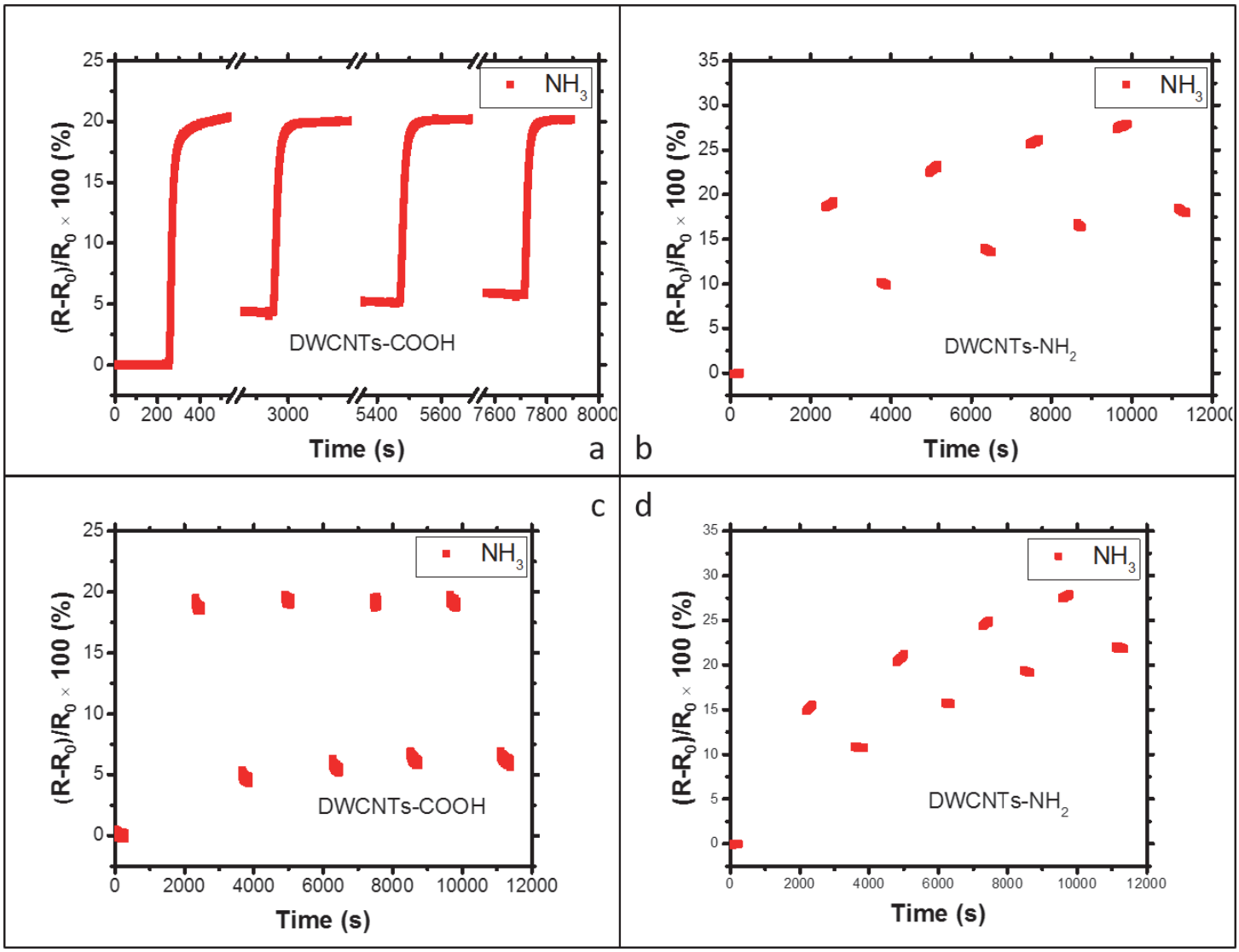


Figure 2.17: Repeated exposure to 17 *ppm* ammonia vapor (in the presence of water vapor) on oxidized DWCNTs gas sensors ((a), (c)) and aminated DWCNTs gas sensors ((b), (d)). Four sensors are integrated in one device. Sensor (a) is arbitrarily selected as monitor of exposure process. As 'becoming stable' is determined by observation during experiment, each exposure cycle has different duration.

Control experiment of water exposure: With the exposure setting described previously, three cycles of water vapor were carried out. The results are plotted in Figure 2.18. Since the device has been previously exposed to ammonia vapor, the resistance of each sensor is higher than its original resistance.

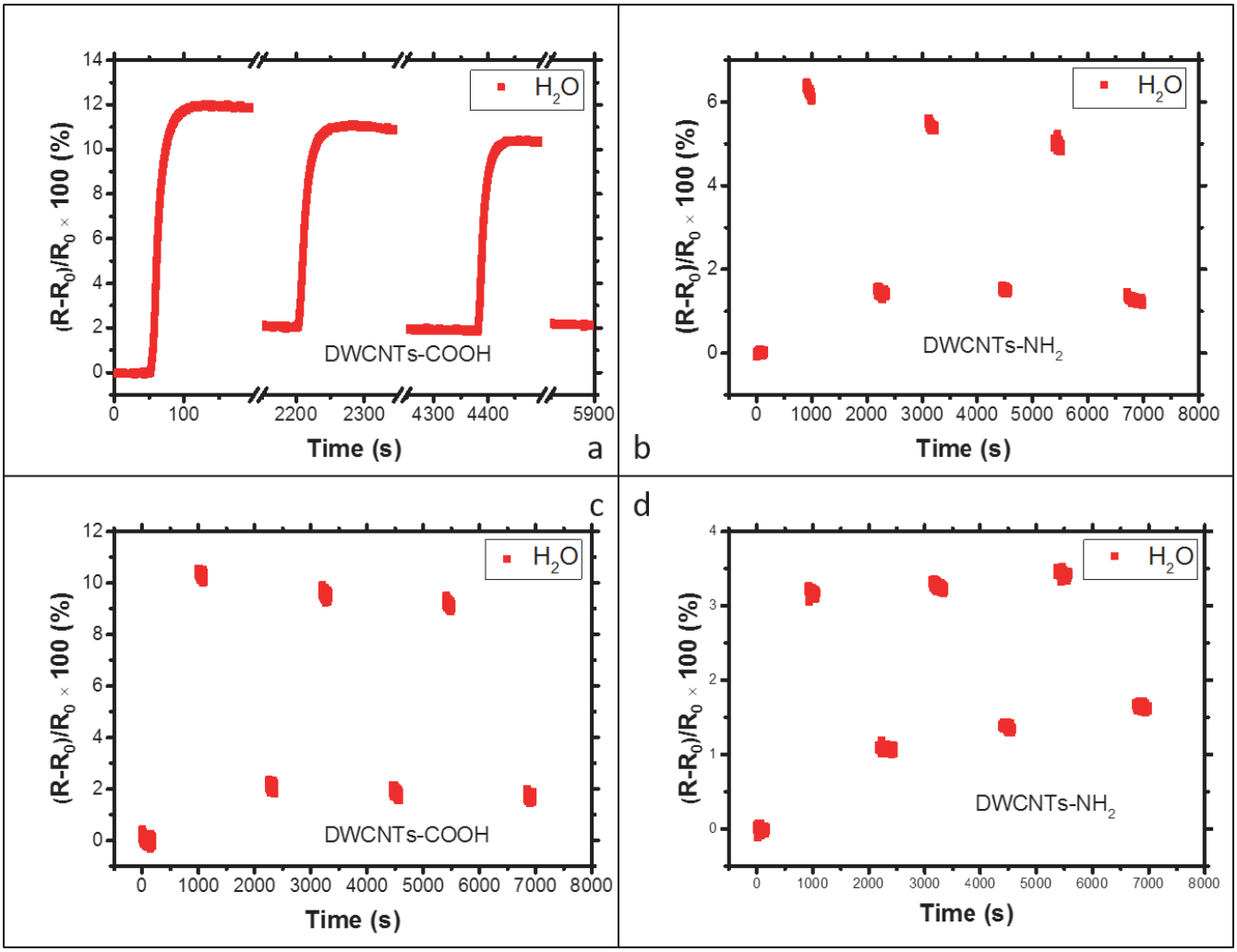


Figure 2.18: Control experiment of repeated exposure to 5690 *ppm* water vapor (in the absence of ammonia vapor) on oxidized DWCNTs gas sensors ((a), (c)) and aminated DWCNTs gas sensors ((b), (d)) corresponding to the sensors in Figure 2.17.

It is clear that the signal detected by oxidized DWCNTs sensors is much higher than that of aminated DWCNTs. The recovery of oxidized DWCNTs sensors is very stable. Despite the differences of resistance between (a) and (c) sensors, both recovered back to a very similar state where the relative resistance responses after recovery are very close to each other. In the case of oxidized DWCNTs sensors, the relative resistance response

of equilibrium state is decreasing with the increase of exposure cycle. This is not always the case for aminated DWCNTs sensors. Though the two aminated DWCNTs sensors have different behaviour to the water exposure in terms of the intensity and evolution of relative resistance response of each equilibrium and recovered state, their signals remain of quite low intensity to the water vapor exposure ($6\% - 3\%$).

Associated with ammonia vapor exposure, it is clear that with the presence of small amount of ammonia, ca. 17 *ppm*, the signal is about two times higher than what it is to the pure water vapor, ca. 5700 *ppm*, exposure. It is also clear that it takes less time to recover from water vapor exposure, and the recovered resistance of each sensor is very close to the initial resistance. As a conclusion, the slowed down recovery from ammonia vapor exposure is due to the absorption of ammonia. Besides, the degree of recovery from ammonia vapor exposure is lower than it is from water vapor exposure. To summarise, longer duration of recovery and lower degree of recovery are observed in the presence of small amount of ammonia.

An interesting phenomenon can be noted from Figure 2.18 when water vapor exposures are repeated, notably in the case of oxidized DWCNTs, after the second exposure the signal recover its original level. This result also means that if a sensor of this type no longer exhibits this property this would be the signature of the presence of some traces of other molecules capable to interact strongly with the DWCNTs surface inside the water vapor. In other words, this suggests that oxidized DWCNTs based sensors are quite immune to humidity.

Conclusion of Repeated Exposure: Oxidized DWCNTs sensors keep a high stability for ammonia detection performance from repeated and prolonged ammonia vapor exposures. Oxidized and aminated DWCNTs sensors are both sensitive to ammonia. The oxidized DWCNTs sensors keep high sensitivity in repeated and prolonged ammonia vapor exposures. The high repeatability and stability is not dependent on oxidized DWCNTs film initial resistance. The oxidized DWCNTs sensors are also sensitive to water vapor but in a much smaller extend compared to ammonia vapor. The oxidized DWCNTs sensors remain much less sensitive to water vapor in repeated and prolonged exposure.

Aminated DWCNTs sensors show high sensitivity when ammonia is present in the ambient atmosphere. Once being exposed to ammonia, aminated DWCNTs sensors' sensitivity is reduced significantly if no active recovery method is used. Though the the resistance variation are not the same from exposure to exposure, due to the partial recovery of the sensor, aminated DWCNTs sensors maintain a good repeatability in repeated exposures. As depicted in Figure 2.10 and Figure 2.18, aminated DWCNTs sensors preserve low sensitivity to water vapor.

2.4.5 Discrimination

Detecting Formaldehyde Vapor

From Section 2.4.1, we learned that our sensors are capable of detecting acetone with a poor sensitivity. Acetone is the simplest Ketone, which structure is shown in Figure 2.19 (a). We thus expect that the oxidized DWCNTs sensors are also poorly sensitive to formaldehyde which has a structure as shown in Figure 2.19 (b). To verify this hypothesis, we first exposed the sensors to formaldehyde vapor of the same concentration, ca. 17 *ppm*, generated from its water solution. The control experiment is DI water vapor exposure.

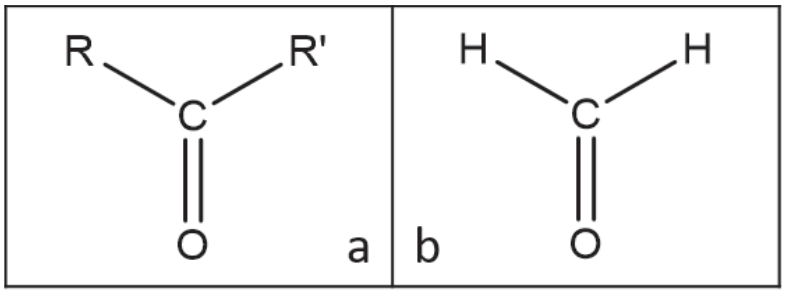


Figure 2.19: Schematic of Ketone (a) and Formaldehyde (b).

The same oxidized DWCNTs sensor that has been exposed to ammonia and water vapor in Section 2.4.2 is utilized to detect formaldehyde vapor. The result is plotted in Figure 2.20 (b). Figure 2.20 (a) is the sensor's response to water vapor exposure from Section 2.4.2

From Figure 2.20, it can be seen that oxidized DWCNTs sensor is merely sensitive to formaldehyde. When formaldehyde is presented in water vapor, the signal of oxidized DWCNTs sensor is only slightly increased (ca. 0.5%). The difference between two responses is too small even it is much larger than the signal noise which is miniature (ca. 0.02%).

While oxidized DWCNTs sensor has small distinguishable difference in response rate between formaldehyde vapor and DI water vapor exposure, aminated DWCNTs sensor is quite inert to formaldehyde in the same condition.

As shown in Figure 2.21, it is difficult to distinguish the signal differences between formaldehyde vapor exposure and water vapor exposure for aminated DWCNTs sensor in this experiment.

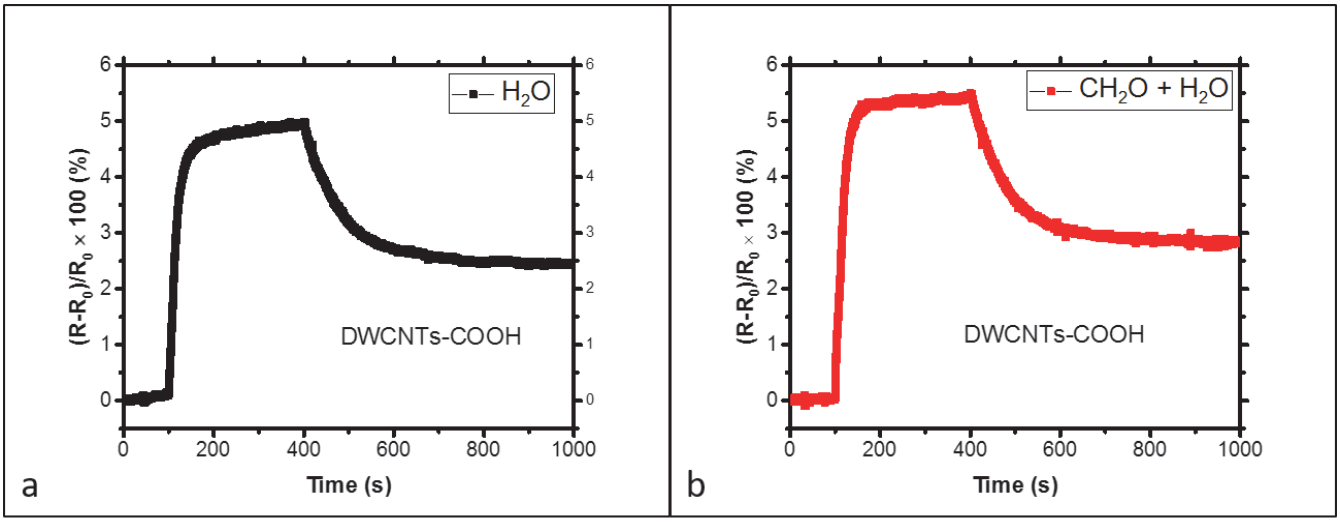


Figure 2.20: The signal response of oxidized DWCNTs sensor to pure DI water vapor exposure (a) and to formaldehyde vapor exposure (b).

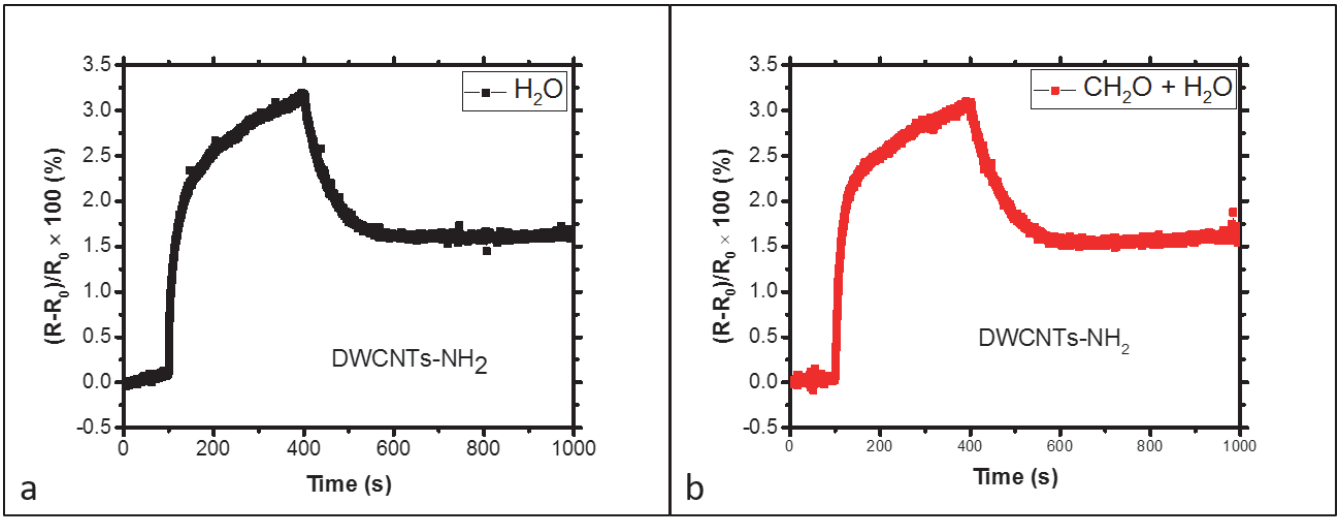


Figure 2.21: The signal response of aminated DWCNTs sensor to pure DI water vapor exposure (a) and to formaldehyde vapor exposure (b).

Multiple Formaldehyde Vapor Exposure: Two sensors, one oxidized DWCNTs sensor and one aminated DWCNTs sensor, are exposed to formaldehyde vapor for three cycles. The experiment process is configured as described in Section 2.4.4. The results are illustrated in Figure 2.22

In Figure 2.22, (a) and (b) are the signal of the oxidized and aminated DWCNTs sensors to three cycles of formaldehyde vapor exposure, respectively. The oxidized DWC-

NTs sensor was selected as monitor of exposure, which is the reason why its response figure have resistance evolution and data gaps characters.

We can observe that in the case of presence of small amount of formaldehyde in the gas vapor, the resistance of oxidized DWCNTs sensors does not recover between successive exposures. This contracts with the observation of Figure 2.18 and indicates that even if formaldehyde is hardly detectable with this kind of sensors by just looking at the signal jump under exposure, the dynamic of the recovery reveals its presence.

For the aminated DWCNTs sensor, it exhibits the similar response behavior to formaldehyde vapor exposure as to ammonia vapor exposure: it shows the best response in the first exposure, and shows smaller response in the following exposure cycles.

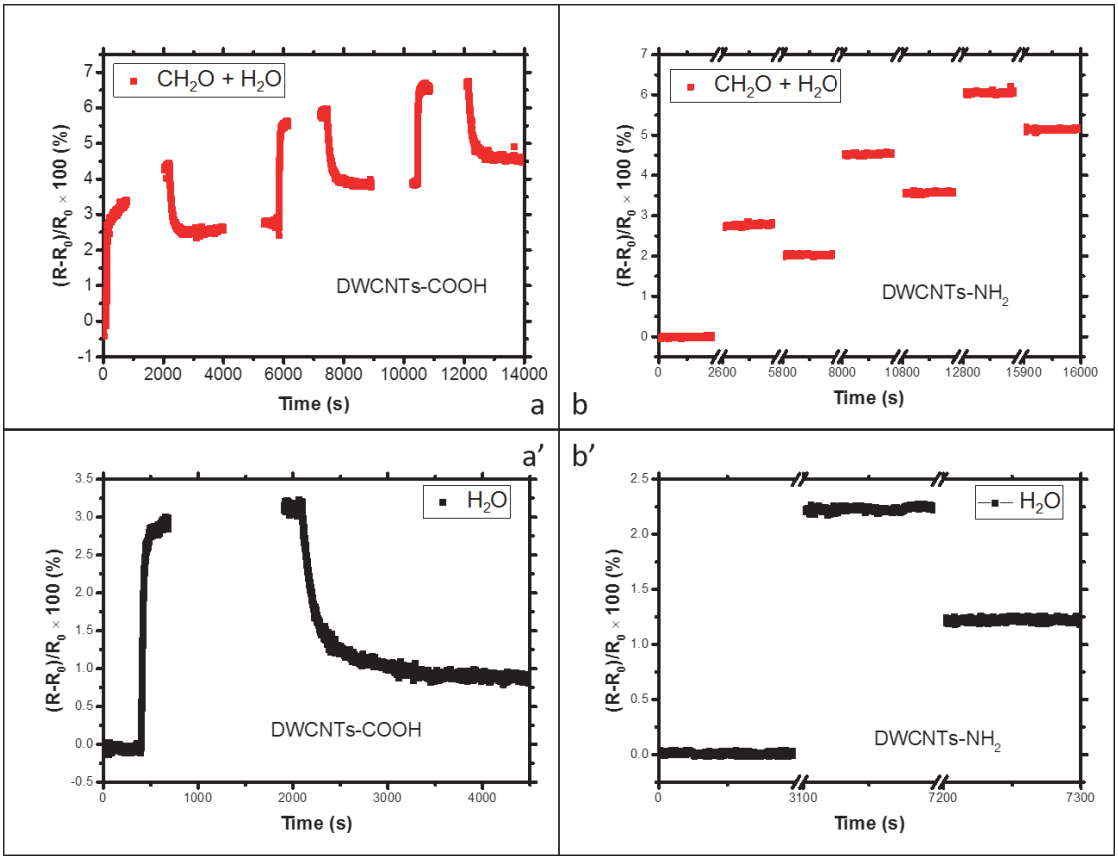


Figure 2.22: The signal of oxidized DWCNTs sensor (a) and aminated DWCNTs sensor (b) to repeated exposures of formaldehyde vapor. (a') and (b') are response of corresponding sensor to DI water vapor exposure, respectively. The R and R_0 are the resistance of sensor in real-time and initial resistance, respectively.

Discrimination of Gas Species

Conventional way of discriminating gases: The signal response. From Section 2.4.2 and 2.4.5, we learn that the functionalized DWCNTs sensors are sensitive to water vapor, ammonia vapor and formaldehyde because each kind of vapor cause different magnitude of signal.

Notice that there are two main differences between response curves to ammonia vapor and response curves to formaldehyde and/or water. The first one shows that oxidized DWCNTs is more sensitive to ammonia than water and/or formaldehyde, which is obvious to find from the amplitude of signal. The second is the dissimilarity in the time evolution of the resistance response. The curves of response to water vapor or to formaldehyde vapor are similar to each other that within a short time the resistances reach a 'plateau'. It is due to the saturation of absorption of water and/or formaldehyde molecules. While for ammonia within the exposure time, a plateau is never reached. This behaviour can be observed in Figure 2.23 for oxidized DWCNTs sensors and Figure 2.24 for aminated DWCNTs sensors.

Thereby, the saturation of adsorption of water molecules does not prevent the oxidized DWCNTs sensor from detecting the existence of ammonia.

We observed the similar results from aminated DWCNTs sensor. In Figure 2.24, it demonstrates the result of the signal to DI water vapor, formaldehyde vapor and ammonia vapor exposure.

Both type of functionalized DWCNTs sensors are much more sensitive to ammonia than to water and formaldehyde. Within exposure window, the response to ammonia vapor is $6-7$ times greater than the response to water and/or formaldehyde vapor. But as pointed above, this is not the only noticeable difference. It is clear that for different gas molecules the shape of the signal, more precisely the rising front, is noticeably different. We thus question if the fine analysis of the time evolution of the signal could not be used as method for discriminating different gases.

Potential novel method of discriminating gases. As it has been discussed, besides the intensity of the signal, the evolution of response differs from detected gas species. This may lead to a novel way of discriminating gases.

In the following, we thus try to draw a phenomenological model for describing the time evolution of the resistance changes. For one sensor, we assume that there are N_0 active sites available in DWCNTs film for interacting with gas molecules and thereby modifying the resistance of the sensor. These sites can be at the surface of DWCNTs, on the defects of the nanotubes and/or at the tunnel junctions.

When gas molecules impinge randomly on the sensor, active sites start to be occupied by gas molecules and are no longer available for further resistance change.

Let us call $N(t)$ the number of active sites available at time t, $N(t=0)=N_0$ when the sensor is not exposed and all the active sites are unoccupied. Then the number of active sites available progressively decrease upon gas exposure.

Meanwhile, we make another assumption that the variation of the number of available active sites dN during an incremental time dt is proportional to the proportion of

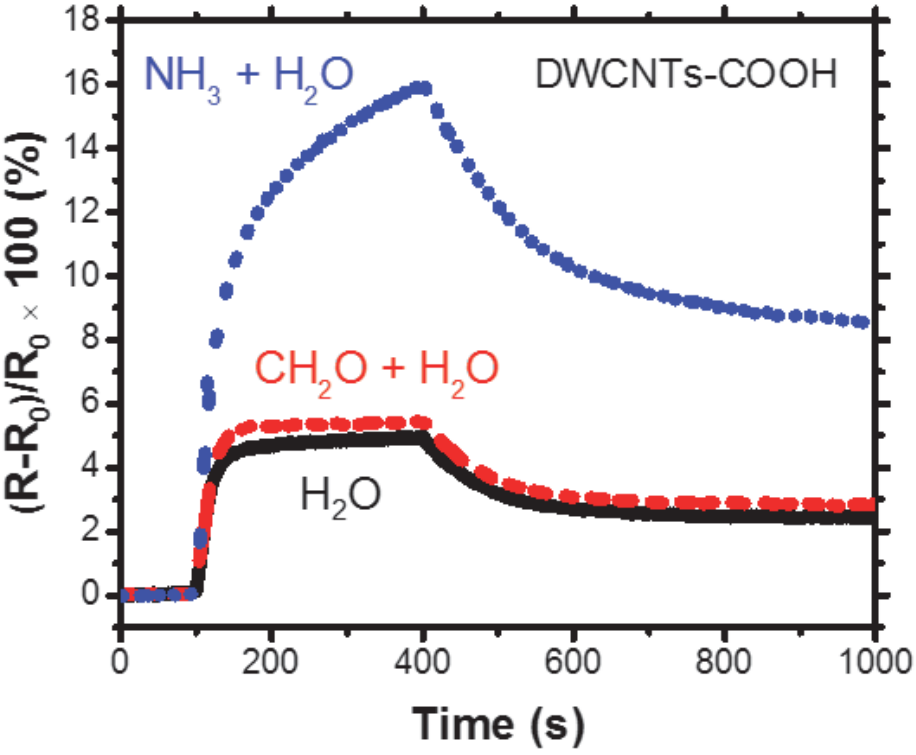


Figure 2.23: The signal of an oxidized DWCNTs sensor to ammonia vapor and formaldehyde vapor. The control experiment is pure DI water vapor exposure.

unoccupied active sites, such that

$$\frac{dN(t)}{dt} = -k\frac{N(t)}{N0} \tag{2.4}$$

where k is the proportionality coefficient and the sign $-$ indicates that the number of available sites are decreasing upon the exposure proceeding. Indeed, the probability for a molecule to encounter an active site is proportional to the proportion of sites that are still available ($\frac{N(t)}{N_0}$).

In the same way, the number of occupied sites at time t is called $O(t)$. Then the increase of $O(t)$ during an incremental time dt is proportional to the probability for a site to be available, i.e. $N(t)/N_0$. As $N(t) + O(t) = N_0$, this probability equals $1 - O(t)/N_0$. Thus we have

$$\frac{dO(t)}{dt} = k\frac{N_0 - O(t)}{N_0} \tag{2.5}$$

In the following context, the evolution of resistance is derived based on the assump-

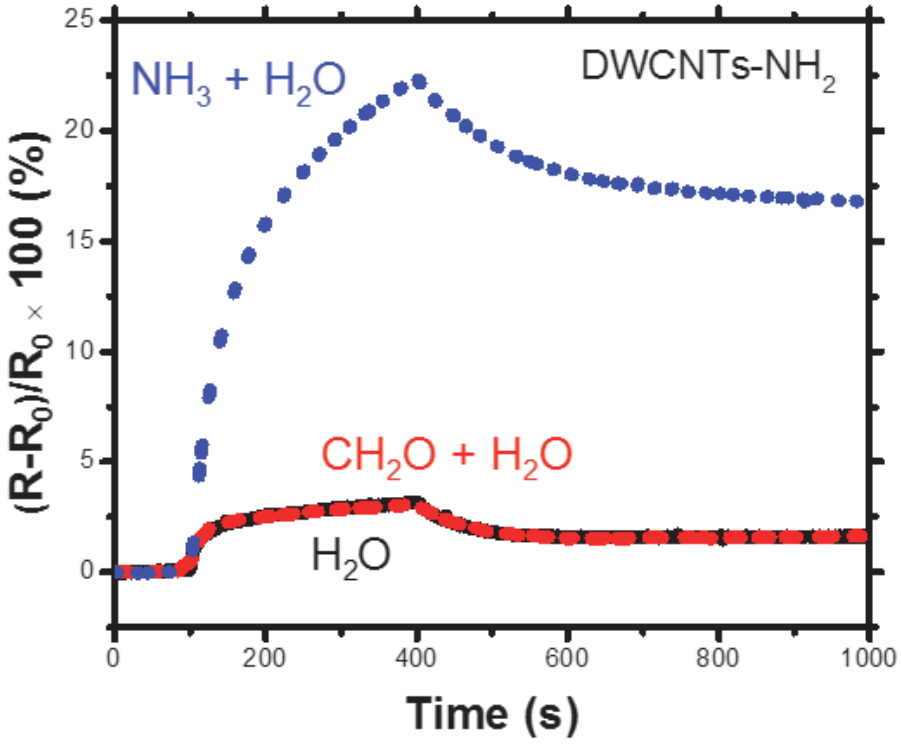


Figure 2.24: The signal of an aminated DWCNTs sensor to ammonia vapor and formaldehyde vapor. The control experiment is pure DI water vapor exposure.

tion above. At time $t = 0$, all the sites are available, $N(t) = N_0$, $O(t) = 0$, and the resistance thus equals its initial value, say $R_{initial}$. If all sites are occupied, $N(t) = 0$ and $O(t) = N_0$, the resistance is higher (we make this hypothesis that the adsorption on an active site increases the resistance) and the resistance reaches its maximum, say R_{max}. Thereby, the evolution of the resistance is the same as the evolution of occupied sites $O(t)$ with the boundary conditions that at $t = 0$, $R = R_{initial}$ and at time infinite $R = R_{max}$. The increment of resistance during an increment of time is then driven by

$$\frac{dR(t)}{dt} = k\frac{R_{max} - R(t)}{R_{max}} \tag{2.6}$$

Taking the boundary condition into account, equation 2.6 is solved as

$$R(t) = R_{max} - (R_{max} - R_{initial})exp(-\frac{kt}{R_{max}}) \tag{2.7}$$

we then re-write the equation above as

$$R(t) = R_{max} - \Delta R exp(-\frac{t}{\tau}) \tag{2.8}$$

where the $\Delta R = R_{max} - R_{initial}$ and the time constant $\tau = R_{max}/k$.

In this model, we consider that the resistance is instantaneously changed upon the occupancy of an active site, by which we assume that the dynamic of the resistance change is simply governed by the rules of random adsorption of gas molecules at the surface. But if time is needed for the adsorption event to be converted into resistance change, this will affect the $R(t)$ revolution. This is much more complex to model because we do not know exactly the mechanisms occurring between the adsorption and the charge transfer, or tunnel junction barrier change. Based on the shape of our experimental measurements, we assume that due to these unknown mechanisms there is also another term to consider which indicates that the resistance increases linearly with time according to a rate which is not dependent on the adsorption mechanism itself.

This new term gives the final phenomenological equation of the resistance evolution as following

$$R(t) = R_{max} - \Delta R exp(-\frac{t}{\tau}) + \alpha t \tag{2.9}$$

where α is a phenomenological parameter accounting for this unknown mechanism.

We have found that this simple model fits quite accurately with our experimental curves. As an example in Figure 2.25, we present the fit obtained in the case of ammonia (a) and formaldehyde (b) vapor detection with an oxidized DWCNTs sensor.

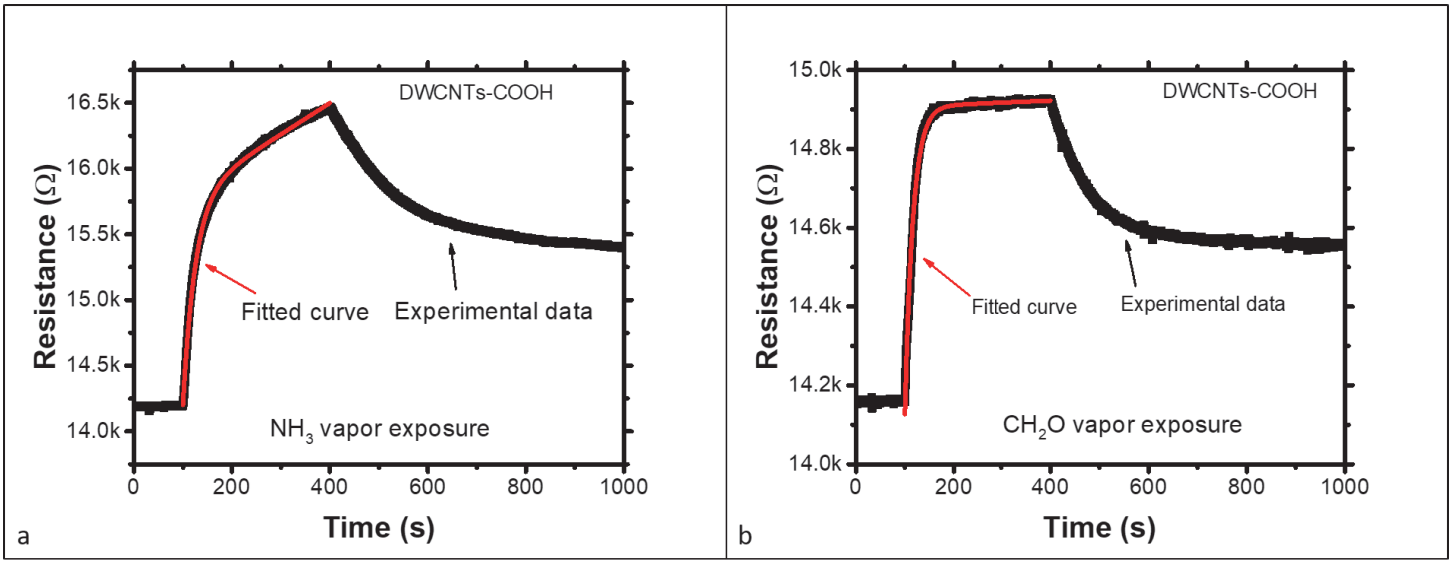


Figure 2.25: An oxidized DWCNTs sensor's resistance evolution (black curves) upon ammonia (a) and formaldehyde (b) vapor exposures with fitted curves (red) using model 2.9.

Applying this model to our experimental observation, we have also found that the τ and α are the two most interesting parameters. Taking the measurements in previous sections as example, for the oxidized DWCNTs sensor in Figure 2.23, applying the model to its resistance evolution upon ammonia, formaldehyde and water vapor, respectively, we then obtain the following table of parameters τ and α.

	$\tau(s)$	$\alpha(\Omega s^{-1})$
NH_3	25.35	2.38
CH_2O	16.60	0.05
H_2O	15.54	0.18

Table 2.1: Parameters τ and α derived from the model 2.9 of the oxidized DWCNTs sensor's resistance variation upon NH_3, CH_2O and H_2O exposure in Figure 2.23.

Similarly, we obtained the parameters τ and α of the aminated DWCNTs sensor's resistance evolution upon NH_3, CH_2O and H_2O vapor exposure from Figure 2.24.

From the fitting results above and the experimental observation, it can be seen that the resistance change is mainly due to the exponential part of the model. Thus, the occupancy of active sites dominates the resistance response, i.e. the exponential part in the model 2.9.

The magnitude of resistance variation can be predicted from parameter τ, the larger the τ is the larger the resistance variation is. For upon two different gases exposure, if the difference of resistance variation of sensor is big, the gases can be distinguished by the resistance variation or the τ parameter. If the difference is small, it is difficult to discriminate gases in the same way, but it turned out that the parameter α is very different between different gases. This differentiation exist not matter the resistance variation is big or small. For example, in Table 2.2, the parameter τ is very different between NH_3 and CH_2O vapor exposure or NH_3 and H_2O vapor exposure, but the τ is very close to each other for CH_2O and H_2O exposure. From previous section we learned that the aminated DWCNTs sensors are capable of detecting CH_2O, however the parameter τ cannot tell this information, but we can clearly see the difference in the parameter α upon CH_2O and H_2O vapor exposure. The same conclusion can be seen from Table 2.1 for oxidized DWCNTs sensor.

For gas sensors made from different functionalized DWCNTs upon the same gas exposure, we can see that the relative resistance variation is proportional to the parameter

	$\tau(s)$	$\alpha(\Omega s^{-1})$
NH_3	37.26	1.12
CH_2O	13.39	0.12
H_2O	14.30	0.08

Table 2.2: Parameters τ and α derived from model 2.9 of the aminated DWCNTs sensor's resistance variation upon NH_3, CH_2O and H_2O vapor exposure in Figure 2.24.

τ by comparing Table 2.1 and 2.2. Taking the NH_3 vapor exposure measurement as an example, the parameter τ of aminated DWCNTs sensor is larger than for oxidized DWCNTs. This result coincides with the fact that the relative resistance response of aminated DWCNTs sensor is clearly higher than that of oxidized DWCNTs (see Figure 2.23 and 2.24).

We thus make a hypothesis that the model 2.9 describes the gas sensing signal in two terms. It first tells the sensor's discriminability in a novel perspective, α, rather than the traditional way which is based on the differences of signals' intensity. This method can discriminate gases even for very similar signals. Secondly, it shows that the sensitivity relies on the functionalization of DWCNTs, which induces the main different behaviour of resistance evolution.

2.4.6 Limit of Detection and Calibration

As it has been observed, oxidized DWCNTs sensors are highly sensitive to ammonia meanwhile maintain better recovery from ammonia vapor exposure compared to aminated DWCNTs sensors. Thereby, the oxidized DWCNTs sensors are used to determine the limit of detection of ammonia in the presence of water.

First, a set of ammonia aqueous solution of different concentration is newly prepared from ammonium hydroxide solution (28-30 $wt\%$, 0.9 g/mL, Sigma-Aldrich). Thereby, ammonia vapor is generated at different concentration in nitrogen atmosphere, from *ca.* 0.5 *ppm* to *ca.* 110 *ppm*. The sensors are set to exposure of ammonia vapor for 10 s. The control experiment is DI water vapor exposure. It starts first with control experiment then continues with repetitive ammonia vapor exposures, from lowest concentration to highest concentration. We have performed two experiments. The first sensor was exposed to ammonia vapor of 0 (pure water vapor), 1, 5 and 8 *ppm*, respectively. We then exposed the sensor to ammonia vapor over a wider range of concentration.

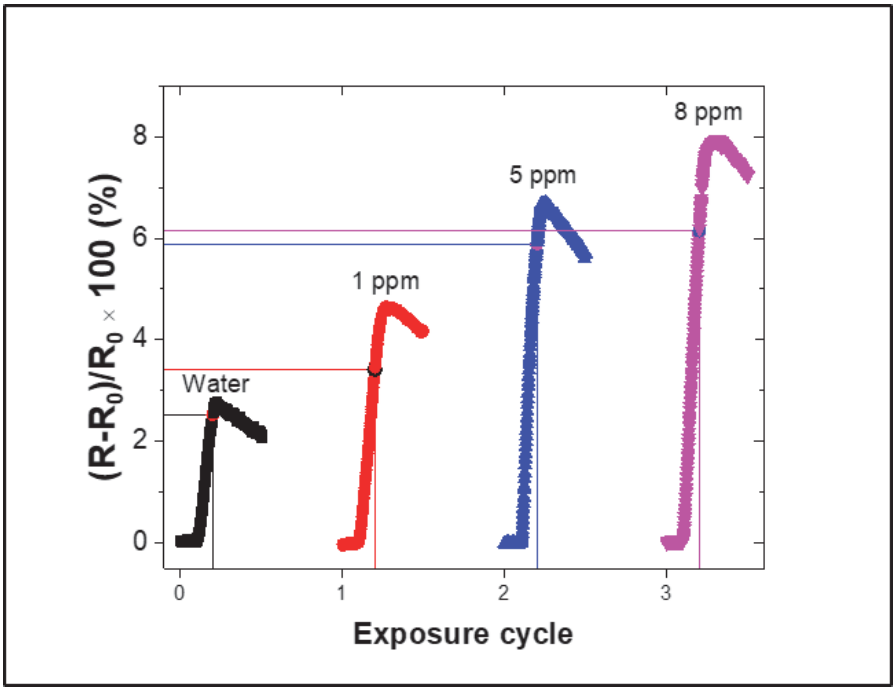


Figure 2.26: The signal of the oxidized DWCNTs sensor to ammonia vapor exposure at different concentration in water vapor.

Figure 2.26 illustrates the signal of an oxidized DWCNTs sensor to ammonia vapors. Due to manual control, the real exposure window differs from each other. Therefore, the labeled data points in Figure 2.26 mark response value of the moment when exposure duration is 10 s, for the purpose of comparison.

The sensor is obviously sensitive to ammonia vapor of low concentration. With very small amount of ammonia vapor, *ca.* 1 *ppm*, it makes response different from that of DI water vapor. The response is increased as a function of ammonia vapor concentration indicating that after calibration our devices could deliver quantitative information.

Figure 2.27 shows the response of another oxidized DWCNTs sensor submitted to ammonia vapor exposures over a larger range of concentration. As the exposure window is manually controlled, the true exposure window duration is *ca.* 11.5 ± 0.5 s.

The minimum concentration of ammonia vapor available with our method of preparation is *ca.* 0.5 *ppm*, however it induces higher signal compared to water vapor exposure. The highest concentration of ammonia that has been tested is *ca.* 110 *ppm*, which is about 55 *times* smaller than DI water concentration but cause more than 4 *times* higher signal. The signal of oxidized DWCNTs sensor is non-linearly proportional to the concentration of ammonia in the nitrogen atmosphere.

From the data of Figure 2.27, we have presented a calibration curve in Figure 2.28. In this figure, we have also reported the electrical measurement noise and the relative resistance variation per $°C$ at room temperature. The range of electrical measurement noise is within 0.07% and the relative resistance response variation per $°C$ at room

temperature is within -0.2%, the sign '$-$' means that resistance change is inversely proportional to the temperature change. The insert shows the first five data points which are hard to read in a large scale of X-axis.

From the Figure 2.28 it can be seen that our sensor can detect trace of ammonia (less than 1 *ppm*) in water vapor. The electrical measurement noise and temperature change induced relative resistance variation at room temperature are negligible compared to the signal caused by ammonia. The red solid curve is only a rough description of the increasing tendency of the signal as a function of ammonia vapor concentration. It is not rigorously studied result.

The calibrated relative resistance variation is non-linearly proportional to the gas concentration, which coincides with the model 2.9, because the resistance change depends on the probability of active sites occupied by gas molecules and this probability is also proportional to the number of gas molecules in unit volume, i.e. concentration. Such that high gas concentration gives high probability for an active site to be occupied by gas molecule(s) within unit time. The resistance is thereby changed more rapidly than the low gas concentration situation. Since the exposure time here is very short, it requires more work to determine whether the 'unknown mechanism' has effect on the measurement, which is very interesting for the future work.

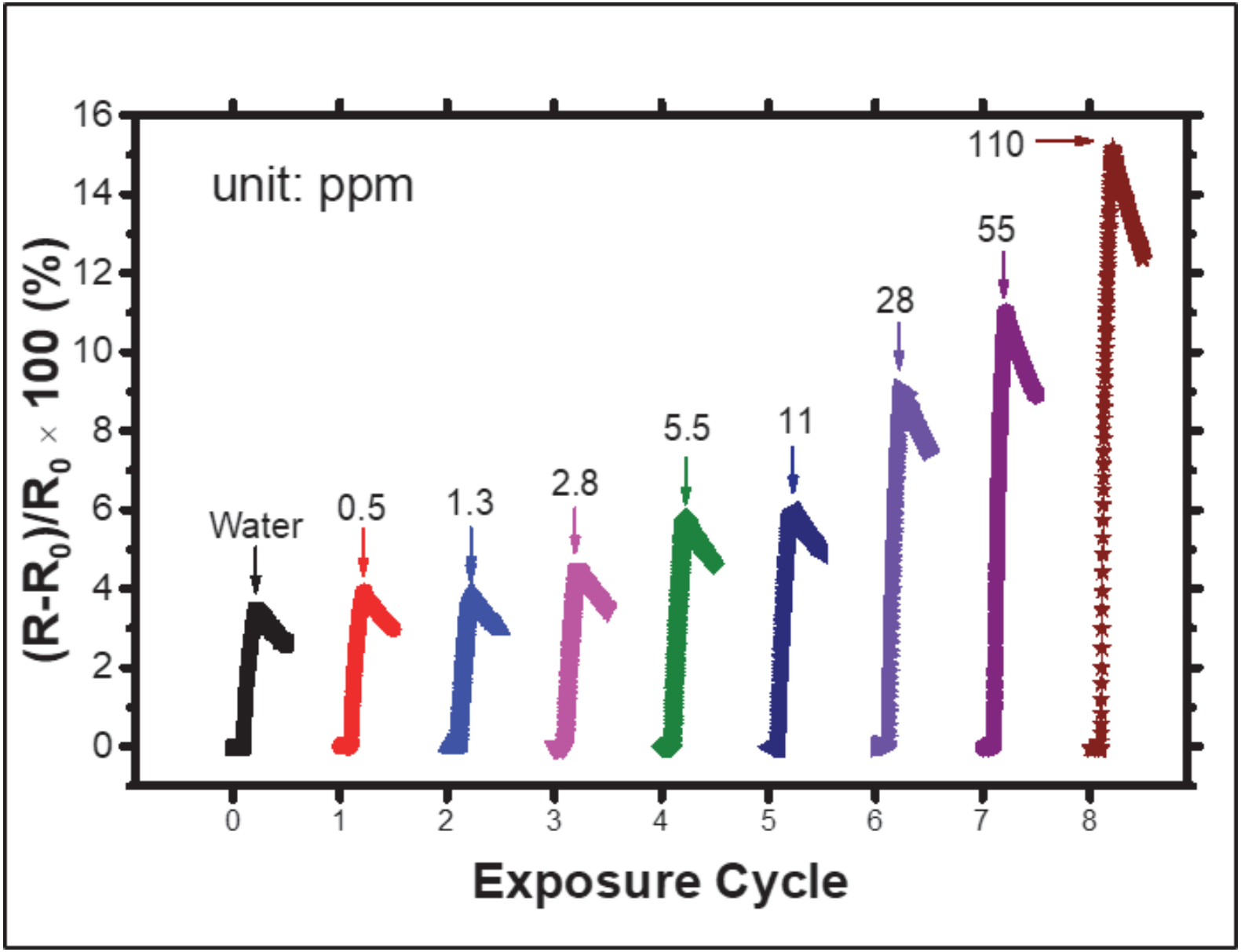


Figure 2.27: The signal of the an oxidized DWCNTs sensor to different concentrations of ammonia vapor.

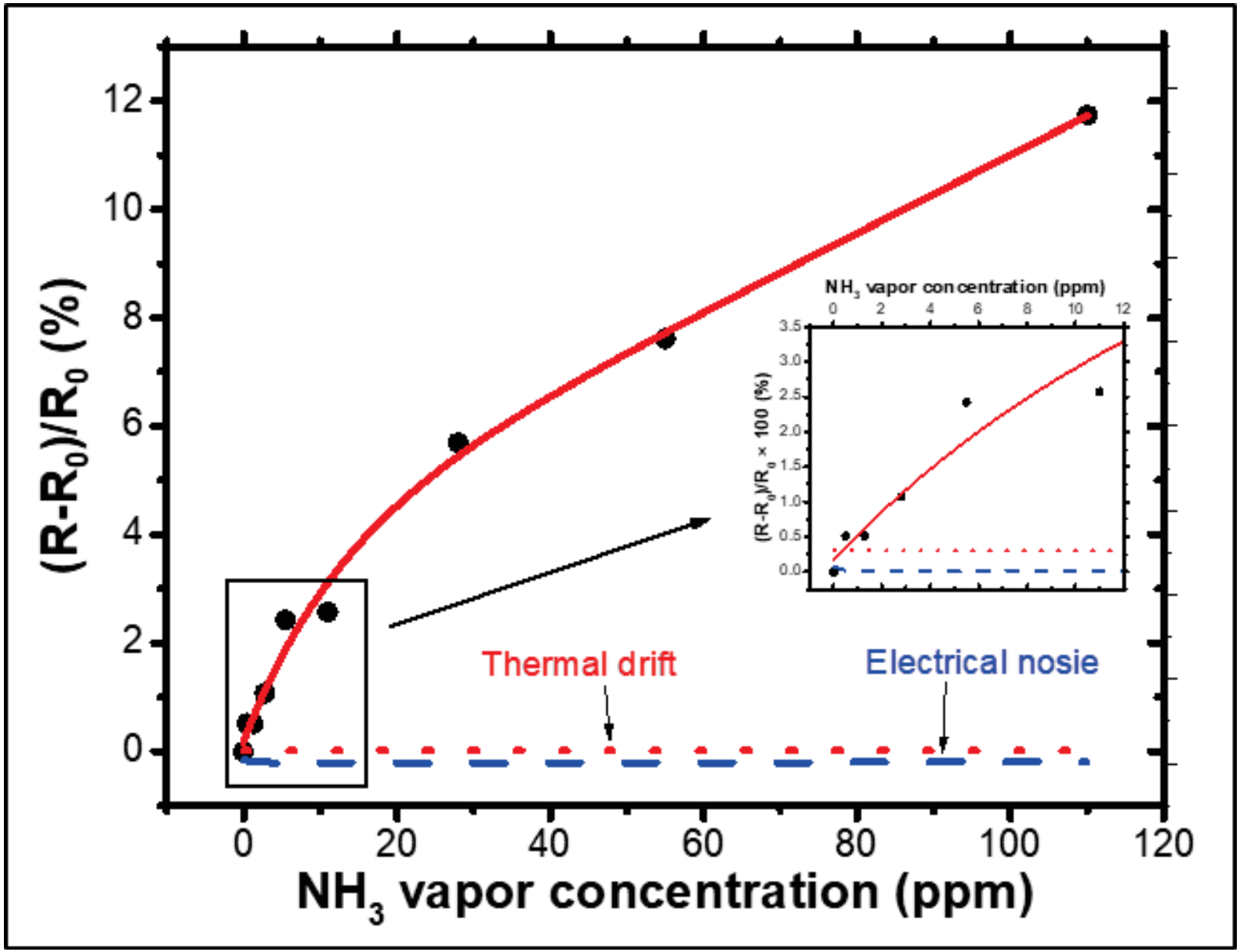


Figure 2.28: The calibrated relative resistance response upon ammonia vapor exposure of different concentrations.

2.4.7 Chlorine Detection

We also tested our sensors with chlorine gas. Chlorine gas is produced by reaction of concentrated Hydrochloric Acid and Postassium Permanganate.

$$2\,KMnO_4 + 16\,HCl \longrightarrow 2\,MnCl_2 + 2\,KCl + 8\,H_2O + 5\,Cl_2 \tag{2.10}$$

The gas is filtered by bubbling through water to remove trace of Hydrochloric Acid. Then, chlorine gas is dried through calcium chloride.

Dry chlorine gas is collected in the tube that compatible to the Fluigent system. Then run the experiment as the exposure of ammonia. Once the sensors are exposed to chlorine gas, the resistance show a cliff-like drop. Figure 2.29 show two independent experiments for oxidized and aminated DWCNTs sensors. Though the proportion of chlorine gas is undetermined, the chlorine gas indeed oxidized the DWCNTs. The devices never recovered from chlorine gas exposure. Thereby, chlorine gas cause permanent fatal damage to the devices. Due to the time constraint, in-depth work was not carried out.

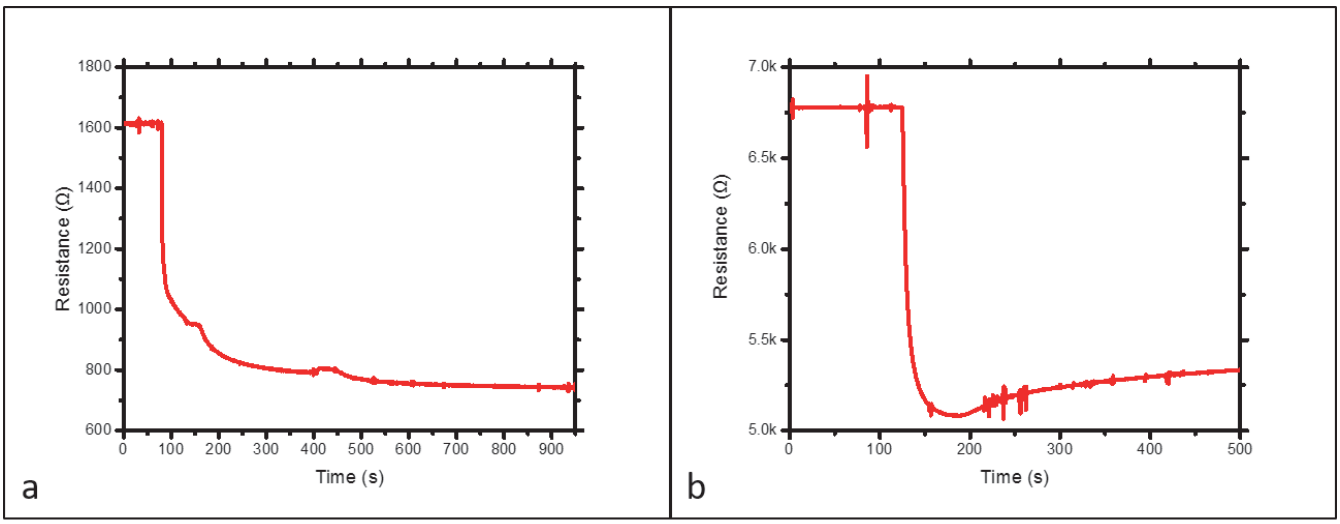


Figure 2.29: Two independent chlorine gas exposure upon oxidized DWCNTs sensor (a) and aminated DWCNTs sensor (b).

In conclusion, the high electronegativity make chloride a strong oxidizer. A decrease of resistance occurred during chloride gas exposure. However, the chloride gas strongly interacts with the sensors and corrodes the device. The resistance measurement does not show any sign of recovery.

2.5 Conclusion

Our sensors are able to detect the pure chemical compounds C_2H_5OH and C_3H_6O. But the sensitivity of all kinds of DWCNTs sensors towards those gas species is poor. However

the functionalized DWCNTs (oxidized, aminated) sensors exhibit superior performance.

Both types of functionalized DWCNTs sensors are very sensitive to the ammonia vapor. The oxidized DWCNTs sensors exhibit a better repeatability upon ammonia vapor exposures than aminated DWCNTs sensors. The oxidized DWCNTs sensors are able to detect ammonia vapor below 1 *ppm* when water vapor is present.

Each type of functionalized DWCNTs sensors have similar relative resistance response upon formaldehyde vapor (in water vapor) exposure compared to the relative resistance response upon water vapor exposure, respectively. But the formaldehyde strongly affects the recovery of sensors' resistance where water does not. Thus the recovery could be a signature of gas species.

We also developed another model to discriminate gas species. This method is unlike the conventional way that relies on the differences of intensity of signals. Indeed we found that the rising of the resistance when gas is exposed exhibit a classical exponential regime governed by stochastic adsorption laws, but also exhibit a linear regime reflecting some time delay between the gas molecule landing and the charge transport induced on an active site. By comparing this linear regime for different gas species, we have shown that it might be used to discriminate different gases.

The oxidized DWCNTs sensor is sensitive to temperature variation but with a poor sensitivity. Thereby, it is reliable from temperature influence when detecting gases.

Our sensors are sensitive to chlorine gas in a different resistance response behaviour compared to other tested gases. But they are vulnerable to the corrosive chlorine gas. For further research on chlorine gas detection with DWCNTs, we suggest using high diluted chlorine gas.

Bibliography

[1] "Ethanol." https://en.wikipedia.org/wiki/Ethanol#Low-temperature_liquid.

[2] B. Tymrak, M. Kreiger, and J. M. Pearce, "Mechanical properties of components fabricated with open-source 3-d printers under realistic environmental conditions," *Materials & Design*, vol. 58, pp. 242–246, 2014.

[3] J. A. Ober, "Mineral commodity summaries 2017," tech. rep., US Geological Survey, 2017.

[4] J. A. Ober, "Mineral commodity summaries 2016," tech. rep., US Geological Survey, 2016.

[5] H. Qi, J. Liu, J. Pionteck, P. Pötschke, and E. Mäder, "Carbon nanotube–cellulose composite aerogels for vapour sensing," *Sensors and Actuators B: Chemical*, vol. 213, pp. 20–26, 2015.

[6] J. G. Speight *et al.*, *Lange's handbook of chemistry*, vol. 1. McGraw-Hill New York, 2005.

[7] Z. Sun, X. Zhang, N. Na, Z. Liu, B. Han, and G. An, "Synthesis of zro2- carbon nanotube composites and their application as chemiluminescent sensor material for ethanol," *The Journal of Physical Chemistry B*, vol. 110, no. 27, pp. 13410–13414, 2006.

[8] M. L. Y. Sin, G. C. T. Chow, G. M. K. Wong, W. J. Li, P. H. W. Leong, and K. W. Wong, "Ultralow-power alcohol vapor sensors using chemically functionalized multiwalled carbon nanotubes," *IEEE Transactions on Nanotechnology*, vol. 6, no. 5, pp. 571–577, 2007.

[9] T. Someya, J. Small, P. Kim, C. Nuckolls, and J. T. Yardley, "Alcohol vapor sensors based on single-walled carbon nanotube field effect transistors," *Nano letters*, vol. 3, no. 7, pp. 877–881, 2003.

[10] R. Martel, V. Derycke, C. Lavoie, J. Appenzeller, K. Chan, J. Tersoff, and P. Avouris, "Ambipolar electrical transport in semiconducting single-wall carbon nanotubes," *Physical review letters*, vol. 87, no. 25, p. 256805, 2001.

[11] S. Heinze, J. Tersoff, R. Martel, V. Derycke, J. Appenzeller, and P. Avouris, "Carbon nanotubes as schottky barrier transistors," *Physical Review Letters*, vol. 89, no. 10, p. 106801, 2002.

[12] V. Derycke, R. Martel, J. Appenzeller, and P. Avouris, "Controlling doping and carrier injection in carbon nanotube transistors," *Applied Physics Letters*, vol. 80, no. 15, pp. 2773–2775, 2002.

[13] B. Philip, J. K. Abraham, A. Chandrasekhar, and V. K. Varadan, "Carbon nanotube/pmma composite thin films for gas-sensing applications," *Smart materials and structures*, vol. 12, no. 6, p. 935, 2003.

[14] S. Aloisio, P. E. Hintze, and V. Vaida, "The hydration of formic acid," *The Journal of Physical Chemistry A*, vol. 106, no. 2, pp. 363–370, 2002.

[15] A. B. Nadykto and F. Yu, "Strong hydrogen bonding between atmospheric nucleation precursors and common organics," *Chemical physics letters*, vol. 435, no. 1, pp. 14–18, 2007.

[16] N. Peng, Q. Zhang, C. L. Chow, O. K. Tan, and N. Marzari, "Sensing mechanisms for carbon nanotube based nh3 gas detection," *Nano letters*, vol. 9, no. 4, pp. 1626–1630, 2009.

[17] J. Kong, N. R. Franklin, C. Zhou, M. G. Chapline, S. Peng, K. Cho, and H. Dai, "Nanotube molecular wires as chemical sensors," *science*, vol. 287, no. 5453, pp. 622–625, 2000.

[18] X. Feng, S. Irle, H. Witek, K. Morokuma, R. Vidic, and E. Borguet, "Sensitivity of ammonia interaction with single-walled carbon nanotube bundles to the presence of defect sites and functionalities," *Journal of the American Chemical Society*, vol. 127, no. 30, pp. 10533–10538, 2005.

[19] C. W. Bauschlicher Jr and A. Ricca, "Binding of n h 3 to graphite and to a (9, 0) carbon nanotube," *Physical Review B*, vol. 70, no. 11, p. 115409, 2004.

[20] J. A. Robinson, E. S. Snow, Ş. C. BaÌÑdescu, T. L. Reinecke, and F. K. Perkins, "Role of defects in single-walled carbon nanotube chemical sensors," *Nano Letters*, vol. 6, no. 8, pp. 1747–1751, 2006.

[21] J. Zhao, A. Buldum, J. Han, and J. P. Lu, "Gas molecule adsorption in carbon nanotubes and nanotube bundles," *Nanotechnology*, vol. 13, no. 2, p. 195, 2002.

[22] J. Li, Y. Lu, Q. Ye, M. Cinke, J. Han, and M. Meyyappan, "Carbon nanotube sensors for gas and organic vapor detection," *Nano letters*, vol. 3, no. 7, pp. 929–933, 2003.

[23] J. Zhao, A. Khalizov, R. Zhang, and R. McGraw, "Hydrogen-bonding interaction in molecular complexes and clusters of aerosol nucleation precursors," *The Journal of Physical Chemistry A*, vol. 113, no. 4, pp. 680–689, 2009.

[24] M. J. Field and I. H. Hillier, "Non-dissociative proton transfer in 2-pyridone–2-hydroxypyridine. an ab initio molecular orbital study," *Journal of the Chemical Society, Perkin Transactions 2*, no. 5, pp. 617–622, 1987.

[25] A. Held and D. W. Pratt, "Ammonia as a hydrogen bond donor and acceptor in the gas phase. structures of 2-pyridone-nh3 and 2-pyridone-(nh3) 2 in their s0 and s1 electronic states," *Journal of the American Chemical Society*, vol. 115, no. 21, pp. 9718–9723, 1993.

[26] A. Held and D. W. Pratt, "Hydrogen bonding in water complexes. structures of 2-pyridone-h2o and 2-pyridone-(h2o) 2 in their s0 and s1 electronic states," *Journal of the American Chemical Society*, vol. 115, no. 21, pp. 9708–9717, 1993.

Partie III : Application Gas Detection in Real Condition

Chapter 1

DWCNTs Sensor Usage in Practice

In previous chapter, we have studied our sensors upon different gas exposure in a complex environment condition. The results show that our sensors are capable of detecting gases like ammonia, formaldehyde in presence of water vapor. These interesting results encourage us to test our sensor in real condition. In this chapter, we will demonstrate the usage of our sensors in a practical way, such as alcohol detection and residual of ammonia detection.

1.1 Alcohol Test

We tested an oxidized DWCNTs sensor for alcohol test. Meanwhile, a commercial breathalyzer was used as a test reference. The test was taken in three steps: the testers first took a breath test before drinking alcoholic beverage, testers then drunk a certain volume of alcoholic beverage, at last the testers took a second breath test one hour later after drinking.

We took two alcohol tests, in first test the testers drunk enough alcoholic beverage within the detection range of the commercial breathalyzer, and in second test the testers took small amount of alcoholic beverage which was out of the detection limit of the commercial breathalyzer.

The test range of the breathalyzer is $0.000 - 2.000\ mg/L$. And the legal limit in most European countries is $0.25\ mg/L$. A conversion table of alcohol concentration by different measurement standard is attached in the Appendix.

Figure 1.1 shows the results of the first test. The testers were two French adults, one female (a) and one male (b). It can be seen in Figure 1.1 that it is difficult to tell if the tester drunk alcohol or not by simply looking at the intensity of the signals. But it is clear that the recovery of signal taken after alcohol drinking is better than it is before alcohol drinking.

The results of second test are plotted in Figure 1.2. The testers were two adults male, one European (a) and one east Asian (b). From Figure 1.2 (a) it can be seen that

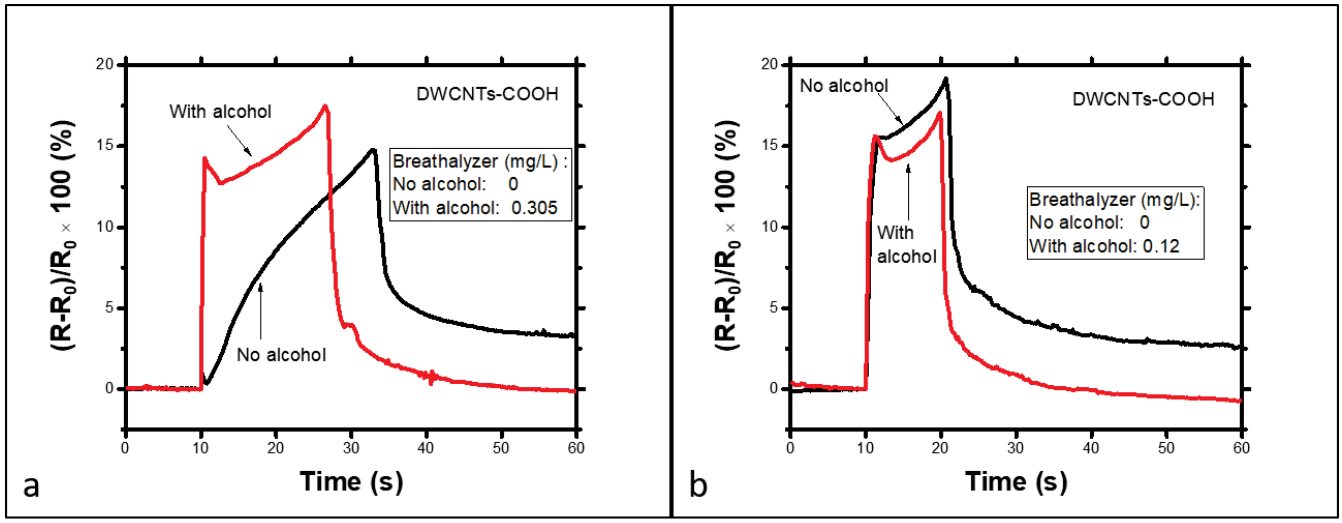


Figure 1.1: The signal of an oxidized DWCNTs sensor to the first alcohol drinking test. The insert box shows the corresponding readings by commercial breathalyzer.

the oxidized DWCNTs sensors detected differences between two breath test while the breathalyzer did not. But breathalyzer detected trace of alcohol from the Asian tester's breath rather than the European tester's, which could be due to the fact that many east Asian carry a gene called Aldehyde dehydrogenase, mitochondrial (ALDH2) which encode a low efficient enzyme for alcohol metabolism. Nevertheless, our sensors can give distinct signals between the breath of low concentration of alcohol and no alcohol.

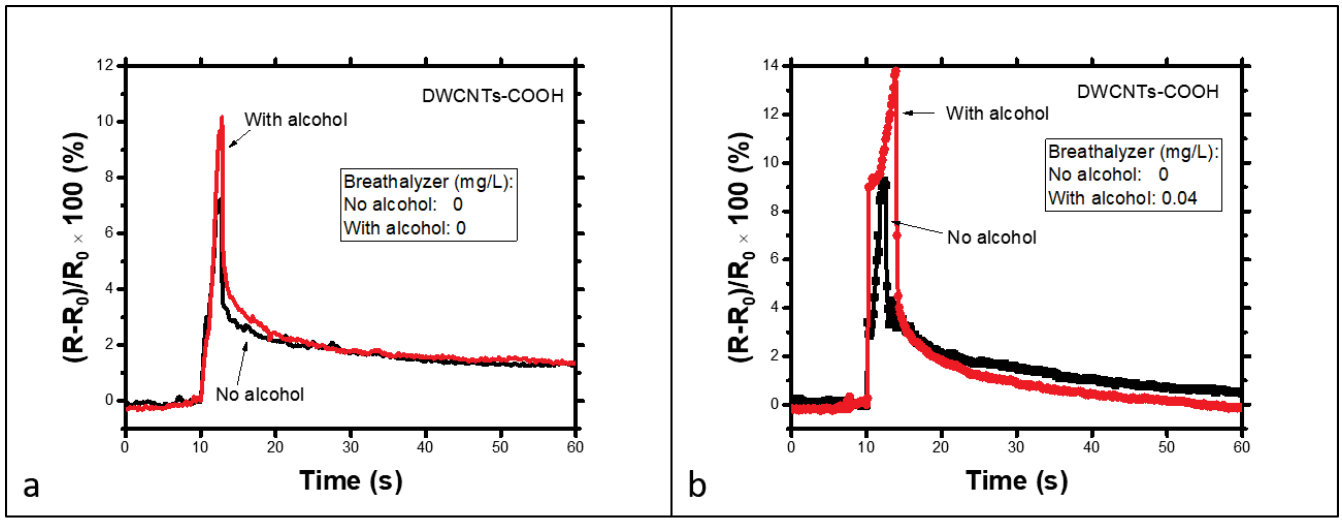


Figure 1.2: The signal of an oxidized DWCNTs sensor to the second alcohol drinking test. The insert box show the corresponding readings by the commercial breathalyzer.

1.2 Detecting Trace of Ammonia

The experiment already presented in Section 2.4.6 showed that our oxidized DWCNTs sensors are able to detect sub *ppm* concentration of ammonia in water vapor. Thus we expect that the oxidized DWCNTs sensor can detect ammonia of much lower concentration in real-life condition. In real-life condition, people are frequently exposed to ammonia vapor through, such as, daily supplies and/or household products. The concentration of ammonia in these goods are normally very low in some case it is lower than the limit of human smell limit ($< 0.04ppm$). Thereby it is interesting to discover whether our sensors are able to detect traces of ammonia at room temperature in open air.

For this purpose, we used an oxidized DWCNTs sensor to detect ammonia residual in the bottom of a tube which was filled with 5 mL $0.03wt\%$ ammonia aqueous solution for more than a month. We run the test two times, the first test was conducted 1-day after cleaning the tube and the second test was done 45-day later after the first test. Before each test, we also rinsed the tube with DI water and dried it with dry nitrogen. The control experiment was done on an unused tube which was rinsed by DI water and dried by dry nitrogen before test. The results are shown in Figure 1.3.

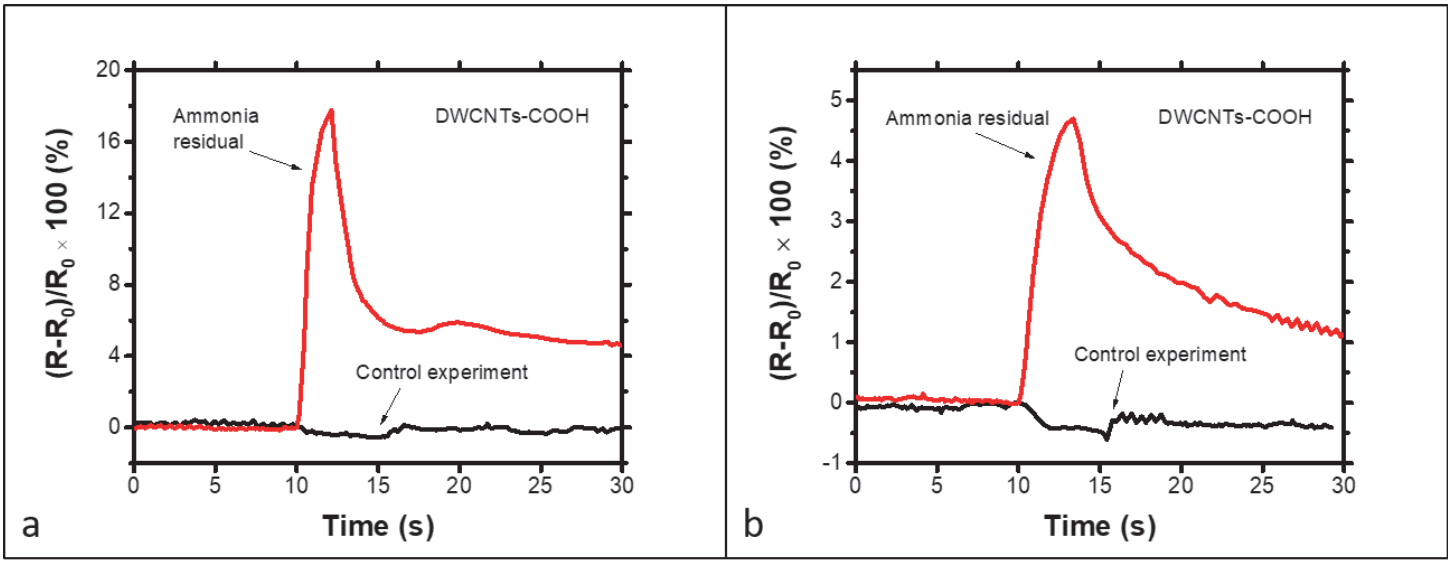


Figure 1.3: Ammonia residual detection by an oxidized DWCNTs sensor 1-day (a) and 46-day (b) after removing ammonia solution. The Tube-1 is the control tube, Tube-2 is the one used to contain ammonia solution. Each test started at 10 s.

It is clear that with a trace of ammonia the oxidized DWCNTs sensors gave highly distinctive signal compared to the control condition. Our oxidized DWCNTs sensor is thus able to detect ammonia of very low concentration in real-life condition.

A video of demo experiment can be download from url:

https://drive.google.com/file/d/1pR0_gVVdlrP_iW6GxHeeRYGH84enjNCy/view?usp=sharing

1.3 Conclusion

We tested our oxidized DWCNTs sensors in real-life condition for alcohol drinking detection and trace of ammonia detection. The oxidized DWCNTs sensor is able to detect small amount of alcohol drinking. Compared to the breathalyzer, which costs around 300 €, our oxidized DWCNTs sensors cost less than 1 €including material preparation and photolithography related equipment usage. If taking hand-fabrication process into account, it is still less than 10 €. In addition, taking the resistance measurement equipment into account, the cost should be less than 300 €. Such low cost sensors are also able to detect very small amount of ammonia in real-life conditions.

Part IV: General Conclusion

The double-walled carbon nanotubes (DWCNTs) are the simplest MWCNTs. They have the highest aspect ratio compared to other types of MWCNTs while preserving the high conductivity property of MWCNTs. Out of the consideration above, in this work, we have successfully fabricated gas sensors based on chemically functionalized double-wall carbon nanotubes (DWCNTs) using a robust and low cost process. The DWCNTs were synthesized by catalytic chemical vapor deposition (CCVD) method. They were then purified before functionalization (oxidation, amination, and fluorination). The sensor devices were fabricated by soft lithography using PDMS (Poly-DiMethylSiloxane) stencils and liquid phase pipetting of a suspension of chemically functionalized DWCNTs in deionized water, rinsing and finally drying in a nitrogen flow. Each device (1 $cm \times 2$ cm) is equipped with a set of 7 DWCNTs based resistors. Each resistor can accommodate a precise chemical functionalization for targeting a specific gas species, allowing a multiplexed detection. Due to their small size and the possibility to fabricate them on soft substrates, they could be used for many kinds of applications including wearable devices. The electrical resistance of the produced resistors turned out to decrease with temperature, suggesting fluctuations induced tunneling conduction through the disordered network of metallic nanotubes. However, we have shown in our work that for realistic applications, gas sensing can be achieved without any temperature regulation of our devices, because the variations of electrical conductance caused by gas molecules adsorption are significantly larger than those caused by possible temperature fluctuations. The as fabricated devices exhibit at room temperature a metallic conducting behavior. Sensors with a resistance less than 100 $k\Omega$ were selected for gas detection. Because the sensing principle is based on the direct measurement of the resistance, our scheme ensures low power consumption (< 1 μW).

Raw (not functionalized) DWCNTs-based gas sensors exhibited a low sensitivity to the tested analytes, including ethanol, acetone, ammonia and water vapor. Functionalized DWCNTs-based gas sensors exhibited a moderate sensitivity to ethanol, acetone and water vapor but the response to ammonia, even in the presence of additional water vapor (ca. 5700 ppm), was excellent. In particular, oxidized DWCNTs based gas sensors exhibited a high stability in the case of prolonged (ca. 1000 s) and repeated gas exposures. The oxidized DWCNTs gas sensors were also able to detect ammonia vapor at sub-ppm concentration in the presence of water vapor at high concentration (ca. 5700 ppm). We believe that the functional groups grafted to the DWCNTs modify the in-

teraction between gas molecules and DWCNTs and that the induced charge transfer is responsible for the modification of the electrical conductivity.

We have built a simple phenomenological model for the analysis of the sensing response curve. This model includes two components for the variations of electrical resistance during gas exposure, an exponential regime and a linear one. In particular, the time constant extracted from the exponential part and the time coefficient of linear part of the response were found to be informative on devices' sensitivity and selectivity.

Finally, we tested our sensors for realistic applications such as trace detection of ammonia, which could be easily detected while far below the detection threshold of human nose (0.04 ppm)

Due to the high stability, ease of fabrication (very simple design, use of low-cost technologies, integration on flexible substrates), robustness (detection in the presence of a large excess of water vapor and resilient to temperature fluctuations) and extremely low amounts of carbon nanotube required, we expect these results to have some potential for a wide range of mass applications in the field of wearable gas sensors for Information and Communication Technologies (ICT) industry. We thus expect our work could help people in many aspects in the future , like food security, household and working environment monitoring.

Appendix

Appendix I: Recipe of Photolithography

NLOF 2035 — 5 µm

PREPARATION

Si/SiO_2/Si_3N_4: H_2O_2/H_2SO_4 2' ou Plasma O_2 800W 5' >> Déshydratation 15' >> HMDS

Métal: Acétone (en fonction des métaux) >> Déshydratation 15'

Verre: H_2O_2/H_2SO_4 2' >> Plasma O_2 800W 15' >> Déshydratation 15' >> HMDS

ENDUCTION

MANUELLE :

Volume :	3mL
Vitesse :	1350
Accélération :	5000
Temps :	30s

AUTOMATIQUE :

SUR EVG 120

RECIPE :
Enduction Nlof 5um 4pouces

RECUIT

110°C *pendant* **90 sec**

DETOURAGE

MANUELLE :

Seringue Acétone

Vitesse :	5000
Accélération :	5000
Temps :	30s

AUTOMATIQUE :

SUR EVG 120

RECIPE :
détourage classique

INSOLATION

Dose : 150 mJ/cm² *Polarité : negative et insolation en Channel 2 (Ci2) 405nm*

APPAREIL	PUISSANCE (fixe)	TEMPS (s)
EVG 620	62 mW/cm²	2.4
MA 150	20 mW/cm²	7.5
MA 6	25 mW/cm²	6
MJB3 Si	30 mW/cm²	5

PEB

110°C *pendant* **90 sec**

AUTOMATIQUE :

SUR EVG 120

RECIPE :
PEB + Révelation Nlof 5um 4pouces

REVELATION

SOLUTION : **MF CD 26**
TEMPS : **2 min environ**
RINCAGE : **EAU DI face AV/AR puis séchage**

CONTRÔLE VISUEL **puis Révélation supplémentaire** ***SI NECESSAIRE***

OPTION

OPTIONNEL

Sur-révélation = lift-off plus facile mais perte de résolution

VERIFICATION

NETTOYAGE FACE ARRIERE

OBSERVATION au MICROSCOPE

MESURE EPAISSEUR au PROFILOMETRE

LAAS-CNRS 30/07/2014 contact : photolithographie@laas.fr

Appendix

Appendix II: Procedure of integration of raw DWCNTs

1. Sonication of DWCNTs suspension

Placing DWCNTs suspension in probe sonication to re-disperse some sediment of DWCNTs. Setting the power at 150 W and intermittent sonication mode (5 s **ON** and 5 s **OFF**) for 10 min.

2. Removal of photoresist

Using acetone and ethanol to clean the residual of photoresist on substrate. The substrate is then rinsed with DI water and dried by nitrogen flow.

3. Air plasma treatment

Placing the substrate in air plasma oven at the maximum power for 5 min.

4. Attach of PDMS stencil

Covering the substrate with stencil after air plasma treatment. Aligning the cavities in stencil along the electrodes on substrate where there are gaps between source and drain electrodes.

5. Integration of raw DWCNTs

a. Dropping 0.6 μL DWCNTs suspension into each cavity via a pipette.

b. To accelerate the evaporation of water, placing the substrate on a hot plat which was pre-heated at 60 °C.

c. Repeating the above steps six times in total.

6. Removal of excessive DWCNTs and surfactant.

a. Peeling off the PDMS stencil.

b. Soaking the substrate in DI water for 3 min.

c. Drying the substrate carefully with gentle nitrogen breeze.

d. Repeating the two steps above for five times in total.

Appendix

Appendix III: Conversion table

Measurement Standard	Mg/l (BrAC) Air	µg/l	(g/l) promile – blood	% (BAC)
Country	France, U.K., Japan, China	New Zealand	Norway, Germany, Spain, Italy, Portugal, Argentina, Austria	U.S.A, Korea, Australia
Increment	0.05	50	0.10	0.01
	0.10	100	0.20	0.02
	0.20	200	0.40	0.04
	0.25	250	0.50	0.05
	0.30	300	0.60	0.06
	0.40	400	0.80	0.08
	0.50	500	1.00	0.10
	0.60	600	1.20	0.12
	0.70	700	1.40	0.14
	0.80	800	1.60	0.16
	0.90	900	1.80	0.18
	1.00	1000	2.00	0.20

* The legal limit in most European countries is 0.25 mg/L (BrAC) in air or 0.50 g/L (promile) in blood.

Summary in English and French

We have successfully fabricated gas sensors based on chemically functionalized double-wall carbon nanotubes (DWCNTs) using a robust and low cost process. The DWCNTs were synthesized by catalytic chemical vapor deposition (CCVD) method. They were then purified before functionalization (oxidation, amination, and fluorination).

The sensor devices were fabricated by soft lithography using PDMS (Poly-DiMethylSiloxane) stencils and liquid phase pipetting of a suspension of chemically functionalized DWCNTs in deionized water, rinsing and finally drying in a nitrogen flow. Each device (1 cm x 2 cm) is equipped with a set of 7 DWCNT based resistors. Each resistor can accommodate a precise chemical functionalization for targeting a specific gas species, allowing a multiplexed (up to 7) detection. Due to their small size and the possibility to fabricate them on soft substrates, they could be used for many kinds of applications including wearable devices. The electrical resistance of the produced resistors turned out to decrease with temperature, suggesting fluctuations induced tunneling conduction through the disordered network of metallic nanotubes. However, we have shown in our work that for realistic applications, gas sensing can be achieved without any temperature regulation of our devices, because the variations of electrical conductance caused by gas molecules adsorption are significantly larger than those caused by possible temperature fluctuations. The as fabricated devices exhibit at room temperature a metallic conducting behavior. Devices with a resistance less than 100 kΩ were selected for gas detection. Because the sensing principle is based on the direct measurement of the resistance, our scheme ensures low power consumption (<1 μW).

Raw (not functionalized) DWCNTs-based gas sensors exhibited a low sensitivity to the tested analytes, including ethanol, acetone, ammonia and water vapor. Functionalized DWCNTs-based gas sensors exhibited a moderate sensitivity to ethanol, acetone and water vapor but the response to ammonia, even in the presence of additional water vapor, was excellent. In particular, oxidized DWCNTs based gas sensors exhibited a high stability in the case of prolonged and repeated gas exposures. The oxidized DWCNTs gas sensors were also able to detect ammonia vapor at sub-ppm concentration in the presence of water vapor at high concentration. We believe that the functional groups grafted to the DWCNTs modify the interaction between gas molecules and DWCNTs and that the induced charge transfer is responsible for the modification of the electrical conductivity.

We have built a simple phenomenological model for the analysis of the sensing response curve. This model includes two components for the variations of electrical resistance during gas exposure, an exponential regime and a linear one. In particular, the time constant extracted from the exponential part of the response was found to be informative on devices' sensitivity and selectivity.

Finally, we tested our sensors for realistic applications such as trace detection of ammonia, which could be easily detected while far below the detection threshold of human nose (0.04ppm)

Due to the high stability, ease of fabrication (very simple design, use of low-cost technologies, integration on flexible substrates), robustness (detection in the presence of a large excess of water vapor and resilient to temperature fluctuations) and extremely low amounts of carbon nanotube required, we expect these results to have some potential for a wide range of mass applications in the field of wearable gas sensors for Information and Communication Technologies (ICT) industry.

Nous proposons dans ce travail une méthode robuste et bas-coût afin de fabriquer des détecteurs de gaz à base de Nanotubes de Carbone bi-parois (DWCNTs) chimiquement fonctionnalisés. Ces nano-objets (DWCNTs) sont synthétisés par dépôt catalytique en phase vapeur (CCVD), puis purifiés avant d'être oxydés ou bien fonctionnalisés par des terminaisons fluorées ou aminées.

Les dispositifs de détection électriques ont été fabriqués par lithographie douce en utilisant un pochoir de PDMS (Poly-DiMethyl Siloxane) et un dépôt en phase liquide à la pipette d'une suspension aqueuse contenant les nanotubes fonctionnalisés, rinçage puis séchage à l'azote sec. Chaque dispositif (1 cm X 2 cm) est équipé d'un jeu de 7 résistors à base de DWCNTs. Chaque résistor peut accueillir des nanotubes fonctionnalisés par une entité chimique différente afin de cibler un gaz spécifique, permettant ainsi une détection multiplexée. En raison de leur faible encombrement et la possibilité de les fabriquer sur tout type de substrat y compris des substrats souples, ces détecteurs pourraient être utilisés pour une large gamme d'applications et notamment les détecteurs de gaz portatifs et intégrés. La résistance électrique des résistors s'avère décroître avec la température suggérant une conduction électrique gouvernée par l'effet tunnel et les fluctuations au sein du tapis désordonné de nanotubes de carbone. Nous avons cependant montré dans ce travail que pour des applications réelles de détection de gaz, une régulation thermique des dispositifs n'est pas nécessaire car les variations de résistance engendrées par l'adsorption de molécules de gaz sont significativement plus grandes que les variations causées par de possibles fluctuations de température. Les dispositifs produits présentent un caractère métallique à température ambiante et pour des applications de détection de gaz nous avons sélectionné des dispositifs présentant des résistances inférieures à 100 kΩ. Le principe de base de la détection de gaz étant basé sur la mesure directe de la résistance électrique du dispositif, la consommation électrique de ces dispositifs reste faible (<1 μW).

La réponse des dispositifs à base de nanotubes de carbone non fonctionnalisés aux analytes testés (éthanol, acétone, ammoniac et vapeur d'eau) est faible. Les nanotubes de carbone fonctionnalisés présentent quant à eux, une réponse modérée à la vapeur d'eau, à l'éthanol et à l'acétone mais montrent une sensibilité excellente à l'ammoniac. En particulier, les nanotubes de carbone oxydés se sont avérés capables de détecter des concentrations sub-ppm d'ammoniac en présence de vapeur d'eau en excès et à température ambiante et ont montré une grande stabilité dans le temps même pour des expositions de gaz répétées. Nous pensons que les groupes chimiques fonctionnels ancrés à la surface des nanotubes de carbone modifient les interactions entre les molécules de gaz et les nanotubes et que le transfert de charges induit provoque les modifications de la conductance électrique du système.

Nous avons construit un modèle phénoménologique pour analyser les réponses électriques de nos dispositifs lors de l'exposition d'un gaz. Ce modèle prend en compte une variation exponentielle de la résistance au cours du temps puis un régime d'accroissement linéaire de cette résistance. Nous montrons en particulier que la constante de temps extraite du régime exponentiel est très informative sur la sensibilité et la sélectivité du détecteur de gaz. Nous avons finalement testé nos dispositifs pour des applications représentatives comme par exemple la détection de traces d'ammoniac qui ont pu être aisément réalisées à des concentrations bien inférieures au seuil de détection du nez humain (0.04ppm). En raison de leur grande stabilité, facilité de fabrication (design très simple, technologies de fabrication bas coût, intégration sur substrats souples), robustesse (détection possible en présence de vapeur d'eau et résiliente aux fluctuations thermiques) et en raison de la faible quantité de nanotubes de Carbone nécessaire, nous pensons que nos résultats sont intéressants pour des applications de masse concernant des détecteurs de gaz portables pour l'industrie des technologies de l'information et de la communication.

Capteurs de Gaz integrant des nanotubes de Carbone bi-parois

Lin Yang, 28 Novembre 2017.

Introduction

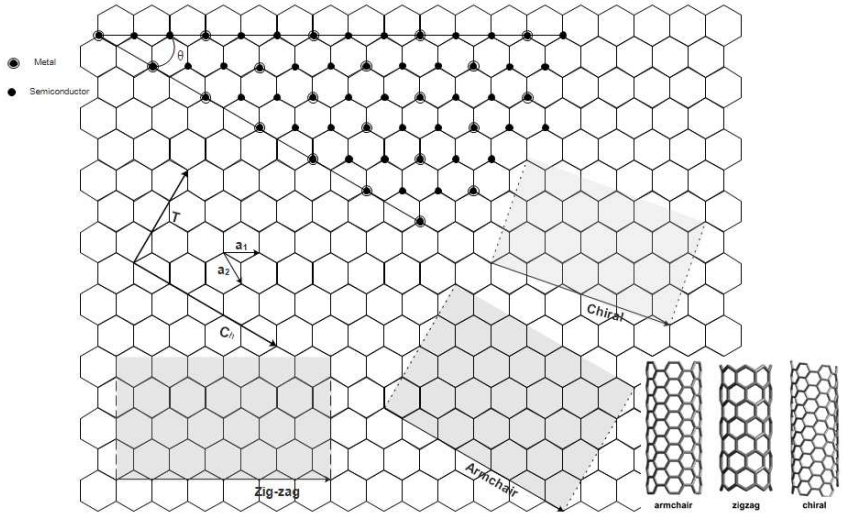
Selon certains scientifiques nous vivons au 21ième siècle une nouvelle ère géologique baptisée l'anthropocène qui marque l'empreinte des activités humaines sur notre planète. Autant dire que les problématiques environnementales sont devenues aujourd'hui un enjeu important dont il faut se soucier activement afin de modifier drastiquement nos comportements et notre manière de vivre. Parmi toutes ces problématiques, la pollution de l'air par toutes sortes d'espèces moléculaires issues de nos véhicules, de nos installations industrielles, de nos traitements agricoles ou par des actes de malveillance est devenue une source inquiétante de menaces. La diminution et le contrôle des effluents gazeux potentiellement nocifs ainsi que la protection des individus exposés, passent par notre capacité à détecter en tous lieux et à chaque instant avec des instruments portatifs et à bas coût, la présence de certaines molécules gazeuses dans l'air ambiant. C'est dans cette très large perspective que les travaux de recherche consignés dans cette thèse ont été menés. Nous avons essayé de concevoir une technologie de fabrication de capteurs de gaz qui remplissent le cahier des charges précédemment évoqué. Nous avons fait le choix d'une méthode de fabrication simple et peu coûteuse, compatible avec la fabrication de masse et une méthode de mesure robuste compatible avec une détection en plein air à température ambiante et dans une atmosphère potentiellement humide. Ce choix nous a orienté vers la fabrication de détecteurs de gaz qui sont de simples résistances électriques formées par des Nanotubes de Carbone bi-parois fonctionnalisés en surface. En effet, il est connu que le transport électrique au sein d'un tapis de nanotubes de carbone est sensible aux espèces moléculaires susceptibles de s'adsorber à la surface de ces nano-objets. Ainsi, par une simple mesure de la variation de résistance électrique il devient possible de révéler des évènements d'adsorption moléculaire. Par la fonctionnalisation chimique de surface nous avons tenté de rendre cette détection spécifique à certaines entités gazeuses et en particulier pouvoir discerner un gaz d'intérêt par rapport à la vapeur d'eau nécessairement présente dans l'air ambiant. Ainsi le prisme sous lequel ces travaux doivent être considérés est celui de la robustesse et de la portabilité de la

détection, plus que celui de la limite de détection ultime, lequel n'a pas constitué le principal enjeu de notre recherche.

Ce travail est composé de trois chapitres principaux. Dans le premier chapitre nous rappelons ce que sont les nanotubes de Carbone et leurs méthodes de synthèse et nous décrivons l'état de l'art de la fabrication de détecteurs de gaz à base de nanotubes de Carbone. Dans un second chapitre nous décrivons les résultats obtenus sur la synthèse et la fonctionnalisation chimique de nanotubes de Carbone bi-parois, sur la fabrication des détecteurs intégrant ces nanotubes au sein de résistances électriques de dimension micrométriques et sur les mécanismes de conduction électrique au sein de ces résistors. Nous montrons également l'influence de l'adsorption de différentes espèces gazeuses sur les caractéristiques électriques de ces dispositifs. Enfin, dans un troisième chapitre nous montrons des expériences de détection « de terrain » réalisées avec nos capteurs de gaz.

Chapitre 1 : Introduction aux nanotubes de Carbone et à leur utilisation pour la détection de gaz

Les nanotubes de carbone, mis en évidence par Iijima il y a maintenant plus de 25 ans, peuvent être décrits comme des cylindres creux formés par enroulement d'un feuillet de graphène (sans recouvrement). Ils peuvent comporter une ou plusieurs parois coaxiales, dans le cas des nanotubes de carbone multiparois (MWNT). La manière dont le plan de graphène est orienté selon l'axe du nanotube de carbone détermine l'ensemble de ses propriétés, et notamment le fait qu'il se comporte comme un métal ou comme un semi-conducteur. La figure ci-dessous décrit les différentes structures possibles dans le cas d'un nanotube de carbone monoparoi (SWNT). La structure d'un NTC monoparoi est totalement définie par un vecteur que l'on note C_h. Ce vecteur définit aussi un angle d'hélicité, θ (Fig.1-3(a)). Le vecteur est défini par la relation suivante : $C_h=na1+ma2$, n et m étant deux entiers positifs, et a1 a2 les deux vecteurs unitaires définissant le plan de graphène.



Description des différentes structures possibles dans le cas d'un Nanotube de carbone monoparoi

Les propriétés des *NTC* notamment électriques, obéissent à certaines règles en lien avec leur chiralité. En effet, lorsque la différence des indices dans le couple (*n,m*) est égale à un multiple de 3 (0 inclus), alors le nanotube aura un caractère métallique (absence de gap entre les bandes de valence et de conduction. Dans tous les autres cas, il est semi-conducteur. Cette relation permet de déterminer très simplement dans le cas d'un *NTC* monoparoi le caractère électrique qu'il possède, à savoir métallique ou semi-conducteur. Le caractère semi-conducteur s'exprime naturellement lorsque $n \neq m$ avec *n-m* non multiple de 3.

- ❒ *NTC zigzag :* $(n,0)\ et\ \theta = 0°$ - Peuvent être métalliques ou semi-conducteurs (métalliques si n est un multiple de 3)
- ❒ *NTC armchair (fauteuil) :* $(n,n)\ et\ \theta = 30°$ - Sont uniquement métalliques.
- ❒ *NTC chiral :* $(n,m)\ et\ 0 < \theta < 30°$

Les propriétés électroniques des NTC dépendent de leur angle d'enroulement et de leur diamètre, ainsi que nous l'avons décrit préalablement. Dans le cas des SWNT, la proportion est de 2/3 de NTC semi-conducteurs pour 1/3 de NTC métalliques. Avec les MWNT, chacun des feuillets est relativement indépendant du point de vue de ses propriétés électriques. En effet, chaque feuillet peut être soit semi-conducteur, soit métallique. Bien qu'un certain couplage entre les parois consécutives soit décrit, il est considéré généralement que la proportion de NTC de type métallique augmente avec

le nombre de parois. Les NTC présentent un très grand intérêt dans le domaine de la microélectronique. Ils peuvent transporter des densités de courant supérieures à 10^9 A/cm² (à 300°C pendant un temps très court). Ces valeurs de densité de courant peuvent être 1000 fois supérieures à celles supportées par les métaux (cuivre, argent). L'augmentation du nombre de parois provoque l'augmentation de la proportion de défauts, et donc une diminution de la conductivité électrique et une dégradation des propriétés mécaniques. Les NTC biparois (DWNT) offrent la conformation géométrique idéale à la frontière des NTC mono et multiparois. Leur caractère métallique est très prononcé (75-80%). Les densités de courant peuvent atteindre par exemple 9.108 A/cm² pour les DWNT oxydés. La distance inter-tube est quelquefois décrite comme une variable qui influence le caractère semi-conducteur des NTC. Par exemple, plus cette distance augmente, plus le NTC interne sera métallique pour les NTC à chiralité zig-zag/zig-zag. En réalité, ce type de conformation est très rare, et en pratique la structure de chacun des NTC composant un DWNT n'est pas contrôlée lors de la synthèse, bien que des travaux récents montrent que certaines configurations (relations entre tube interne et externe) soient favorisées alors que d'autres sont au contraire défavorisées. Cependant, la distance inter-parois varie peu (entre 0,34 et 0,35 nm). Les Nanotubes de carbone biparois utilisés dans ces travaux sont donc considérés comme présentant majoritairement un caractère de conducteur métallique, ceci étant d'autant plus vrai qu'ils sont le plus souvent organisés sous forme de faisceaux de nanotubes et que dans de telles structures, les nanotubes métalliques assurent la conductivité électrique de l'ensemble.

Méthodes de synthèse

Il existe diverses méthodes pour synthétiser les NTC. Celles-ci sont toutes basées sur le même principe utilisant une source carbonée, sous forme solide ou gazeuse, et le plus généralement la présence d'un catalyseur. Les différentes techniques disposent généralement d'une panoplie de conditions opératoires permettant de générer, selon les conditions expérimentales, tous les types de NTC (SWNT, DWNT, MWNT), sans que leurs caractéristiques structurales / physico-chimiques (chiralité, qualité, pureté) soient totalement contrôlées. Trois techniques majeures se distinguent : l'arc électrique, l'ablation laser et le dépôt chimique catalytique en phase

vapeur (CCVD). Le dépôt chimique catalytique est une voie de synthèse dite à «température modérée», contrairement aux deux autres qui sont considérées comme des voies de synthèse à haute température.

Décharge par arc électrique

Le principe de la décharge par arc électrique repose sur l'application d'un champ électrique intense sous atmosphère inerte et à faible pression entre deux électrodes de graphite. Cet état provoque l'apparition d'un plasma engendrant la sublimation de l'anode (>3000°C température de fusion du graphite) et ainsi la production de produits carbonés de différentes natures à la cathode (électrodes imprégnés par des métaux de transitions (Fe, Ni, Co, Yttrium)). Ce type de synthèse fut utilisé initialement pour la synthèse des fullerènes, et par la suite des sous-produits comme les SWNT ou MWNT. Malheureusement, cette technique ne peut être industrialisée, car elle conduit à des produits hétérogènes, c'est à dire à une grande variété de matières carbonées, nécessitant plusieurs étapes de purification (et une augmentation du coût de production). La génération de l'arc devient aussi rapidement problématique lorsque le diamètre des électrodes augmente.

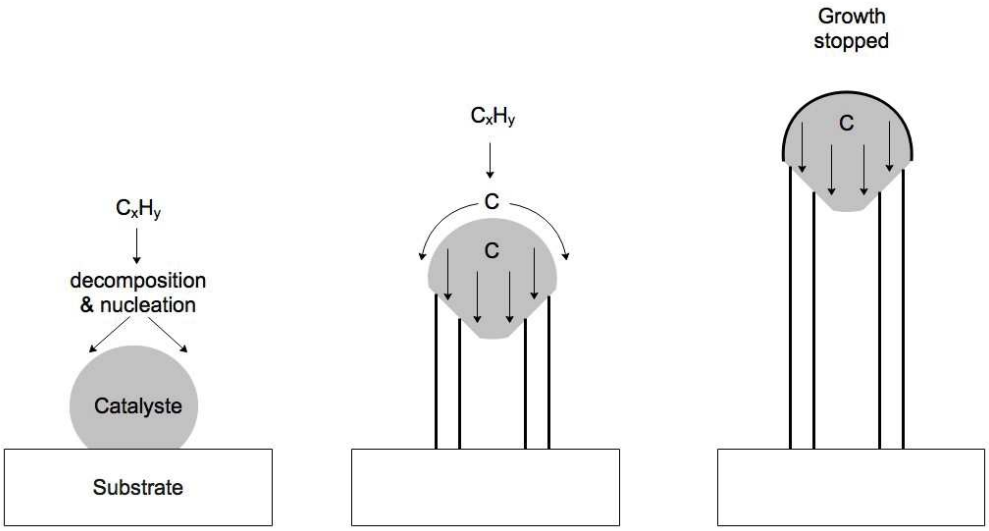
Synthèse par ablation laser

La méthode de synthèse par ablation laser a initialement permis de découvrir les fullerènes. Cette méthode consiste à insérer un bloc de graphite dans un four chauffé à une température avoisinant les 1200°C. Le carbone est vaporisé sous l'application d'un rayonnement laser de haute énergie (pulsé ou continu). Les produits carbonés ainsi obtenus sont entrainés par un flux de gaz inerte et récupérés au niveau d'un collecteur en cuivre refroidi. En ajoutant des catalyseurs métalliques (Co, Ni) au graphite, il est possible d'obtenir des SWNT. Cette méthode permet d'obtenir des NTC de grande pureté, avec cependant de faibles rendements. Elle est de plus très coûteuse.

Dépôt chimique catalytique en phase vapeur (CCVD : Catalytic Chemical Vapour Deposition

Cette technique est l'une des méthodes de synthèse des NTC les plus utilisées, notamment pour la production industrielle, permettant la production de SWNT ou de MWNT, selon les conditions expérimentales. Des quantités industrielles allant jusqu'à

la tonne peuvent être préparées. Le principe de cette méthode est relativement simple et basé sur la décomposition d'un gaz carboné à la surface de nanoparticules catalytiques le plus souvent métalliques, à des températures généralement comprises entre 400 et 1200 °C. Le carbone décomposé diffuse en surface des nanoparticules, jusqu'à précipiter à la saturation pour former un "chapeau" qui se soulève suite à l'apport constant en carbone, formant ainsi un nanotube de carbone tel qu'illustré par exemple sur la figure ci-dessous :

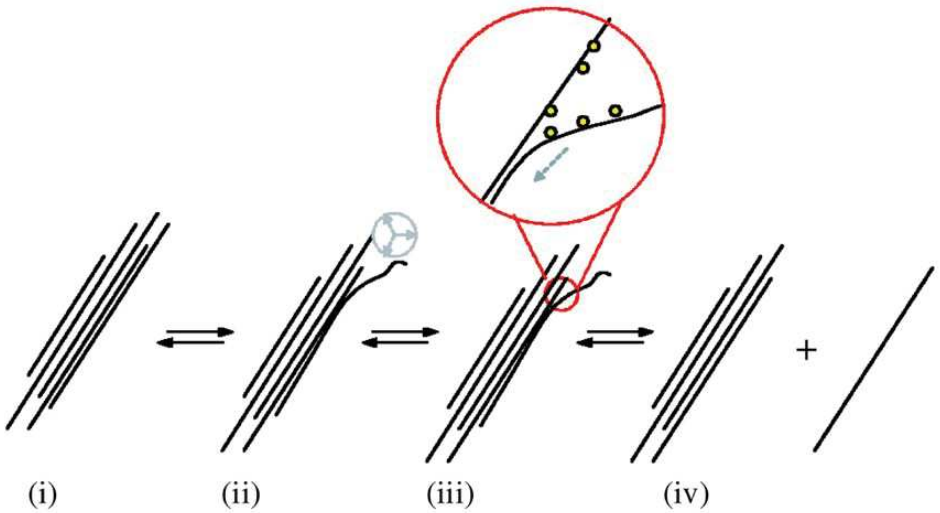


Croissance des nanotubes de carbone sur particule métallique : (a) «tip-growth model», (b) «base- growth model»

D'un point de vue mécanistique, le dépôt de type «tip-growth» (ci-dessus) implique une interaction faible entre le catalyseur et le substrat et la source de carbone se décompose en surface de la particule. Les produits migrent ensuite vers le bas via la particule métallique. Les NTC croissent sous la particule métallique, poussant ainsi l'intégralité de la particule hors du substrat. Pour le dépôt de type «base-growth», le mécanisme fait intervenir la création d'un chapeau de graphène qui se forme sur le dessus de la particule. Le chapeau se décolle lorsque la paroi du NTC croit. La taille de la particule catalytique détermine ainsi généralement le diamètre des NTC. La nanoparticule peut donc se trouver à une des deux extrémités du NTC, en fonction du mécanisme de croissance. Eventuellement dans le cas des MWNT, la particule peut se fragmenter au cours de la croissance et ainsi être emprisonnées à l'intérieur du NTC. Un large éventail de sources carbonées peut être utilisé, comme par exemple le monoxyde de carbone (CO), des hydrocarbures comme le méthane

(CH_4), l'acétylène (C_2H_2), le propylène (C_3H_6), ou encore le benzène, le toluène ou même les alcools. La composition des catalyseurs est également variée. En général, il s'agit de nano particules métalliques, dispersées sur un substrat, soit directement mises en contact avec le gaz carboné (aérosols), soit générées in situ lors de la synthèse. Les catalyseurs sont souvent composées de fer (Fe), cobalt (Co), ou nickel (Ni). Il est également possible d'utiliser des mélanges constitués de particules bimétalliques Co/Molybdène, Fe/Co, Co/Ni. La mise en œuvre de catalyseurs sous forme de solutions solides permet la génération in situ des nanoparticules et donc d'éviter leur croissance exagérée. Cette technique est celle qui a été utilisée pour la synthèse des DWNT au cours de ces travaux de thèse.

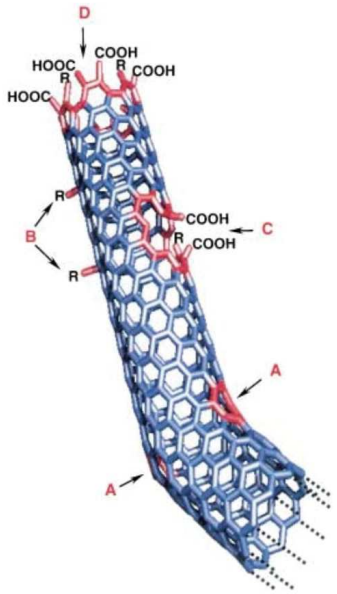
Nous nous intéressons ici essentiellement aux applications des nanotubes de carbone dans le domaine des capteurs de gaz et la fonctionnalisation est une des méthodes proposées pour améliorer la sélectivité des nanotubes de carbone. La fonctionnalisation peut être covalente ou non selon les méthodes employées. La figure ci-dessous illustre comment la fonctionnalisation non covalente est mise en œuvre pour séparer les nanotubes de carbone dans un faisceau et les individualiser.



Individualisation des nanotubes de carbone par insertion progressive de surfactant adsorbé à la surface.

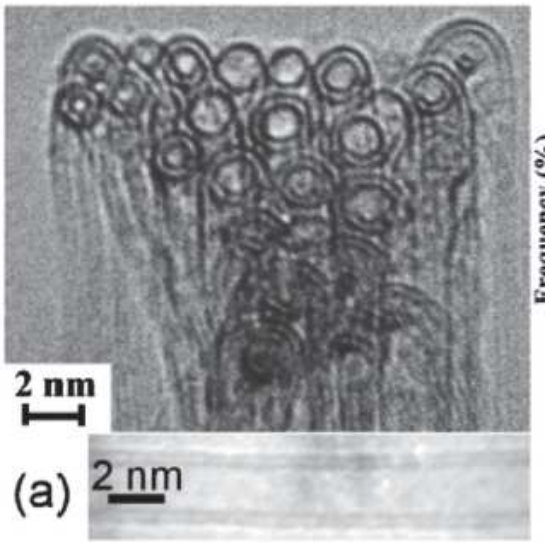
Nous avons choisi dans nos travaux de nous focaliser sur la fonctionnalisation covalente par greffage de fonctions oxygénées ou aminées. Les fonctions oxygénées sont obtenues par traitement à l'acide nitrique à reflux, ce qui est la méthode la plus

répandue dans la bibliographie. Une illustration des fonctions carboxyliques ainsi obtenues est donnée ci-dessous, ces dernières sont localisées essentiellement aux extrémités des nanotubes de carbone (probablement ouvertes après ce traitement), ou encore le long de la paroi là où des défauts de structure (repérés par la lettre A : pentagone ou heptagone) sont potentiellement présents :



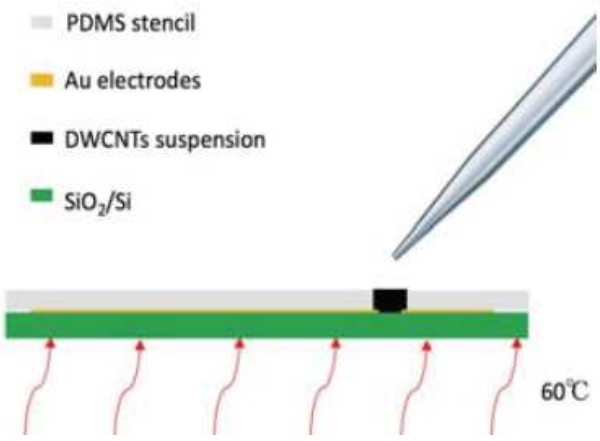
Chapitre 2 : Résultats expérimentaux

Les nanotubes de Carbone bi-parois ont été obtenus par dépôt catalytique en phase vapeur à partir d'un précurseur gazeux de type méthane. Le résultat de cette synthèse produit une poudre solide contenant les objets présentés sur l'image suivate obtenue par microscopie électronique en transmission.

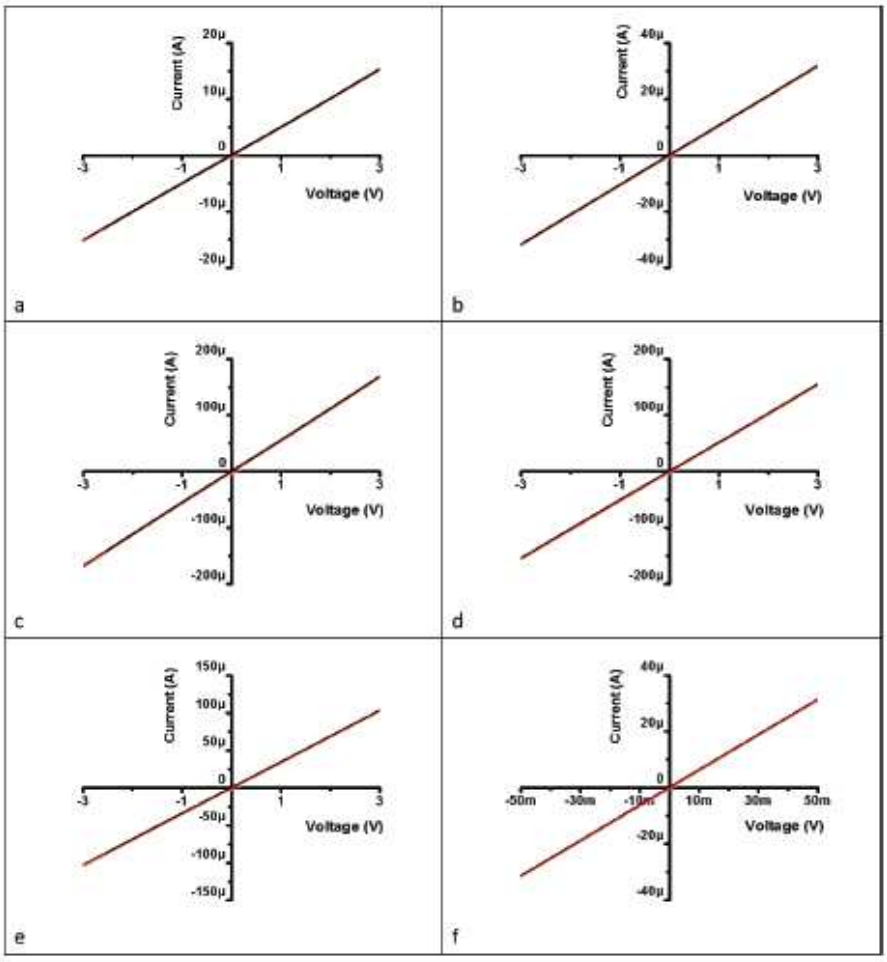


On observe clairement au sein de cette poudre une quantité importante de nanotubes cylindriques bi-parois (80% des espèces produites) d'un diamètre d'environ 2 nm et de longueur variable située autour de 10 µm. Après nettoyage de cette poudre solide par de l'acide chlorhydrique, ces nanotubes de carbone sont fonctionnalisés chimiquement par greffage covalent de terminaux de type COOH on parle alors de nanotubes de carbone oxydés ou par des terminaux de type NH2, on parlera alors de nanotubes aminés. A la fin de ces procédés, des dispersions dans l'eau de ces nanotubes de Carbone fonctionnalisés sont obtenues et stabilisées avec du SDS pour les nanotubes aminés ou du CMC pour les nanotubes oxydés.

Ces nanotubes de carbone (NTCs) sont ensuite intégrés au sein d'un capteur comportant un réseau de 7 résistances électriques par une méthode simple et originale de **pochoir en phase liquide**. A la surface d'une puce (1cm X 2cm) de Silicium comportant un jeu de microélectrodes de 600 µm de large nous déposons localement les NTCs en pipetant directement un volume contrôlé de ces dispersions au sein de cavités d'un pochoir plastique en PDMS puis en évaporant le solvant aqueux. Le réseau de microélectrodes est obtenu par lithographie optique conventionnelle et le pochoir en PDMS par moulage direct sur un moule fabriqué par usinage mécanique. Ainsi les ingrédients de notre fabrication sont conventionnels et très peu coûteux à produire. Le schéma suivant présente succinctement le procédé de dépôt localisé en phase liquide à l'aide d'un pochoir.

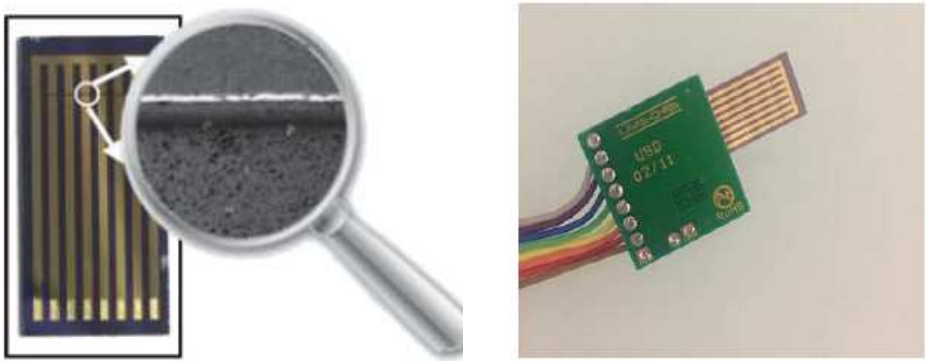


A la fin du procédé de fabrication nous générons 7 résistances électriques qui sont composées chacune par un tapis désordonné de NTCs bi-parois fonctionnalisés, la longueur de chaque résistance est de 80 µm et la largeur 200 µm. Après rinçage qui permet d'enlever le surplus de NTCs mal fixés à la surface et de nettoyer les NTCs des traces de SDS ou de CMC, nous obtenons de manière très reproductible des dispositifs électriques présentant un comportement ohmique à température ambiante. Notons que pour l'ensemble du procédé de fabrication, la consommation de NTCs est très faible (de l'ordre du µg).

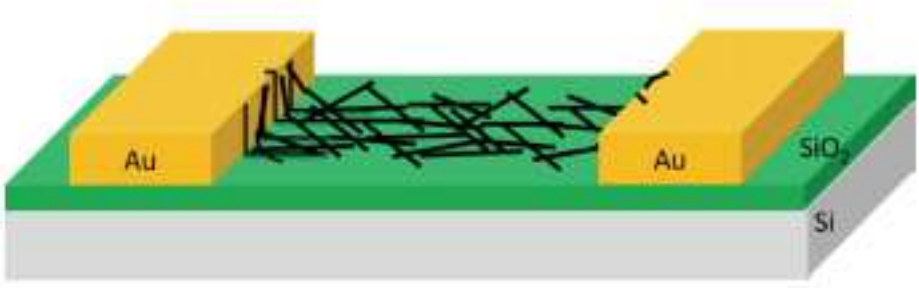


Caractéristiques électriques I(V) à température ambiante de six capteurs différents intégrant ds NTCs oxydés. Les résistances varient entre 2 et 200 kΩ.

Les figures suivantes présentent des images des différents éléments de notre capteur : à gauche la puce en silicium équipée des microélectrodes et un zoom sur la région du gap entre les électrodes où ont été intégrés les NTCs fonctionnalisés et à droite un capteur connecté à un circuit de mesure externe.



En étudiant les mécanismes de conduction électrique au travers de ce tapis désordonné de NTCs bi-parois fonctionnalisés, nous avons mis en évidence que d'une microélectrode à l'autre les électrons de conduction doivent passer au travers du réseau formé par les nanotubes par effet tunnel. En effet, les NTCs bi-parois ont un comportement métallique à température ambiante mais pour connecter le gap entre les microélectrodes de 80 µm, il faut emprunter plusieurs de ces NTCs comme le schématise la figure çi-dessous.

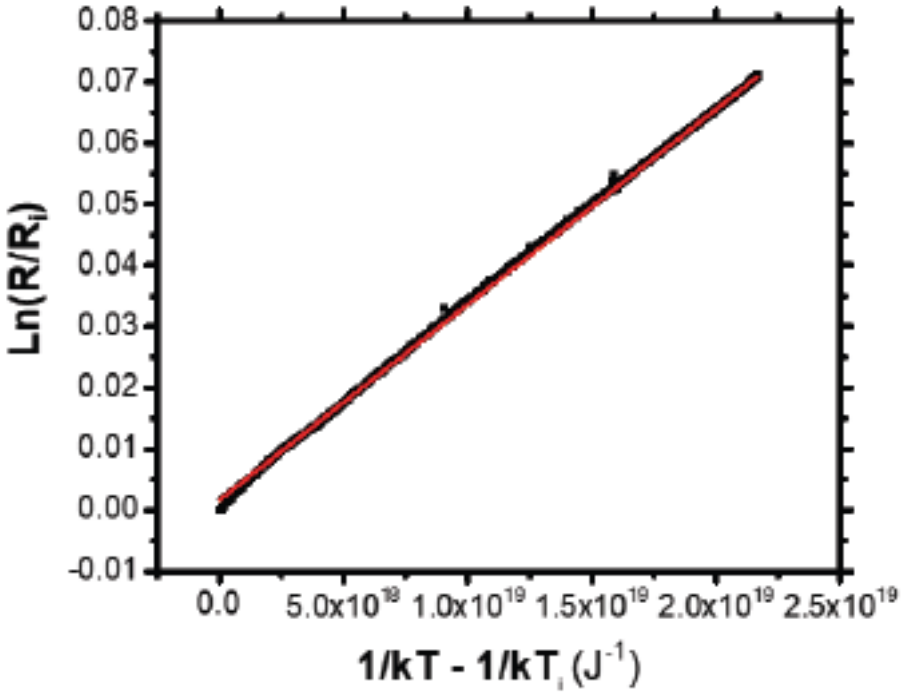


Ainsi, le courant mesuré au travers de la résistance dépend de la conductivité intrinsèque des NTCs mais aussi des jonctions tunnels entre NTCs. Dans de tels systèmes la conduction est donc gouvernée par l'effet tunnel et les fluctuations de potentiel liées au caractère désordonné du réseau. Nous avons pu vérifier que le modèle proposé en 1980 par P. Sheng pour décrire de tels systèmes s'applique très

bien à nos dispositifs. La résistance du dispositif est activée thermiquement et peut s'écrire sous la forme :

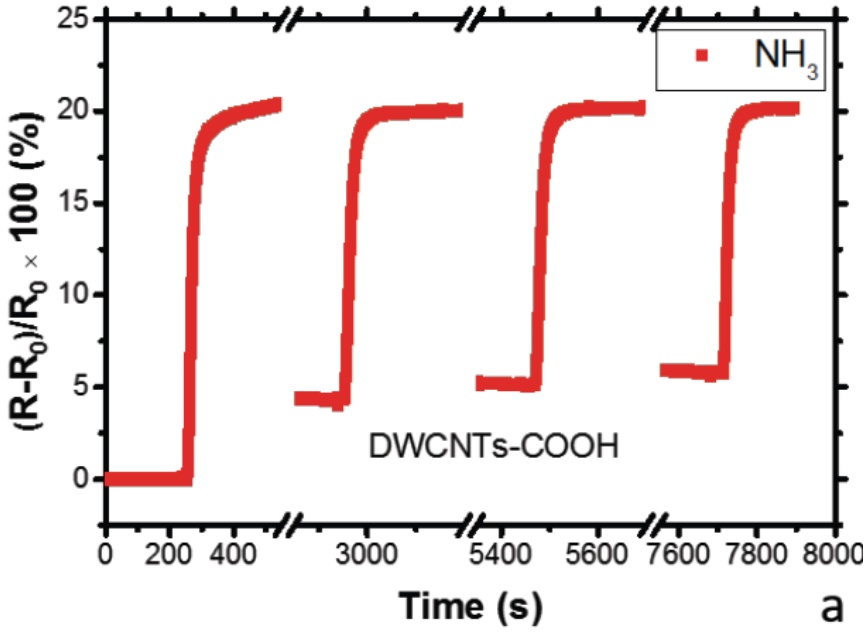
$$R=R_0 \exp(-E_{act}/kT)$$

Ce modèle permet donc d'établir la variation de la résistance de ces dispositifs avec la température. Dans le cas de nos dispositifs nous obtenons une diminution de la résistance lorsque la température augmente et cette variation autour de la température ambiante est d'environ 0.3% par degré Celsius. C'est un résultat très important pour notre application car il montre que en situation d'utilisation réelle où la température n'est pas régulée et peut fluctuer pendant le temps de la mesure, les variations aléatoires de la résistance électrique liées à ces fluctuations thermiques restent très faibles.



Variation thermique de la résistance électrique d'un capteur à base de NTCs oxydés représentée de manière à montrer l'adéquation avec la formule dériuvée du modèle de P. Sheng.

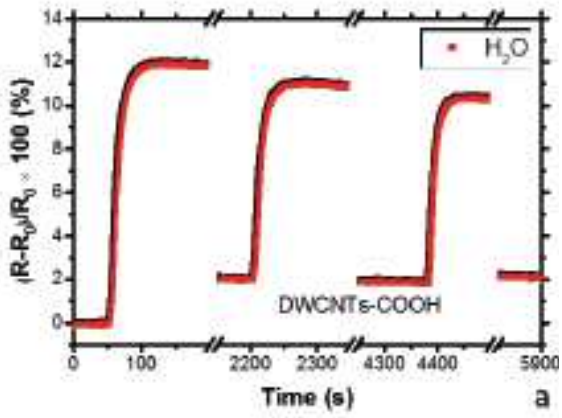
Nous avons ensuite soumis ces résistances électriques à base de NTCs fonctionnalisés à différents types d'exposition par des gaz simples (Acétone, Ethanol, Ammoniac, vapeur d'eau). Nous montrons clairement que l'adsorption des molécules du gaz à la surface des NTCs et au voisinage des jonctions tunnels modifie de manière importante et reproductible la résistance électrique du capteur à température ambiante. Nous expliquons principalement ces modifications par un transfert de charges entre la molécule adsorbée et les NTCs. Ces transferts de charges modifient le dopage des NTCs et donc leur conductivité et également modifient la hauteur de barrière des jonctions tunnel. Ces modifications sont dépendantes de la fonctionnalisation de surface des NTCs et de la nature des gaz adsorbés. Ainsi, par la fonctionnalisation nous pouvons améliorer la sensibilité de la détection et également sa spécificité. La plus belle réussite de ce travail est représentée sur la figure suivante.



Expositions répétées de traces d'ammoniac (17 ppm) diluées dans une concentration de vapeur d'eau de 5000 ppm et détectées électriquement par un capteur à base de NTCs oxydés.

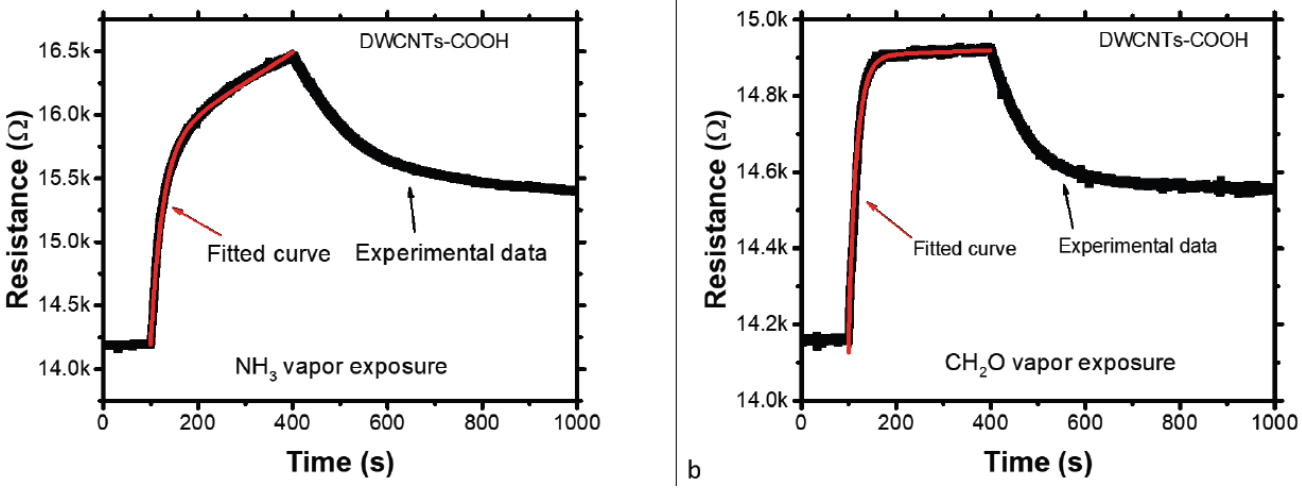
Nous observons les variations relatives de la résistance électrique pour une exposition répétée à un gaz contenant 17 ppm d'ammoniac en présence d'une concentration 500 fois supérieure de vapeur d'eau. Ces variations sont de l'ordre de 20 % alors que ce même capteur, soumis à une concentration similaire de vapeur

d'eau en l'absence de toute trace d'ammoniac ne montre des variations de résistance que de l'ordre de 10% (voir figure çi-dessous).



Expositions répétées de vapeur d'eau de concentration 5000 ppm et détectées électriquement par un capteur à base de NTCs oxydés.

On voit donc que grâce à la fonctionnalisation de surface il devient possible de détecter une toute petite concentration d'ammoniac, même en présence d'une très forte humidité résiduelle, à température ambiante et sans régulation thermique.
Nous avons ensuite étudié la dynamique de notre signal et modélisé de manière phénoménologique la variation de la résistance de nos capteurs au cours du temps R(t) lors de l'exposition à une vapeur gazeuse donnée. Nous montrons que notre modèle permet d'ajuster proprement nos courbes expérimentales (figure çi-dessous).

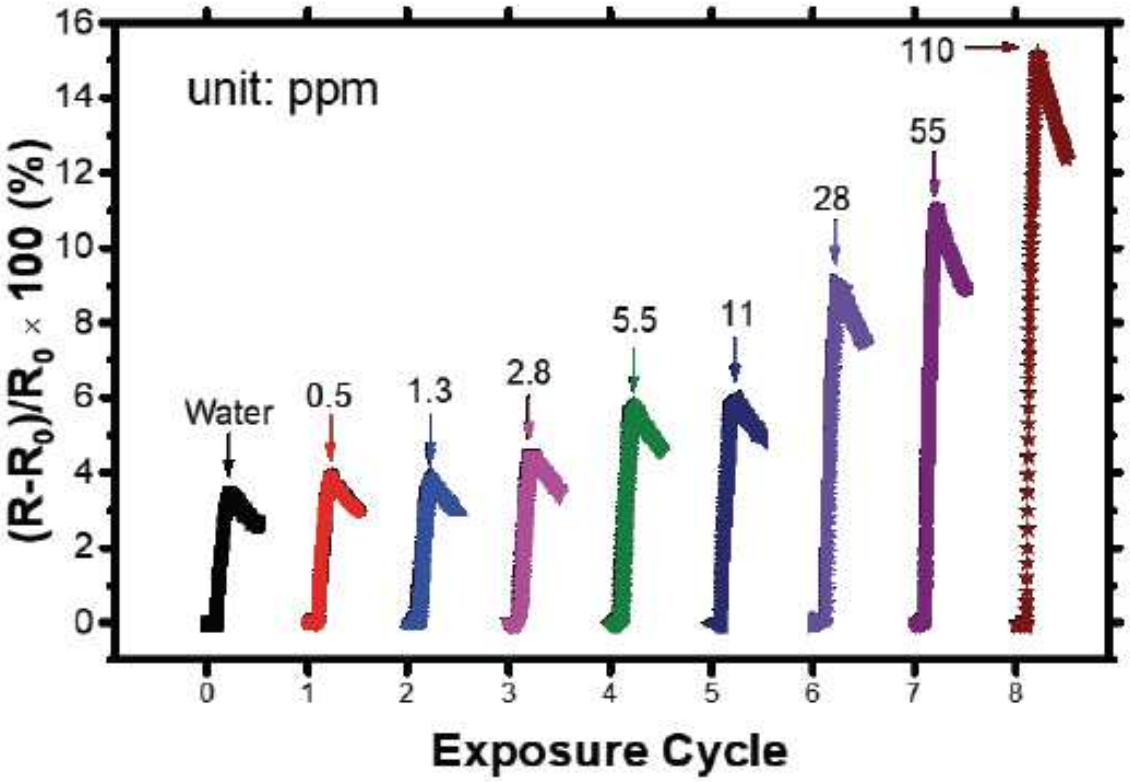


Nous observons à gauche, un signal de détection pour un capteur à base de NTCs oxydés en présence d'une trace d'ammoniac au sein de vapeur d'eau et à droite, en présence d'une trace de formaldéhyde au sein de vapeur d'eau. Les courbes noires montrent les mesures expérimentales et les courbes rouges le résultat de nos ajustements.

Grâce à ce modèle d'ajustement nous pouvons à partir d'un signal mesuré extraire deux paramètres : τ, la constante de temps de montée de la résistance juste après l'exposition : régime exponentiel et α, le taux d'accroissement de la résistance dans le régime linéaire. Ces paramètres, en plus de l'amplitude de la variation relative de la résistance électrique, peuvent être utilisés pour différencier les espèces gazeuses ayant interagi avec le capteur. La table suivante montre, par exemple, comment ces paramètres dépendent de la molécule détectée pour des capteurs à base de NTCs oxydés.

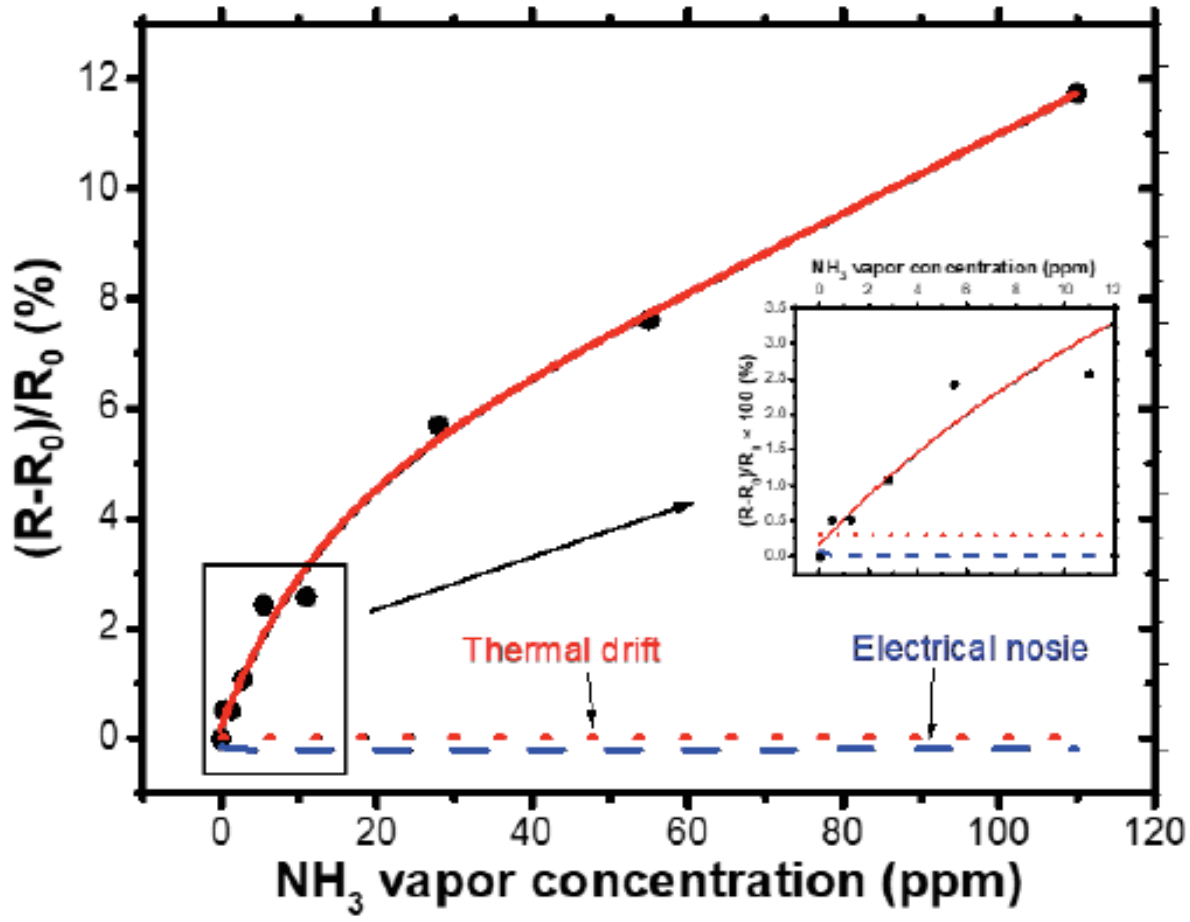
	$\tau(s)$	$\alpha(\Omega s^{-1})$
NH_3	25.35	2.38
CH_2O	16.60	0.05
H_2O	15.54	0.18

Finalement, nous nous sommes également intéressés à la détermination de la sensibilité de nos capteurs et l'éventuelle possibilité de les calibrer. Pour cela nous avons sélectionné des capteurs à base de NTCs oxydés et nous les avons exposés avec des traces d'ammoniac à des concentrations variant de 0.5 à 110 ppm au sein d'une concentration d'environ 500 ppm de vapeur d'eau. La figure suivante représente les résultats obtenus.



Signal de détection typique d'un capteur à base de NTC oxydés exposé avec des traces d'ammoniac à des concentrations variant de 0.5 à 110 ppm au sein d'une concentration d'environ 500 ppm de vapeur d'eau.

Nous observons que des traces d'ammoniac peuvent être détectées au sein de vapeur d'eau jusqu'à des concentrations inférieures au ppm et que le signal du capteur dépend bien de la concentration de l'espèce gazeuse. Il est à noter que pour cette expérience les différentes concentrations ont été exposées de manière séquentielle en commençant par la plus faible. Cette expérience montre la bonne stabilité de nos capteurs pour des expériences longues (environ 2 heures ici), leur bonne récupération entre deux détections et leur bonne reproductibilité d'une détection à l'autre. Ces résultats peuvent également être présentés sous la forme d'une courbe de calibration.



Courbe de calibration d'un capteur à base de NTC oxydés pour la détection de traces d'ammoniac diluées dans 500 ppm de vapeur d'eau

Le signal n'évolue pas linéairement avec la concentration. Sur cette figure nous avons également reporter quel est le bruit de la mesure électrique en bleu c'est à dire avec quelle précision la résistance électrique du dispositif est mesurée et le résultat d'une dérive de la température de 1°C en rouge.

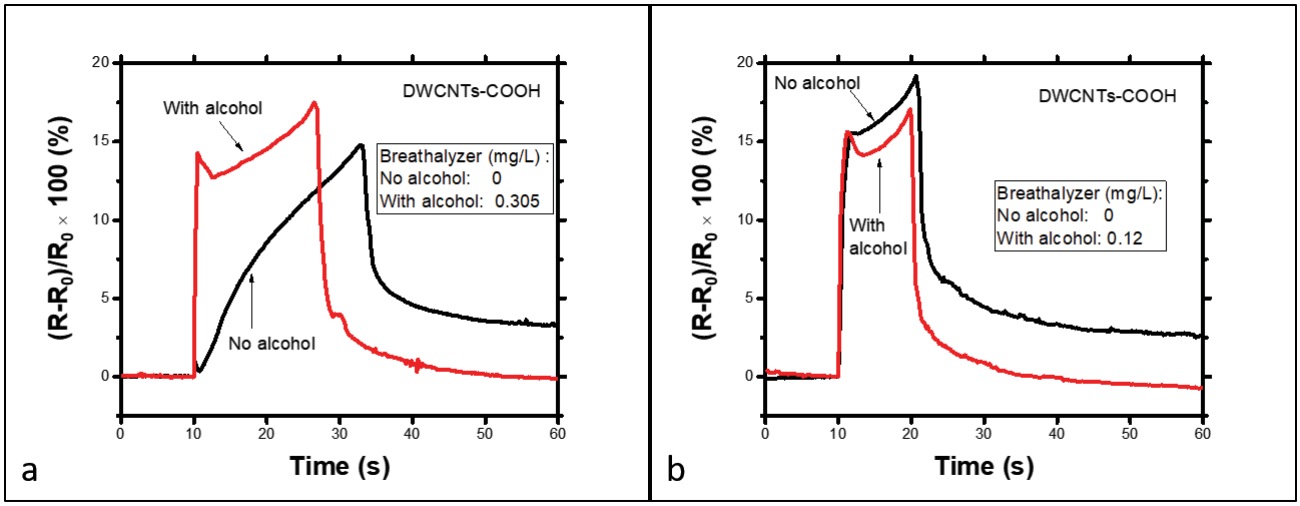
En résumé de ce chapitre nous avons montré que les capteurs à base de NTCs fonctionnalisés étaient capables de détecter différentes espèces gazeuses comme l'acétone, l'éthanol, l'ammoniac et le formaldéhyde. Pour les deux fonctionnalisations de surface privilégiées dans cette étude (COOH et NH2) nous avons obtenu la meilleure sensibilité pour la détection de l'ammoniac ou du formaldéhyde et cela, même en présence d'une forte concentration concurrente de vapeur d'eau. Nos capteurs ne sont pas affectés par des variations de température raisonnables de quelques degrés autour de la température ambiante et peuvent donc être employés

sans aucune régulation thermique. La limite de détection dans le cas de traces d'ammoniac est inférieure à 1ppm. Le temps de réponse de nos capteurs est relativement court (τ = 10 à 30 s, en fonction des espèces gazeuses). Après exposition le temps de retour de ces capteurs est également relativement court (entre 1 et 2 minutes). Ainsi à température ambiante, le capteur se régénère spontanément au bout de quelques minutes à la suite de la désorption progressive des molécules adsorbées à sa surface. Des cycles répétés d'exposition ont pu ainsi être réalisés.

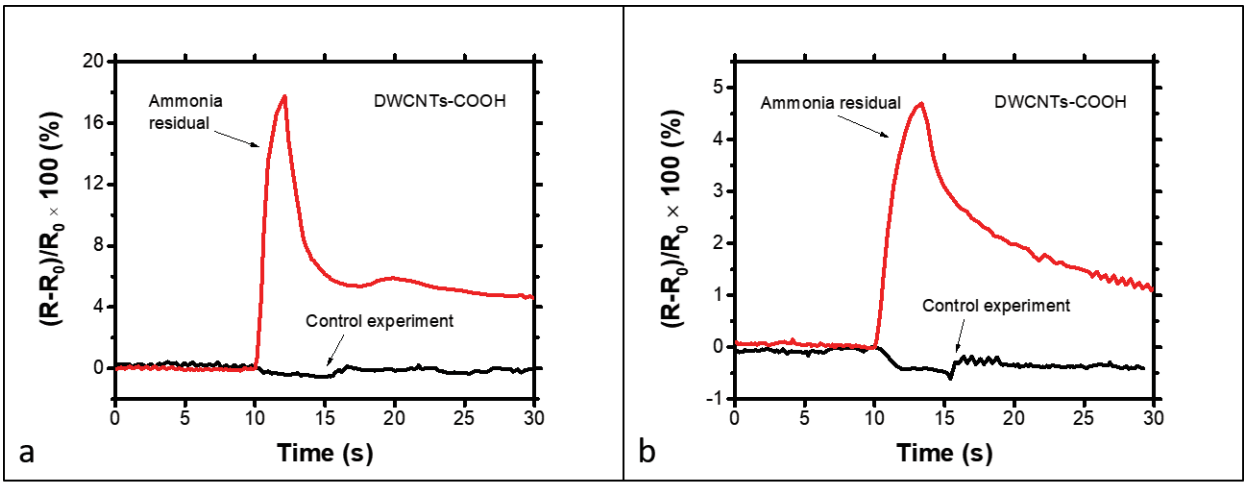
L'ensemble de ces caractéristiques montre que la technologie mise en place et les choix opérés au cours de ce travail de thèse permettent réellement de remplir les objectifs initiaux à savoir : une détection simple et robuste, utilisable à température ambiante et en atmosphère ouverte pour un coût de production extrêmement réduit et compatible avec une fabrication de masse.

Chapitre 3 : Application à la détection de gaz en conditions réelles d'utilisation

Pour terminer, nous avons souhaité tester notre dispositif dans des conditions réelles d'utilisation, par exemple en tant qu'éthylomètre. La figure ci-dessous illustre les résultats encourageants obtenus avec des nanotubes de carbone oxydés, et les compare à ceux obtenus avec un éthylomètre du commerce. Ceci démontre le fort potentiel applicatif de nos dispositifs puisque en essayant d'estimer l'ensemble des coûts incluant les matières premières (dont les DWNT) et les coûts de production, le prix de revient de nos capteurs est estimé autour de 1€, à mettre en comparaison avec le prix de l'appareil commercial (300€).



Un autre exemple concerne la détection de traces d'ammoniac, en particulier en présence d'humidité (air ambiant). La figure ci-dessous illustre les résultats obtenus et démontre ici encore à la fois la sensibilité et la sélectivité de nos dispositifs.



Détection de traces d'ammoniac à l'aide de capteurs à base de DWNT oxydés dans un flacon ayant contenu de l'ammoniac : (a) 24h après avoir rincé le flacon et (b) 46 jours après. L'expérience de contrôle correspond à un flacon identique mais n'ayant jamais contenu d'ammoniac. Dans tous les cas, la mesure commence à t=10s (introduction du capteur dans le flacon).

Conclusion du travail

Nous avons développé dans ce travail une méthode robuste et bas-coût afin de fabriquer des détecteurs de gaz à base de Nanotubes de Carbone bi-parois (DWCNTs) chimiquement fonctionnalisés. Ces nano-objets (DWCNTs) ont été synthétisés par dépôt catalytique en phase vapeur (CCVD), puis purifiés avant d'être oxydés ou bien fonctionnalisés par des terminaisons fluorées ou aminées.
Les dispositifs de détection électriques ont été fabriqués par lithographie douce en utilisant un pochoir de PDMS (Poly-DiMethyl Siloxane) et un dépôt en phase liquide à la pipette d'une suspension aqueuse contenant les nanotubes fonctionnalisés, rinçage puis séchage à l'azote sec. Chaque dispositif (1 cm X 2 cm) est équipé d'un jeu de 7 résistors à base de DWCNTs. Chaque résistor peut accueillir des nanotubes fonctionnalisés par une entité chimique différente afin de cibler un gaz spécifique, permettant ainsi une détection multiplexée. En raison de leur faible encombrement et

la possibilité de les fabriquer sur tout type de substrat y compris des substrats souples, ces détecteurs pourraient être utilisés pour une large gamme d'applications et notamment les détecteurs de gaz portatifs et intégrés. La résistance électrique des résistors s'avère décroître avec la température suggérant une conduction électrique gouvernée par l'effet tunnel et les fluctuations au sein du tapis désordonné de nanotubes de carbone. Nous avons cependant montré dans ce travail que pour des applications réelles de détection de gaz, une régulation thermique des dispositifs n'est pas nécessaire car les variations de résistance engendrées par l'adsorption de molécules de gaz sont significativement plus grandes que les variations causées par de possibles fluctuations de température. Les dispositifs produits présentent un caractère métallique à température ambiante et pour des applications de détection de gaz nous avons sélectionné des dispositifs présentant des résistances inférieures à 100 kΩ. Le principe de base de la détection de gaz étant basé sur la mesure directe de la résistance électrique du dispositif, la consommation électrique de ces dispositifs reste faible (<1 µW).

La réponse des dispositifs à base de nanotubes de carbone non fonctionnalisés aux analytes testés (éthanol, acétone, ammoniac et vapeur d'eau) est faible. Les nanotubes de carbone fonctionnalisés présentent quant à eux, une réponse modérée à la vapeur d'eau, à l'éthanol et à l'acétone mais montrent une sensibilité excellente à l'ammoniac. En particulier, les nanotubes de carbone oxydés se sont avérés capables de détecter des concentrations sub-ppm d'ammoniac en présence de vapeur d'eau en excès et à température ambiante et ont montré une grande stabilité dans le temps même pour des expositions de gaz répétées. Nous pensons que les groupes chimiques fonctionnels ancrés à la surface des nanotubes de carbone modifient les interactions entre les molécules de gaz et les nanotubes et que le transfert de charges induit provoque les modifications de la conductance électrique du système.

Nous avons construit un modèle phénoménologique pour analyser les réponses électriques de nos dispositifs lors de l'exposition d'un gaz. Ce modèle prend en compte une variation exponentielle de la résistance au cours du temps puis un régime d'accroissement linéaire de cette résistance. Nous montrons en particulier que la constante de temps extraite du régime exponentiel est très informative sur la sensibilité et la sélectivité du détecteur de gaz. Nous avons finalement testé nos dispositifs pour des applications représentatives comme par exemple la détection de

traces d'ammoniac qui ont pu être aisément réalisées à des concentrations bien inférieures au seuil de détection du nez humain (0.04ppm). En raison de leur grande stabilité, facilité de fabrication (design très simple, technologies de fabrication bas coût, intégration sur substrats souples), robustesse (détection possible en présence de vapeur d'eau et résiliente aux fluctuations thermiques) et en raison de la faible quantité de nanotubes de Carbone nécessaire, nous pensons que nos résultats sont intéressants pour des applications de masse concernant des détecteurs de gaz portables pour l'industrie des technologies de l'information et de la communication.